Two Coating Problems: Thin Film Rupture and Spin Coating

by

Mihaela Froehlich

Department of Mathematics
Duke University

Date: _____

Approved:

_____
Thomas P. Witelski, Advisor

_____
J. Thomas Beale

_____
Anita Layton

_____
Stephanos Venakides

Dissertation submitted in partial fulfillment of the requirements for the degree of
Doctor of Philosophy in the Department of Mathematics
in the Graduate School of Duke University
2009

Abstract
(Mathematics)

Two Coating Problems: Thin Film Rupture and Spin Coating

by

Mihaela Froehlich

Department of Mathematics
Duke University

Date: _____

Approved:

_____
Thomas P. Witelski, Advisor

_____
J. Thomas Beale

_____
Anita Layton

_____
Stephanos Venakides

An abstract of a dissertation submitted in partial fulfillment of the requirements for the degree of Doctor of Philosophy in the Department of Mathematics in the Graduate School of Duke University
2009

Abstract

We study two fluid dynamics problems which are of particular interest in industries where thin film coating is a part of a production process, like optical coating, insulating layers in micro-circuitry, adhesives and painting.

Experiments show that for very thin films of viscous liquids van der Waals intermolecular forces can produce instabilities leading to film ruptures. We consider this problem of thin film rupture driven by van der Waals forces and look for axisymmetric steady state solutions. Small perturbations from these solutions will lead to finite-time rupture. Using different numerical approaches we look for the solutions close to rupture. We obtain more solutions via shooting method and show that finite difference schemes on uniform grids are inferior to shooting for this problem.

The second problem comes from a process called spin coating, one of the methods used to coat uniform thin films onto solid surfaces in variety of industrial applications such as manufacturing magnetic and optical discs. In spin coating a drop of liquid spreads radially due to centrifugal effects from spinning and eventually yields a thin film of uniform thickness formed on the solid surface. In experiments fingering instabilities at the expanding front of the fluid layer have been observed. This has renewed interest in the study of the nonlinear dynamics of such problems. We derive the evolution equation for thin films in rotating polar coordinates. We solve the axisymmetric problem and give numerical and analytical results for steady states. For large fluid volumes in rotating cylinders, we show that when centrifugal and

gravity forces dominate, steady state solution free-surface profiles are parabolas for the angular velocity less then the critical velocity, and for higher velocities film ruptures, producing truncated parabolic profiles with circular contact lines. We find the similar results for the steady state case when centrifugal and surface tension forces are dominant, and when gravity, centrifugal and surface tension forces are dominant. Finally, we study the dynamics of the spin coating again considering the three cases, as well as including the influence of van der Waals and Marangoni forces.

Contents

List of Figures

Acknowledgements

This research project would not have been possible without the support of many people. Partial support and funding was provided by National Science Foundation research grant FRG 0244498 and CAREER 0239125.

The author wishes first to express her deepest gratitude to her supervisor Prof. Thomas P. Witelski for offering her the opportunity to work on such interesting topics and for all his trust, advice and guidance in supervising this research. His doors were always open for any questions no matter how small or big they were. Without his unwavering support this thesis would have never seen the light of day.

Regarding the understanding of the experiments relevant to the problem, the gratitude goes to Dr. Shomeek Mukhopadhyay for all the experimental work he has done on spin coating problems, and Prof. Robert P. Behringer with whose help the experiments were conducted. A special thank-you goes to the Thin Films Research Group for all the valuable input and discussions.

It is important to mention many professors who directly and indirectly supported me throughout my education and schooling: Prof. J. Thomas Beale, Prof. Anita Layton, Prof. Harold Layton, Prof. Michael C. Reed, and Prof. Stephanos Venakides from Duke University; Prof. Lee S. Dewald, Prof. Philip B. Peters, Prof. George Piegari, Prof. Troy J. Siemers, Prof. Daniela Topasna, Prof. Gregory A. Topasna, and Prof. Stacia M. Vargas from Virginia Military Institute; Prof. Robert P. Bennell from Zayed University, UAE, and Prof. Alexander Oron from Israel Institute of

Technology.

The author wishes to express her love and gratitude to her beloved family: to her mother and father for providing the atmosphere where learning was encouraged, their endless support, unconditional love and allowing her freedom to go and make her own life experiences; to her brothers and sister for sharing the good and the not so good of our family's spartan way of living; to her daughter for being her companion, medicine in times of stress but also keeping her on her toes; and finally to her good-looking husband who has been a rock for her for such a long time - breathing again.

1

Introduction

1.1 Historical context

Interest in fluids and fluid flow is as old as the human kind. The fascination comes from observing fluids in the nature; from watching ripples formed by the rock thrown into a pond and flow of a river through a canal, to desire to understand the flow of the blood around our bodies or wind and weather in the atmosphere. Ancient civilizations had the knowledge to solve certain flow problems and apply them to better their lives. The focus at the time was on building canals, aqueducts, irrigation systems, and sailing ships.

The improvement in designs of those systems continued but it was not until 15th century when Leonardo Da Vinci (1452-1727), great Italian artist and engineer, first started to analyze the world of fluids and fluid flow. He was an experimentalist and in his notes carefully described phenomena such as waves, eddies, falling water, interference of waves and many other then newly observed phenomena. He was also the first to derive the equation of conservation of mass in one-dimensional steady flow.

Leonardo Da Vinci was followed by Isaac Newton (1642-1727), English scientist whose great contribution was his postulates of laws of motion and the law of viscosity of linear fluids. His theory led eighteen century mathematicians such as Leonhard Euler (1707-1783), who derived equations which describe the conservation of momentum and mass for inviscid fluids, and others to produce many solutions to frictionless-flow problems. Engineers of the time rejected these mathematical theories as unrealistic and begun relying on experiments and in process developed the science of hydraulics. Much data was produced at this time on fluid flows such as open channels, pipe flows, and waves. This was also the time when French scientist Claude Louis Marie Henry Navier (1785-1836) and Irish scientist George Gabriel Stokes (1819-1903) introduced viscous transport into the Euler equations resulting in the famous Navier-Stokes equations [39].

The complexity of the equations made them too difficult to apply to arbitrary flows. It was not until the 1960s and 1970s with the development of computers that the equations could be solved for real flow problems. These equations are the basis of the modern fluid dynamics.

In this work we consider a simplification of Navier-Stokes equations to a single partial differential equation called the Reynolds lubrication equation. In 1886 Osborn Reynolds [43] applied the Navier-Stokes equation to slow viscous flow and derived the fundamental differential equation called Reynolds lubrication equations. He also found approximate solutions for this equation and compared his theoretical results to earlier experiments. In his theory of lubrication he introduced the idea of the lubrication limit in which one of the dimensions in the problem is assumed to have a much smaller scale compared to other two. For all the problems in this work we assume that the scale for the height of the fluid is much less that its lateral length scales. This allows us to model the flow by applying lubrication theory to Navier-Stokes equations and obtain so-called thin film equations.

Thin films appear in many natural phenomena such as lava flows in geology, tear films in the eye in biophysics, and industry such as application of paints and adhesives [40]. Thin film flows display a variety of interesting dynamics which has been observed experimentally. They can rupture, flows with contact lines can change structure leading to fingered patterns, or since the interface between the liquid film and the air is deformable, they can display wave motion. All of these flow phenomena can be described by the thin film equation

$$h_t = \nabla \cdot \left(h^3 \nabla P(h) \right) \tag{1.1.1}$$

where h is the height of the thin film spreading over a solid substrate, and $P(h)$ is a pressure due to any forces effecting the problem. For example, simple assumption that the height scale of the fluid is much smaller than the length scales of microscopic films leads to the conclusion that for those fluids gravity forces are dominated by surface tension forces. Assuming a constant surface tension, pressure is then proportional to curvature or

$$P(h) = -\nabla^2 h. \tag{1.1.2}$$

In equation (1.1.1) this surface tension term wants to flatten the surface. It minimizes the curvature of surface and smooths out jumps in the height of the surface. This model has been a subject of many studies both numerical and analytical, and a basis for study many other thin film flows. Researchers often start with equation (1.1.1) and add terms which describe the influence of different forces which effect their particular problem. In our work we study two interesting problems both which arise from the phenomena related to industry of optical coating, microcircuitry, paints and adhesives.

We first consider the problem of rupture of thin films of viscous fluids on solid substrates. For films of very small heights of $100 - 1000$ Å intermolecular van der Waals forces between the fluid and surface begin to influence the fluid flow. The

expression for the force has been a subject of many studies [24, 25, 56, 48]. In this model we follow a work by Williams and Davis [51] and model the pressure as a sum of contributions from a disjoining pressure due to attractive van der Waals forces and a linearized curvature term corresponding to surface tension effect

$$P(h) = \frac{1}{3h^3} - \nabla^2 h \tag{1.1.3}$$

which substituted into (1.1.1) gives a fourth order nonlinear partial differential equation

$$h_t = -\nabla \cdot \left(h^{-1}\nabla h\right) - \nabla \cdot \left(h^3 \nabla \nabla^2 h\right). \tag{1.1.4}$$

Since the work of Williams and Davis this equation and related models have been used in many studies of linear and non-linear stability of liquid films and has been extended to include effects such as thermocapillarity, evaporation, inertia, repulsive van der Waals forces [53].

The second problem described in this work comes from the industrial process called spin coating used, for example, in a production of silicon microchips. The small fluid drop is deposited in the center of the solid surface and spun. Ideally the fluid spreads axisymmetrically. After the fluid covers the surface and excess fluid spills over the edges, a thin relatively uniform layer is left on the surface. Unfortunately, the industrial process and experimental work showed formation of fingering structures and instabilities in free-surface flows of rotating fluids. This has made the study of films in rotating systems of great interest. Since early work done by Emslie et al. [18] which involved simple analysis of axisymmetric flow on an infinite smooth disk with centrifugal force being balanced by viscous resistance, much research has been done on the flow of a thin film on a rotating disk. Studies included effects such as air shear [36], surface tension [49], non-Newtonian fluids [3], uneven solid substrates [17], and evaporation [42]. Meyers and Charpin in [38] give a

detailed analysis of the influence of Coriolis force and derive evolution equation which includes centrifugal, surface tension, disjoining pressure and gravity force effects. Wu in [55] derives an evolution equation for spin model in which he includes effects of centrifugal, surface tension, disjoining pressure, external air shearing and Marangoni forces, result of surface tension gradients. Wu further imposes nonuniform surface tension profiles to the surface of the solid and study their effects on the flow. In our work we derive the thin film equation which includes effects of centrifugal, surface tension, disjoining pressure, gravity and Marangoni forces

$$h_t + \nabla \cdot \left[\frac{h^3}{3} \left(\mathrm{Ca}^{-1} \vec{\nabla} \left(\nabla^2 h \right) - \mathrm{St}^{-1} \nabla h - \mathrm{Ha} \nabla \Pi + \vec{r} \omega^2 \right) + \frac{h^2}{2} \mathrm{Ma} \nabla \sigma \right]. \qquad (1.1.5)$$

For thin films of small hight scales, surface tension is a dominant force and, if it is not constant, Marangoni forces control the motion of the fluid by driving the film flow toward lower temperature regions. Following previous work done in the study of gravity flows and use of thermal effects to drive thin film dynamics [22, 55], we study the influence of competing centrifugal and Marangoni forces on some axisymmetric spin coating problems.

1.2 Numerical methods

The governing systems modeling the two problems described in this work have only special analytic solutions. In order to solve our models we have to use numerical tools to solve these nonlinear partial differential equations with boundary conditions. For the most part, solving problems via implicit method involves more than just direct calculation at each time step in explicit methods. Instead, a root finding method, such as Newton's method, must be used in order to find the solution at next time step. That makes implementation of implicit methods more difficult and requires more work. However, in return implicit methods grant efficiency when dealing with

stiff and non-linear problems. Because the equations in our work are very stiff due to the presence of fourth order diffusive terms, we need to use implicit time-stepping methods. Such methods are necessary for stability with larger time steps [47]. For such problems use of explicit schemes would be long, tedious and even impossible since those methods are limited to very small time steps to maintain stability. The systems of equations produced by implicit schemes in this work use finite difference equations to discretize both the spatial (x, or r) and time (t) variables. Implicit schemes are then solved using Newton's method which will be discussed in the following sections.

1.2.1 Finite difference schemes

There are many important computational advantages to finite difference schemes. Most importantly, they are very easily implemented in a variety of problems since they can be simply written by replacing derivatives in governing differential equations with their corresponding difference approximations. Even very complicated problems can be implemented in computer programs with the aid of computer algebra packages (Maple). The disadvantages of finite difference methods are seen when we encounter more complex problems with difficult geometry, complex boundary conditions or nonuniform characteristics. For such complex problems the accuracy of methods like the finite elements method might outweigh the simplicity of use of finite difference methods. But for our problems, finite differences will be sufficient and simple to implement.

The challenging problem in our equations will be singular terms in the evolution equations and boundary conditions. In such cases the usual methods might fail to perform as well as expected. So in order to see how to formulate numerics for the difference stencils and boundary conditions of spinning problem we set up simpler problems with similar underlying issues. We start by making sure that the accuracy

of finite difference discretization is preserved by testing our codes first on a linear parabolic PDE problem in cylindrical coordinates and then on a simpler non-linear problem, but with similar underlying issues to our full problem.

1.2.2 Newton's method

The problem of finding the solution of a set of nonlinear equations is much more difficult than that of linear equations. Unlike with linear equations, values of the system at next step cannot be expressed explicitly. Instead, we have to use Newton's method [19] to solve nonlinear systems of form

$$\vec{F}\left(\vec{x}\right) = \vec{0} \tag{1.2.1}$$

where $\vec{x}$ is the vector of unknown solution values, $\vec{F}$ contains the coefficients which are result of the discretizaton and in non-linear problem depends on $\vec{x}$.

To describe the idea behind the Newton's method we first look at the simplest case, finding a root of a scalar function $f\left(x\right)$. Newton's method starts with an initial guess $x^{\{k\}}$ which is reasonable close to the true root x^*. Function is first approximated by its tangent line at the initial guess

$$f\left(x\right) \approx f\left(x^{\{k\}}\right) + f'\left(x^{\{k\}}\right)\left(x - x^{\{k\}}\right), \tag{1.2.2}$$

and the x-intercept of that line is then typically a better approximation to the original guess

$$x^{\{k+1\}} = x^{\{k\}} - \frac{f\left(x^{\{k\}}\right)}{f'\left(x^{\{k\}}\right)}. \tag{1.2.3}$$

This equation is then iterated until desired accuracy is achieved with convergence $x^{\{k\}} \to x^*$ for $k \to \infty$.

In general, to solve the system of equations (1.2.1) we write the expansion (1.2.2)

$$\vec{F}\left(\vec{x}\right) \approx \vec{F}\left(\vec{x}^{\{k\}}\right) + \mathbf{J}\left(\vec{x}^{\{k\}}\right)\left(\vec{x} - \vec{x}^{\{k\}}\right) \tag{1.2.4}$$

so

$$\vec{x}^{\{k+1\}} = \vec{x}^{\{k\}} - \left(\mathbf{J}\left(\vec{x}^{\{k\}}\right)\right)^{-1} \vec{F}\left(\vec{x}^{\{k\}}\right). \tag{1.2.5}$$

Here $\mathbf{J}\left(\vec{x}^{\{k\}}\right)$ is the Jacobian. The elements of $\mathbf{J}\left(\vec{x}^{\{k\}}\right)$ are

$$\mathbf{J}_{ij}\left(\vec{x}^{\{k\}}\right) = \left.\frac{\partial F_i}{\partial x_j}\right|_{\vec{x}^{\{k\}}}. \tag{1.2.6}$$

In most problems, and in all problems in this work, this Jacobian matrix is banded. This simplifies calculation and cuts on the numerical costs as the linear systems of banded matrices can be solved using LU decomposition. In our codes we use bandec and banbks as described in Numerical Recipes for Fortran 77.

If the initial guess, $\vec{x}^{\{0\}}$, was close to true root, $\vec{x}^{*}$, Newton's method will converge quadratically with respect to k, $\vec{x}^{\{k\}} \to \vec{x}^{*}$. However, if the initial guess was far off, the method might never converge. Sometimes Newton's method might be taking steps which are too aggressive. In such cases, an adaptive under relaxed Newton's method can be helpful. This method changes the correction slowly by introducing the relaxation parameter λ, $0 < \lambda \leq 1$, in the iteration equation

$$\vec{x}^{\{k+1\}} = \vec{x}^{\{k\}} - \lambda\left(\mathbf{J}\left(\vec{x}^{\{k\}}\right)\right)^{-1} \vec{F}\left(\vec{x}^{\{k\}}\right). \tag{1.2.7}$$

1.3 Outline

Following this introduction we begin our study of thin film with a general derivation of the thin films evolution equation (1.1.1) in Chapter 2. We start with the Navier-Stokes equations to which we apply the thin film lubrication limit to obtain a general partial differential equation describing the motion of the fluid. This derivation follows the work of Oron, Davis and Bankoff in their review of modern research of thin liquid films [40].

In Chapter 3 we consider a problem of thin film rupture driven by van der Waals forces. We give brief history of the problem and continue on the previous work

done by Witelski and Bernoff in [53]. We then apply and discuss some numerical schemes for finding the solutions of the steady state axisymmetric problem. We first consider a shooting approach via Runge-Kutta fourth order method, and a standard boundary value problem solver via finite difference scheme and Newton's method, both on uniform grid. Realizing that in order to capture the solution structure near the origin closer to rupture we need more information around that point, we introduce a geometric type of grid with points which get denser closer to origin and describe a new difference scheme proposed by Buckmire [10, 11] which can be compared to the standard difference scheme.

In Chapters 4 and 5 we study the second thin film problem, problem of rotating thin film flow. The full derivation of the evolution equation is described in chapter 4. We begin with the Navier-Stokes equations in cylindrical coordinates and apply lubrication theory to obtain the axisymmetric thin film equation in the cylindrical coordinates. We proceed to study the equation in Chapter 5 and find the analytical and numerical solutions to steady state problems. We begin by testing our numerical code on a linear fourth order heat problem with a known analytical solution. This problem has many of the similar difficulties to the full spin-coating problem. We also test the code on a non-linear fourth order partial differential equation which is even more similar to the full problem. We the proceed with analytical and numerical study of three versions of the spin coating problem. We find the critical angular velocities for each case numerically and analytically. Finally we consider the whole problem and study the influence of Marangoni force on the dynamics of the flow.

2

Derivation of the evolution equation for thin films

2.1 Governing equations and boundary conditions

We study problems involving free-surface lubrication flow of a thin film of viscous incompressible Newtonian liquid bounded below by a horizontal solid surface and bounded above by a liquid-air interface. The fluid is subject to conservative body forces $\nabla\phi$, and surface forces on the interface with the air which yield normal and tangential stresses. We begin with the Navier-Stokes equations and use the lubrication theory [39, 43] to derive the evolution equation for the height of a thin fluid layer in terms of general boundary conditions and body forces. We amend this general evolution equation for each problem studied later in order to describe their specific nature.

We begin by setting up the coordinate system with xy-plane along coinciding with solid surface, and z-axis normal to the xy-plane, as shown in Figure 2.1.1. We are interested in the evolution of the liquid-air interface, $h(x, y, t) = z$. The Navier-Stokes and continuity equations for viscous incompressible flow are of the form

$$\rho\frac{D\vec{u}}{Dt} = -\nabla p + \mu\nabla^2\vec{u} + \nabla\phi \tag{2.1.1a}$$

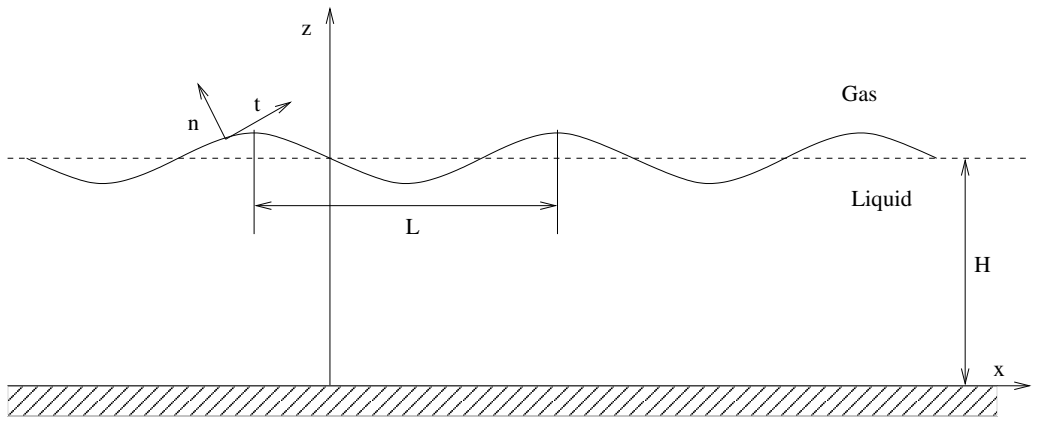

FIGURE 2.1.1: Scheme of a liquid film with a mean thickness H and typical wavelength L. Here y axis is coming out of the plane.

$$\nabla \cdot \vec{u} = 0 \tag{2.1.1b}$$

where the material derivative is

$$\frac{D}{Dt} = \frac{\partial}{\partial t} + \vec{u} \cdot \nabla, \tag{2.1.2}$$

and in rectangular coordinates the Laplacian operator is

$$\nabla^2 = \frac{\partial^2}{\partial x^2} + \frac{\partial^2}{\partial y^2} + \frac{\partial^2}{\partial z^2}. \tag{2.1.3}$$

These equations describe the evolution of the velocity field

$$\vec{u} = (u(x, y, z, t), v(x, y, z, t), w(x, y, z, t))$$

for a Newtonian fluid of constant density ρ and constant dynamic viscosity μ. Pressure of the fluid is given by p and the body force is $\nabla\phi$ [1, 13, 15, 31].

The boundary conditions between the liquid and the solid are classical no-slip and no-flux conditions [1, 31], which say that fluid particles on the solid plate will stick onto and move with the plate and not penetrate the interface,

$$\vec{u}|_{z=0} = \vec{0}. \tag{2.1.4}$$

It is known that the no slip boundary condition is incompatible with the motion of fluid contact line on dry solid surfaces [26]. If we wished to allow for the case where the motion of the contact line exists and there is a slip between the liquid and the solid (liquid spreads on the surface and displaces the gas), instead of non-slip condition for the velocities in the x and y directions we would have

$$u|_{z=0} = \beta_x \frac{\partial u}{\partial z} \tag{2.1.5a}$$

and

$$v|_{z=0} = \beta_y \frac{\partial u}{\partial z}, \tag{2.1.5b}$$

called Navier-slip boundary conditions, where $\beta_{x,y}$ are the slip coefficients in x and y directions respectively. In the case of no slip $\beta_{x,y} = 0$ [32].

On the interface with the air we have the kinetic boundary condition which says that fluid particles never leave the surface

$$\frac{Df}{Dt} = 0 \tag{2.1.6}$$

where we defined the fluid-gas boundary as the level set of $f(x, y, z, t) = z - h(x, y, t) = 0$ so that

$$\frac{Dh}{Dt} = w|_{z=h(x,y,t)}. \tag{2.1.7}$$

On the interface, $z = h(x, y, t)$, we have the stress balance condition which says that the sum of all forces has to be zero

$$-\vec{T}_{gas} + \vec{T}_{fluid} + \kappa\sigma\vec{n} - \nabla_s\sigma = \vec{0} \tag{2.1.8}$$

where $\vec{T}_{gas}$ is the surface traction of the gas on the fluid, $\vec{T}_{fluid}$ is the surface traction of fluid on the gas, $\vec{t}$ is the unit vector tangential to the interface, κ is the mean

curvature, σ is the surface tension, and s the arc-length along the interface. Under the assumption that the gas is an empty space it follows

$$\vec{T}_{gas} = \vec{0}. \tag{2.1.9}$$

In Newtonian fluid

$$\vec{T}_{fluid} = \tau\vec{n} \tag{2.1.10}$$

so that the stress balance condition (2.1.8) can be rewritten as

$$\tau\vec{n} + \kappa\sigma\vec{n} - \nabla_s\sigma = \vec{0} \tag{2.1.11}$$

where in general

$$\tau = -p\mathbf{I} + \lambda(\nabla \cdot \vec{u})\mathbf{I} + \mu\left(\nabla\vec{u} + (\nabla\vec{u})^T\right), \tag{2.1.12}$$

and λ is bulk viscosity. Further, if fluid is incompressible and Newtonian

$$\tau = -p\mathbf{I} + \mu\left[\nabla\vec{u} + (\nabla\vec{u})^T\right]. \tag{2.1.13}$$

The boundary conditions given by the vector equation (2.1.11) at $z = h(x, y, t)$ consist of three scalar equations. In the normal direction normal stress is balanced by the product of the surface tension and mean curvature

$$\vec{n} \cdot \tau\vec{n} + \kappa\sigma = 0. \tag{2.1.14}$$

In the two tangential directions we balance the shear stress on the interface and the surface gradient of the surface tension σ,

$$\vec{t}_x \cdot \tau\vec{n} - \vec{t}_x \cdot \nabla_s\sigma = 0, \tag{2.1.15}$$

and

$$\vec{t}_y \cdot \tau\vec{n} - \vec{t}_y \cdot \nabla_s\sigma = 0. \tag{2.1.16}$$

In the rectangular coordinates the unit outward vector normal to the interface $\vec{n}$, and the unit vectors tangential to the interface, $\vec{t_x}$ and $\vec{t_y}$, are given by equations

$$\vec{n} = \frac{\nabla f}{|\nabla f|} = \frac{(-h_x, -h_y, 1)}{\sqrt{1 + h_x^2 + h_y^2}}, \tag{2.1.17a}$$

$$\vec{t_x} = \frac{(1, 0, h_x)}{\sqrt{1 + h_x^2}}, \tag{2.1.17b}$$

$$\vec{t_y} = \frac{(0, 1, h_y)}{\sqrt{1 + h_y^2}}, \tag{2.1.17c}$$

with $\vec{n} \cdot \vec{t}_{x,y} = 0$. The surface curvature is given by $\kappa = -\nabla \cdot \vec{n}$ where

$$\kappa = \frac{h_{xx} + h_{yy} + h_{xx}h_y^2 - 2h_x h_y h_{xy} + h_{yy}h_x^2}{\left(1 + h_x^2 + h_y^2\right)^{\frac{3}{2}}}. \tag{2.1.18}$$

2.2 Scaled system of equations

Now that we have determined the governing equations and boundary conditions, we will introduce scalings which will allow us to nondimensionalize the system. To simplify the derivation, we consider the problem in one dimension in terms of the height $z = h(x, t)$ of the free surface. Later we will generalize to the two dimensional problem where $z = h(x, y, t)$.

Consider length scale in the x direction defined by wavelength L on a film of mean thickness H defining the length scale in z direction.

Then dimensionless $\tilde{x}$, and $\tilde{z}$ coordinates are

$$\tilde{x} = \epsilon \frac{x}{H}, \tag{2.2.1a}$$

and

$$\tilde{z} = \frac{z}{H} \tag{2.2.1b}$$

where $\epsilon = \frac{H}{L}$ is a nondimensional parameter called the aspect ratio. We assume $\epsilon \to 0$ is a small parameter called lubrication or long-wave limit.

The dimensionless fluid velocity in the x direction is

$$\tilde{u} = \frac{u}{U} \tag{2.2.2}$$

where U is the characteristic velocity of the problem. The equation of the continuity then requires that the dimensionless fluid velocity in the z direction be

$$\tilde{w} = \frac{v}{\epsilon U}. \tag{2.2.3}$$

The time is scaled with $T = \frac{L}{U} = \frac{H}{\epsilon U}$

$$\tilde{t} = \epsilon \frac{Ut}{H}. \tag{2.2.4}$$

Balancing the pressure and viscous force terms gives pressure and force potential scales

$$P = \Phi = \frac{\mu U L}{H^2} = \frac{\mu U}{\epsilon H} \tag{2.2.5}$$

so

$$\tilde{p} = \frac{\epsilon H}{\mu U} p, \tag{2.2.6}$$

and

$$\tilde{\phi} = \frac{\epsilon H}{\mu U} \phi. \tag{2.2.7}$$

From now on we will consider the modified pressure $\bar{p}$ which directly incorporates the body forces

$$\bar{p} = p + \phi, \tag{2.2.8}$$

where the body force ϕ consists of force due to the gravity $\rho g z$ and intermolecular force so

$$\phi = \rho g z + \frac{A'}{6\pi} \Pi(h). \tag{2.2.9}$$

In thin film problems it is important to incorporate intermolecular forces. These forces become significant as the film thickness nears to a range of couple of hundred Angstroms. One such type of forces are van der Waals forces which are attractive or repulsive forces between the molecules caused by fluctuating polarization of their neighboring molecules [40]. In general they compete with electrical forces from electrical double layers but for a typical material they dominate when film thicknesses are of order $0.1\mu m$, with instabilities developing on horizontal length scales of $50 - 100$ times the film thickness consistent with lubrication approximation [53]. Their strength depends on dimensional Hamaker constant A' and potential $\Pi(h)$ definition of which depends on the wetting properties of the surface [24]. In our case we chose common dewetting/wetting form for the van der Waals pressure [44]

$$\Pi(h) = \left[\left(\frac{h_{min}}{h}\right)^n - \left(\frac{h_{min}}{h}\right)^m\right] \tag{2.2.10}$$

where h_{min} is the wetting height, a very thin precursor layer of constant height, and m and n are integers such that $m > n \geq 3$. We use model where $n = 3$ and $m = 4$ [6]. This model will prevent the height of the fluid from decreasing to zero thickness and by doing that we avoid analytical and numerical difficulties which come with zero height solutions [5].

The scaled reduced pressure is

$$\tilde{p_R} = \tilde{p} + \mathrm{St}^{-1}\tilde{z} + \mathrm{Ha}\tilde{\Pi}(\tilde{h}) \tag{2.2.11}$$

with the inverse Stokes number

$$\mathrm{St}^{-1} = \epsilon\frac{\rho g H^2}{\mu U}, \tag{2.2.12}$$

and Hamaker constant

$$\mathrm{Ha} = \frac{A'\epsilon}{6\pi\mu U H^2}. \tag{2.2.13}$$

The Navier-Stokes equations are now expressed in terms of nondimensional variables

$$\epsilon \mathrm{Re}\left(\tilde{u}_{\tilde{t}} + \tilde{u}\tilde{u}_{\tilde{x}} + \tilde{w}\tilde{u}_{\tilde{z}}\right) = -\tilde{p_{R\tilde{x}}} + \epsilon^2 \tilde{u}_{\tilde{x}\tilde{x}} + \tilde{u}_{\tilde{z}\tilde{z}}, \tag{2.2.14a}$$

$$\epsilon^3 \mathrm{Re}\left(\tilde{w}_{\tilde{t}} + \tilde{u}\tilde{w}_{\tilde{x}} + \tilde{w}\tilde{w}_{\tilde{z}}\right) = -\tilde{p_{R\tilde{z}}} + \epsilon^2 \left(\epsilon^2 \tilde{w}_{\tilde{x}\tilde{x}} + \tilde{w}_{\tilde{z}\tilde{z}}\right) \tag{2.2.14b}$$

$$\tilde{u}_{\tilde{x}} + \tilde{w}_{\tilde{z}} = 0. \tag{2.2.14c}$$

At solid wall $\tilde{z} = 0$

$$\tilde{u} = 0, \tag{2.2.15a}$$

$$\tilde{w} = 0. \tag{2.2.15b}$$

At moving boundary $\tilde{z} = \tilde{h} = \frac{h}{H}$ we have the kinematic boundary condition

$$\tilde{w} = \tilde{h}_{\tilde{t}} + \tilde{u}\tilde{h}_{\tilde{x}}, \tag{2.2.16}$$

as well as the normal stress balance (2.1.14)

$$-\tilde{p}\left(1 + \epsilon^2 \tilde{h}_{\tilde{x}}^2\right) + 2\epsilon^4 \tilde{u}_{\tilde{x}} \tilde{h}_{\tilde{x}}^2 - 2\epsilon^2 \left[\tilde{h}_{\tilde{x}}\left(\tilde{w}_{\tilde{x}} + \tilde{u}_{\tilde{z}}\right) - \tilde{w}_{\tilde{z}}\right] + \mathrm{Ca}^{-1} \frac{\tilde{h}_{\tilde{x}\tilde{x}}}{\sqrt{1 + \epsilon^2 \tilde{h}_{\tilde{x}}^2}} = 0, \tag{2.2.17}$$

and the tangential stress balance (2.1.15)

$$-2\epsilon^2 \tilde{h}_{\tilde{x}}\left(\tilde{u}_{\tilde{x}} - \tilde{w}_{\tilde{z}}\right) + \epsilon^2 \tilde{w}_{\tilde{x}} + \tilde{u}_{\tilde{z}} - \epsilon^2 \tilde{h}_{\tilde{x}}^2 \left(\epsilon^2 \tilde{w}_{\tilde{x}} + \tilde{u}_{\tilde{z}}\right) = \tilde{\sigma}_{\tilde{x}} \left(1 + \epsilon^2 \tilde{h}_{\tilde{x}}^2\right) \tag{2.2.18}$$

where the Reynolds number Re is given by

$$\mathrm{Re} = \frac{UH}{\nu}, \tag{2.2.19}$$

$\tilde{\sigma} = \frac{\epsilon\sigma}{\mu U}$ is the dimensionless surface tension, and $\mathrm{Ca} = \epsilon^{-3} \frac{U\mu}{\sigma_0}$ is capillary number with the surface tension σ_0 at room temperature T_∞.

In order to include thermocapillarity effects caused by the variation of surface tension we need to add additional energy equation and corresponding boundary conditions to the governing system of equations [40].

From conservation of energy

$$\rho c_\rho \left(T_t + uT_t + wT_t\right) = k_{th}\nabla^2 T \tag{2.2.20}$$

where c_ρ is the specific heat of the fluid of density ρ, k_{th} is its thermal conductivity. The boundary condition at $z = 0$ is the imposed temperature

$$T = T_0(x), \tag{2.2.21}$$

and at $z = h(x,t)$

$$k_{th}\nabla T \cdot \vec{n} + \alpha_{th}\left(T - T_\infty\right) = 0. \tag{2.2.22}$$

The first boundary condition says that at the interface with the solid temperature T is the same as the temperature of solid. The second boundary condition is a consequence of Newton's cooling law with α_{th} being the heat transfer coefficient which describes the rate of heat transfer from the liquid to the gas which is at constant room temperature [40].

To obtain the nondimensional equations we scale temperature T

$$\tilde{T} = \frac{T - T_\infty}{\Delta T} \tag{2.2.23}$$

where ΔT is the maximum of temperature gradient. The nondimensional conservation of energy equation is then

$$\epsilon \mathrm{RePr}\left(\tilde{T}_{\tilde{t}} + \tilde{u}\tilde{T}_{\tilde{x}} + \tilde{w}\tilde{T}_{\tilde{z}}\right) = \epsilon^2 \tilde{T}_{\tilde{x}\tilde{x}} + \tilde{T}_{\tilde{z}\tilde{z}} \tag{2.2.24}$$

where we introduce new dimensionless parameter called Prandtl number and define it as

$$\mathrm{Pr} = \frac{\mu c_\rho}{k_{th}}. \tag{2.2.25}$$

At $\tilde{z} = 0$ the nondimensionalized boundary condition is

$$\tilde{T} = \tilde{T}_0(\tilde{x}), \tag{2.2.26}$$

and at the surface $\tilde{z} = \tilde{h}(\tilde{x}, \tilde{t})$

$$\tilde{T}_{\tilde{z}} - \epsilon^2 \tilde{T}_{\tilde{x}} \tilde{h}_{\tilde{x}} + \mathrm{Bi}\tilde{T}\sqrt{1 + \epsilon^2 \tilde{h}_{\tilde{x}}^2} = 0 \tag{2.2.27}$$

where Biot number

$$\mathrm{Bi} = \frac{\alpha_{th} H}{k_{th}} \tag{2.2.28}$$

describes the ratio of temperature flux escaping from the surface and the temperature conduction within the fluid layer.

Finally, to have a complete system we need to describe the relation between the surface tension and the temperature. In most liquids the surface tension decreases with an increase of local temperature at the free-surface $T_s = \tilde{T}(\tilde{z} = \tilde{h})$ according to linear relationship [55]

$$\sigma = \sigma_0 - \gamma(T_s - T_\infty) \tag{2.2.29}$$

where σ_0 is the surface tension of the liquid at a referential temperature T_∞ (room temperature), γ is a positive constant. The scaled tangential surface tension gradient from equation (2.1.11) under these conditions is

$$\frac{\partial \tilde{\sigma}}{\partial \tilde{x}} = -\mathrm{Ma}\frac{\partial \tilde{T}_s}{\partial \tilde{x}} \tag{2.2.30}$$

where the Marangoni constant is

$$\mathrm{Ma} = \frac{\epsilon \gamma \Delta T L}{\mu U_0}. \tag{2.2.31}$$

Further, assuming the thin film is spreading over slowly changing temperature profiles and the ratio of thermal advection to diffusion is small (Peclet number, $\mathrm{Pe} = \mathrm{Pr} \cdot \mathrm{Re}$), then the uniform temperature is achieved quickly across the film thickness [22]. In addition we assume that the the ratio of heat transfer at the surface and resistance to heat transfer inside of the body, the Biot number, is very small

(Bi $= O(\epsilon)$). Then the temperature distribution is independent of z and temperature on the free surface is the same as the temperature on the interface with the solid

$$T_s(x) = T_0(x). \tag{2.2.32}$$

We study flows in which we impose a linear temperature distribution

$$T_s(x) = T_\infty - \tau x \tag{2.2.33}$$

where τ is the uniform temperature gradient so that

$$\frac{\partial \tilde{\sigma}}{\partial \tilde{x}} = \mathrm{Ma} \tag{2.2.34}$$

with Marangoni constant

$$\mathrm{Ma} = \frac{\epsilon \gamma \tau L}{\mu U_0} \tag{2.2.35}$$

and then (2.2.18) becomes

$$-2\epsilon^2 \tilde{h}_{\tilde{x}} \left(\tilde{u}_{\tilde{x}} - \tilde{w}_{\tilde{z}}\right) + \epsilon^2 \tilde{w}_{\tilde{x}} + \tilde{u}_{\tilde{z}} - \epsilon^2 \tilde{h}_{\tilde{x}}^2 \left(\epsilon^2 \tilde{w}_{\tilde{x}} + \tilde{u}_{\tilde{z}}\right) = \mathrm{Ma} \left(1 + \epsilon^2 \tilde{h}_{\tilde{x}}^2\right). \tag{2.2.36}$$

2.3 Leading order problem and lubrication approximation

Assuming Reynolds number Re $= O(1)$ and taking the lubrication limit $\epsilon \to 0$ we obtain the leading order equations

$$0 = -\tilde{p_{R\tilde{x}}} + \tilde{u}_{\tilde{z}\tilde{z}}, \tag{2.3.1a}$$

$$0 = -\tilde{p_{R\tilde{z}}}, \tag{2.3.1b}$$

$$\tilde{u}_{\tilde{x}} + \tilde{w}_{\tilde{z}} = 0. \tag{2.3.1c}$$

At $\tilde{z} = 0$

$$\tilde{u} = 0, \tag{2.3.2a}$$

$$\tilde{w} = 0. \tag{2.3.2b}$$

At $\tilde{z} = \tilde{h} = \frac{h}{H}$

$$\tilde{w} = \tilde{h}_{\tilde{t}} + \tilde{u}\tilde{h}_{\tilde{x}} \tag{2.3.3a}$$

$$\tilde{u}_{\tilde{z}} = \mathrm{Ma} \tag{2.3.3b}$$

$$\tilde{p} = -\mathrm{Ca}^{-1}\tilde{h}_{\tilde{x}\tilde{x}}. \tag{2.3.3c}$$

Notice that from equation (2.3.1b) modified pressure is dependent only on variable x and time so using condition (2.3.3c) we have

$$\tilde{p_R} = \tilde{\phi}|_{\tilde{z}=\tilde{h}} - \mathrm{Ca}^{-1}\tilde{h}_{\tilde{x}\tilde{x}} = \mathrm{St}^{-1}\tilde{h} + \mathrm{Ha}\tilde{\Pi}(\tilde{h}) - \mathrm{Ca}^{-1}\tilde{h}_{\tilde{x}\tilde{x}}. \tag{2.3.4}$$

Now we can solve the system by first integrating twice equation (2.3.1a) to obtain

$$\tilde{u}(\tilde{x},\tilde{z},\tilde{t}) = \frac{\partial \tilde{p_R}}{\partial \tilde{x}}\frac{\tilde{z}^2}{2} + C_0(\tilde{x},\tilde{t})\tilde{z} + C_1(\tilde{x},\tilde{t}). \tag{2.3.5}$$

The no-slip condition at $\tilde{z} = 0$ and stress condition at $\tilde{z} = \tilde{h}(\tilde{x},\tilde{t})$ further determine constants C_0 and C_1 so that

$$\tilde{u}(\tilde{x},\tilde{z},\tilde{t}) = \frac{\partial \tilde{p_R}}{\partial \tilde{x}}\left[\frac{\tilde{z}^2}{2} - \tilde{h}\tilde{z}\right] + \mathrm{Ma}\tilde{z} \tag{2.3.6}$$

or

$$\tilde{u}(\tilde{x},\tilde{z},\tilde{t}) = \left(\mathrm{St}^{-1}\tilde{h}_{\tilde{x}} + \mathrm{Ha}\tilde{\Pi}_{\tilde{x}}(\tilde{h}) - \mathrm{Ca}^{-1}\tilde{h}_{\tilde{x}\tilde{x}\tilde{x}}\right)\left[\frac{\tilde{z}^2}{2} - \tilde{h}\tilde{z}\right] + \mathrm{Ma}\tilde{z}. \tag{2.3.7}$$

Combining equations (2.3.1c)(2.3.2b), and (2.3.3a) gives

$$\frac{\partial \tilde{h}}{\partial \tilde{t}} + \frac{\partial}{\partial \tilde{x}}\int_0^{\tilde{h}} \tilde{u}(\tilde{x},\tilde{z},\tilde{t})d\tilde{z} = 0. \tag{2.3.8}$$

From there we can obtain the one dimensional evolution equation

$$\frac{\partial \tilde{h}}{\partial \tilde{t}} - \frac{\partial}{\partial \tilde{x}}\left[\tilde{h}^3\frac{\partial}{\partial \tilde{x}}\left(\mathrm{St}^{-1}\frac{\tilde{h}}{3} + \mathrm{Ha}\tilde{\Pi}\frac{\tilde{h}}{3} - \frac{\mathrm{Ca}^{-1}}{3}\frac{\partial^2 \tilde{h}}{\partial \tilde{x}^2}\right) - \mathrm{Ma}\frac{\tilde{h}^2}{2}\right] = 0. \tag{2.3.9}$$

In two dimensions one can show that the evolution equation has the form

$$\frac{\partial \tilde{h}}{\partial \tilde{t}} - \nabla \cdot \left[\frac{\tilde{h}^3}{3} \nabla \left(\mathrm{St}^{-1} \tilde{h} + \mathrm{Ha} \tilde{\Pi}(\tilde{h}) - \mathrm{Ca}^{-1} \nabla^2 \tilde{h} \right) - \frac{\tilde{h}^2}{2} \mathrm{Ma} \nabla \tilde{\sigma} \right] = 0. \tag{2.3.10}$$

or

$$\frac{\partial \tilde{h}}{\partial \tilde{t}} - \nabla \cdot \left[\tilde{h}^3 \nabla P - \frac{\tilde{h}^2}{2} \mathrm{Ma} \nabla \tilde{\sigma} \right] = 0, \tag{2.3.11}$$

where pressure P is a function of $\tilde{h}$ and is determined by the problem, here

$$P = \frac{1}{3} \left(\mathrm{St}^{-1} h + \mathrm{Ha} \Pi(\tilde{h}) - \mathrm{Ca}^{-1} \nabla^2 h \right). \tag{2.3.12}$$

3

Thin Film Rupture

3.1 Introduction

In this chapter we consider a problem of thin film rupture driven by van der Waals forces described by

$$\frac{\partial h}{\partial t} = -\nabla \cdot (h^{-1}\nabla h) - \nabla \cdot (h^3 \nabla \nabla^2 h). \tag{3.1.1}$$

In thin films of viscous fluid on solid substrates, rupture, represented by finite-time singularities with $h \to 0$, describes the formation of dry spots and changes the geometry of the flow. This is a problem which is of particular interest in industry where thin film coating is a part of the production process (optical coatings, insulating layers in micro-circuitry, adhesives, painting) where nonuniformity is highly undesirable [53].

As described in work of Williams and Davis [51], equation (3.1.1) is derived from the lubrication equation (2.3.11) which holds for low Reynolds number flow of a thin layer of a viscous fluid on a solid substrate with pressure

$$P = \frac{1}{3h^3} - \nabla^2 h, \tag{3.1.2}$$

which consists of disjoining pressure due to attractive van der Waals force and a linearized curvature term which represents the effects of surface tension.

Much work has been done on linear and nonlinear stability of liquid films whose behavior is described by the equation (3.1.1), and similar models which included effects like thermocapillarity, evaporation, surface reaction, inertia, and repulsive van der Waals forces since Williams and Davis published their study [51]. Bertozzi and Pugh studied behaviors of contact lines and weak solutions of the generalized lubrication equation [7, 8, 9]

$$\frac{\partial h}{\partial t} = -\nabla \cdot (h^n \nabla \nabla^2 h \pm h^m \nabla h) \tag{3.1.3}$$

while Laugesen and Pugh analyzed the properties of its steady state solutions [33]. Earlier work on rupture driven by van der Waals forces described by (3.1.1) found that in planar case rupture occurs at points [12, 29], and that axisymmetric problem for the lubrication equation as a model of van der Waals driven bubble merging suggested that axisymmetric rupture or merging could occur either as a point at the origin or as a ring rupture with a finite radius [57, 58]. Zhang and Lister [59] studied the problem of rupture in (3.1.1) associated with singularity forming with $h \to 0$ at finite time t_c and showed that first-type similarity solutions exist for both planar line and axisymmetric point rupture with $h = \mathcal{O}((t_c - t)^{\frac{1}{5}})$ and $x = \mathcal{O}((t_c - t)^{\frac{2}{5}})$ as $t \to t_c$. Using those scalings they were able to reduce (3.1.1) to a fourth order ordinary differential equation for the self-similar profiles. Then they used a shooting method to find some of the solutions. Witelski and Bernoff followed Zhang and Lister [59] but used Newton's method to calculate the self-similar profiles as solutions of a nonlinear two-point boundary value problem [52] which gave linear stability of solutions as well as ordered set of self-similar profiles unlike the shooting method. Later they extended their analysis to include the geometry and dynamics of rupture of full three-dimensional thin films [53].

In this chapter we apply and discuss some numerical schemes for finding the solutions of the steady state axisymmetric problem. In particular, the solutions we want to find belong to the family of solutions on the first bifurcation branch when height of the fluid at the origin gets small. We first try solving the problem using shooting via fourth order Runge-Kutta with Newton's method, and standard finite difference scheme for the boundary value problem with Newton's method, both on uniform grid. Realizing that in order to capture the solution structure near the origin closer to rupture we need more information around that point, we introduce a geometric type of grid with points which get denser closer to origin. We also describe a new difference scheme proposed by Buckmire [10, 11] which can be compared to the standard finite-difference scheme.

3.2 Description of the Problem

Following the work of Witelski and Bernoff [53] we consider a thin layer of fluid confined within an impermeable cylindrical container of finite size. The film thickness is assumed to be nonzero everywhere before the rupture. We also assume there is no flux of fluid through the boundary of the circular region Ω, an area of the container in $r\theta$- plane,

$$\vec{n} \cdot \nabla p = 0 \qquad \text{on} \qquad \partial\Omega. \tag{3.2.1}$$

Here $\vec{n}$ is unit outer normal. Additionally, we take the fluid surface to be normal to the container walls,

$$\vec{n} \cdot \nabla h = 0 \qquad \text{on} \qquad \partial\Omega. \tag{3.2.2}$$

This condition means that we are neglecting any positive or negative meniscus on the wetting or non wetting walls of the container. The uniform fluid layer solution $h(r, \theta) = \bar{h}$ is then an exact solution of the full problem.

Since equation (3.1.1) is a conservation equation, a consequence of the no flux

boundary condition (3.2.1) is that the fluid volume

$$V(t) = \iint_{\Omega} h dA \tag{3.2.3}$$

is conserved

$$\frac{dV}{dt} = \frac{d}{dt} \iint_{\Omega} h dA = 0. \tag{3.2.4}$$

Further, in all our calculations we consider a fixed domain with $R = 1$ and average film thickness $\bar{h} = \frac{V}{A}$ where A is area of Ω.

Witelski and Bernoff [53] defined the energy associated with each instantaneous state of the fluid layer as

$$\mathcal{E}(h) = \iint_{\Omega} \left(\frac{1}{2} |\nabla h|^2 - \frac{1}{6} h^{-2} \right) dA. \tag{3.2.5}$$

Taking the time derivative of (3.2.5) yields dissipation of energy for all solutions

$$\frac{d\mathcal{E}}{dt} = \iint_{\Omega} \frac{\delta \mathcal{E}}{\delta h} \frac{\partial h}{\partial t} dA \tag{3.2.6}$$

where $\frac{\delta \mathcal{E}}{\delta h}$ is the first variation of the energy functional. To find it we disturb the solution h by some small perturbation ϵy where $\epsilon \to 0$ is a small parameter and y is

a perturbation function. Then

$$\begin{aligned}
\frac{\delta \mathcal{E}}{\delta h} y &= \lim_{\epsilon \to 0} \frac{\mathcal{E}(h+\epsilon y) - \mathcal{E}(h)}{\epsilon} \\
&= \lim_{\epsilon \to 0} \frac{1}{\epsilon} \iint_\Omega \left(\frac{1}{2} |\nabla (h+\epsilon y)|^2 - \frac{1}{6} (h+\epsilon y)^{-2} - \frac{1}{2} |\nabla h|^2 + \frac{1}{6} h^{-2} \right) dA \\
&= \lim_{\epsilon \to 0} \iint_\Omega \left(\nabla h \cdot \nabla y + \frac{y}{3} h^{-3} + \mathcal{O}(\epsilon) \right) dA \\
&= \iint_\Omega \left(\nabla h \cdot \nabla y + \frac{y}{3} h^{-3} \right) dA \\
&= \oint_{\partial \Omega} y \vec{n} \cdot \nabla h \, ds + \iint_\Omega \left(y \left(-\nabla \cdot \nabla h \right) + \frac{y}{3} h^{-3} \right) dA \\
&= \iint_\Omega y \left(-\nabla \cdot \nabla h + \frac{1}{3} h^{-3} \right) dA \\
&= \iint_\Omega yp \, dA
\end{aligned}$$

where we have used the integration by parts in the sixth line, and the first term of that expression vanishes due to the boundary condition (3.2.2). From the seventh line $\frac{\partial \mathcal{E}}{\partial h} = p$ so

$$\begin{aligned}
\frac{d\mathcal{E}}{dt} &= \iint_\Omega p \nabla \cdot (h^3 \nabla p) \, dA \qquad (3.2.8) \\
&= \oint_{\partial \Omega} p h^3 \nabla p \cdot \vec{n} \, ds - \iint_\Omega h^3 \nabla p \cdot \nabla p dA \\
&= - \iint_\Omega h^3 |\nabla p|^2 \, dA
\end{aligned}$$

where on the second line we used Green's first identity and the first term vanished due to boundary condition (3.2.1). Since h is positive everywhere in Ω from it follows that energy is decreasing unless pressure is uniformly constant, and energy is constant as well.

$$\frac{d\mathcal{E}}{dt} = - \iint_\Omega h^3 |\nabla p|^2 \, dA \leq 0 \qquad (3.2.9)$$

Since $\frac{d\mathcal{E}}{dt} = 0$ at the equilibrium, equilibrium solutions must have uniform pressure

$$\frac{1}{3}h^{-3} - \nabla^2 h = \bar{p}. \tag{3.2.10}$$

Solutions to (3.2.10) are also subject to boundary conditions (3.2.2),

$$\oint_{\partial\Omega} \nabla h \cdot \vec{n}\, ds = 0, \tag{3.2.11}$$

and as $\vec{n}$ is an outer unit normal vector of $\partial\Omega$, a boundary of a closed bounded region Ω and h has continuous first and second derivative we invoke divergence theorem so

$$\iint_{\Omega} \nabla \cdot \nabla h\, dA = 0. \tag{3.2.12}$$

Since $\nabla \cdot \nabla h = \nabla^2 h$, we can substitute (3.2.10) in (3.2.12),

$$\iint_{\Omega} \left(\frac{1}{3}h^{-3} - \bar{p}\right) dA = 0, \tag{3.2.13}$$

to obtain the compatibility condition which defines the average pressure

$$\bar{p} = \frac{1}{A}\iint_{\Omega} \frac{1}{3}h^{-3} dA > 0. \tag{3.2.14}$$

Note that for non-uniform solutions the average pressure is always greater than the pressure for uniform fluid layers,

$$\bar{p} = \frac{1}{3\bar{h}^3} > 0. \tag{3.2.15}$$

Besides the uniform solution, $h = \bar{h}$, which exists for all $\bar{h} > 0$, there exist critical values $\bar{h}_c$ where families of solutions bifurcate from the uniform solutions. To find those solutions we expand the pressure and the film thickness in the neighborhood of the bifurcation point

$$\bar{p} = \bar{p}_c + \delta + \ldots, \tag{3.2.16}$$

$$h(r) = \bar{h} + \epsilon h_1(r) + \epsilon^2 h_2(r) + \dots \tag{3.2.17}$$

where $\epsilon \ll 1$ and $\delta \ll 1$ are small perturbation parameters with $O(\delta) \leq O(\epsilon)$. Using (3.2.15) uniform solution is then

$$\bar{h} = \frac{1}{3\bar{p}^{\frac{1}{3}}} = \frac{1}{(3\bar{p}_c + 3\delta + O(\delta^2))^{\frac{1}{3}}} = \frac{\frac{1}{3\bar{p}_c{}^{\frac{1}{3}}}}{(1 + \frac{\delta}{\bar{p}_c} + O(\delta^2))^{\frac{1}{3}}} = \bar{h}_c + O(\delta) \tag{3.2.18}$$

where

$$\bar{h}_c = \frac{1}{(3\bar{p}_c)^{\frac{1}{3}}}. \tag{3.2.19}$$

Substituting into (3.2.10) we have a regular perturbation problem which at $O(\epsilon)$ gives

$$\frac{1}{\bar{h}_c^4} + \nabla^2 h_1 = 0 \tag{3.2.20}$$

subject to Neumann boundary condition (3.2.2). The bifurcation values $\bar{h}_c = \frac{1}{\sqrt{\Lambda}}$ are obtained from the positive eigenvalues Λ^2, of the Helmholtz equation with Neumann boundary conditions

$$\Lambda^2 h_1 + \nabla^2 h_1 = 0 \tag{3.2.21a}$$

$$\vec{n} \cdot \nabla h = 0. \tag{3.2.21b}$$

In particular, for axisymmetric problem, when $h = h(r)$ and equilibrium solutions must satisfy

$$\frac{1}{3} h^{-3} - \frac{1}{r}\left(r \frac{dh}{dr}\right) = \bar{p} \qquad \text{on } 0 \leq r \leq 1, \tag{3.2.22a}$$

$$h_r(0) = h_r(1) = 0 \tag{3.2.22b}$$

the linearized equation (3.2.20) is Bessel's equation of zero order

$$h_{1rr} + \frac{1}{r} h_{1r} + \Lambda^2 h_1 = 0 \tag{3.2.23}$$

with roots of the Bessel function $J_1(\Lambda_n) = 0$ for $n = 1, 2, \ldots$ as eigenvalues which correspond to bifurcation solutions

$$\bar{h}_n = \frac{1}{\sqrt{\Lambda_n}} \qquad h_{1,n}(r) = A_n J_0(\Lambda_n r). \tag{3.2.24}$$

In the proceeding section we will use numerical methods to find the branches of solutions corresponding to first two bifurcation points.

3.3 Solving the Axisymmetric Problem Numerically

To solve the axisymmetric problem we could use a variety of numerical methods. In this chapter we consider three:

1. a shooting approach via Runge-Kutta fourth order method (RK-4)
2. a boundary value problem (BVP) solver via finite difference scheme and global iterative relaxation scheme
3. a BVP solver with a non-standard difference scheme as used by Buckmire [10, 11] on problem in cylindrical coordinates, and global iterative relaxation scheme.

We also study how well the two BVP solver schemes compare to each other.

3.3.1 Shooting via Runge-Kutta-4 and Newton's Method

We want to solve axisymmetric boundary value problem for a range of values of pressure $\bar{p}$. For each pressure value we have

$$\frac{1}{3}h^{-3} - \frac{1}{r}\left(r\frac{dh}{dr}\right) = \bar{p} \qquad \text{on } 0 \le r \le 1 \tag{3.3.1a}$$

$$h_r(0) = h_r(1) = 0. \tag{3.3.1b}$$

Here, to solve the axisymmetric problem we use a shooting method via the initial value problem

$$\frac{d^2h}{dr^2} = \frac{1}{3}h^{-3} - \frac{1}{r}\frac{dh}{dr} - \bar{p}, \tag{3.3.2a}$$

$$h(0) = \alpha \tag{3.3.2b}$$

$$h_r(0) = 0. \tag{3.3.2c}$$

For each value of the shooting parameter α the initial value problem gives one solution. All the solutions of the initial value problem make a family of the solutions but only one of the values α solves the original axisymmetric boundary value problem with boundary condition $h_r(1) = 0$.

$$F(\alpha) = h_r(1, \alpha) = 0. \tag{3.3.3}$$

We want to find the root α of this equation. In order to apply Newton's method to this problem we need to determine $F'(\alpha)$. To do that we differentiate the initial value problem (3.3.2a) with respect to the parameter α which gives us an additional initial value problem on $0 \leq r \leq 1$. With $w = \frac{\partial h}{\partial \alpha}$ the additional initial value problem is

$$\frac{d^2w}{dr^2} = -h^{-4}w - \frac{1}{r}\frac{dw}{dr}, \tag{3.3.4a}$$

$$w(0) = 1 \tag{3.3.4b}$$

$$w_r(0) = 0. \tag{3.3.4c}$$

At $r = 0$ both equations (3.3.2a) and (3.3.4a) are singular. This singularity can be removed by multiplying the equations by r, however that does not help the difficulty when solving problem numerically. To resolve this problem we derive Taylor series for $h(r)$ and $w(r)$ at $r = 0$ using initial conditions. We then use it to approximate the values of the two functions at $r = \epsilon$, some small value close to origin, while at the

same time making sure it matches ordinary differential equations (3.3.2a) and(3.3.4a) to the fourth order at that position. Taylor series around $r = 0$ are

$$h(r) = \alpha + \frac{r^2}{2}h''(0) + \frac{r^3}{6}h'''(0) + \frac{r^4}{24}h^{(4)}(0) + O(\Delta r^5) \tag{3.3.5}$$

and

$$w(r) = 1 + \frac{r^2}{2}w''(0) + \frac{r^3}{6}w'''(0) + \frac{r^4}{24}w^{(4)}(0) + O(\Delta r^5). \tag{3.3.6}$$

Then we plug the series into equations (3.3.2a) and (3.3.4a) and keep the terms up to $O(r^5)$ to obtain conditions on the coefficients in two expansions

$$h''(0) = \frac{1}{2}\left(\frac{1}{3\alpha^3} - \bar{p}\right), \tag{3.3.7a}$$

$$h^{(3)}(0) = 0, \tag{3.3.7b}$$

$$h^{(4)}(0) = -\frac{3}{8\alpha^4}\left(\frac{1}{3\alpha^3} - \bar{p}\right), \tag{3.3.7c}$$

and

$$w''(0) = -\frac{1}{2\alpha^4}, \tag{3.3.8a}$$

$$w^{(3)}(0) = 0, \tag{3.3.8b}$$

$$w^{(4)}(0) = -\frac{3}{4\alpha^8}\left(\frac{7}{3} - 4\alpha^3\bar{p}\right). \tag{3.3.8c}$$

We can now use series to approximate values of $h(r)$, $h'(r)$, $w(r)$ and $w'(r)$ at some $r = \epsilon$ with $O(\epsilon^5)$ accuracy so

$$h(\epsilon, \alpha) = \alpha + \frac{\epsilon^2}{4}\left(\frac{1}{3\alpha^3} - \bar{p}\right) - \frac{\epsilon^4}{64\alpha^4}\left(\frac{1}{3\alpha^3} - \bar{p}\right) + O(\epsilon^6), \tag{3.3.9a}$$

$$h'(\epsilon, \alpha) = \frac{\epsilon}{2}\left(\frac{1}{3\alpha^3} - \bar{p}\right) - \frac{\epsilon^3}{16\alpha^4}\left(\frac{1}{3\alpha^3} - \bar{p}\right) + O(\epsilon^5) \tag{3.3.9b}$$

and

$$w(\epsilon,\alpha) = 1 - \frac{\epsilon^2}{4\alpha^4} + \frac{\epsilon^4}{64\alpha^8}\left(\frac{7}{3} - 4\alpha^3\bar{p}\right) + O(\epsilon^6), \tag{3.3.10a}$$

$$w'(\epsilon,\alpha) = -\frac{\epsilon}{2\alpha^4} + \frac{\epsilon^3}{16\alpha^8}\left(\frac{7}{3} - 4\alpha^3\bar{p}\right) + O(\epsilon^5). \tag{3.3.10b}$$

We will use this approximation at the first step of numerical integration,$\epsilon = \Delta r$.

If we let $y_1 = h$, $y_2 = h_r$, $y_3 = w$, and $y_4 = w_r$ then we have an initial value problem on $\epsilon \le r \le 1$,

$$\frac{dy_1}{dr} = y_2 \qquad y_1(\epsilon) = h(\epsilon,\alpha) \tag{3.3.11}$$

$$\frac{dy_2}{dr} = \frac{1}{3y_1^3} - \frac{1}{r}y_2 - \bar{p} \qquad y_2(\epsilon) = h'(\epsilon,\alpha) \tag{3.3.12}$$

$$\frac{dy_3}{dr} = y_4 \qquad y_3(\epsilon) = w(\epsilon,\alpha) \tag{3.3.13}$$

$$\frac{dy_4}{dr} = -\frac{y_3}{y_1^4} - \frac{1}{r}y_4 \qquad y_4(\epsilon) = w'(\epsilon,\alpha) \tag{3.3.14}$$

For every α the non-singular initial value problem (3.3.11) is solved using the standard fourth-order Runge-Kutta scheme [19], which is fourth-order accurate method. Numerical integration cannot be started at $r = 0$ because of the $1/r$ singular coefficients, hence the use of the Taylor series approximations introduced above.

Here α is a shooting parameter and we define a objective function

$$F(\alpha) = y_2(1) \tag{3.3.15}$$

which measures the difference between the current solution and the desired right side boundary condition. We iterate the value of the shooting parameter using Newton's method so that if the solution for α_k is not within of the solution α_* by a prescribed error tolerance we try a new shooting parameter given by

$$\alpha_{k+1} = \alpha_k - \frac{F(\alpha_k)}{F'(\alpha_k)} \tag{3.3.16}$$

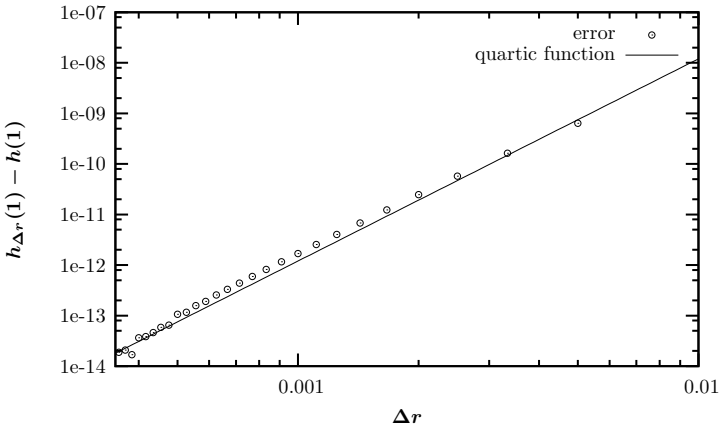

FIGURE 3.3.1: Numerical error of $h(1)$ when $p = 1.8$ for different numbers of grid points.

where

$$F'(\alpha) = \frac{dF}{d\alpha} = \frac{d}{dr}\left(\frac{dh}{d\alpha}\right)\bigg|_{r=1} = \frac{dw}{dr}\bigg|_{r=1} = y_4(1). \tag{3.3.17}$$

We check the RK-4/Newton scheme for accuracy by solving it for pressure, $p = 1.8$, with different step sizes Δr. Figure 3.3.1 shows the error at $h(1)$ for different step sizes. From the log-log plot we see that the error decreases like $O(\Delta r^4)$ as the step gets smaller. This confirms the fourth order accuracy of Runge-Kutta method and approximation at the first step.

Figures 3.3.2 and 3.3.3 show scaled version of the solutions of (3.3.2a), (3.3.2b), and (3.3.2c) for a range of values of $\bar{p}$. Figure 3.3.2 shows a family of solutions with minima at the origin. Figure 3.3.3 shows a family of solutions with minima at the outer edge, $r = 1$.

Figure 3.3.4 is a plot of bifurcation diagram of first two branches of solutions to the axisymmetric steady state rupture problem with $h(0)$ being a function of a parameter $\bar{h}$, the diagonal straight line represents all uniform solutions (flat film). Figure 3.3.5 shows the same but on a semi log scale which enables us to see better details of the graph, especially the part where the first bifurcation curve begins to oscillate. Similarly, while Figure 3.3.6 shows the diagrams of first two bifurcation

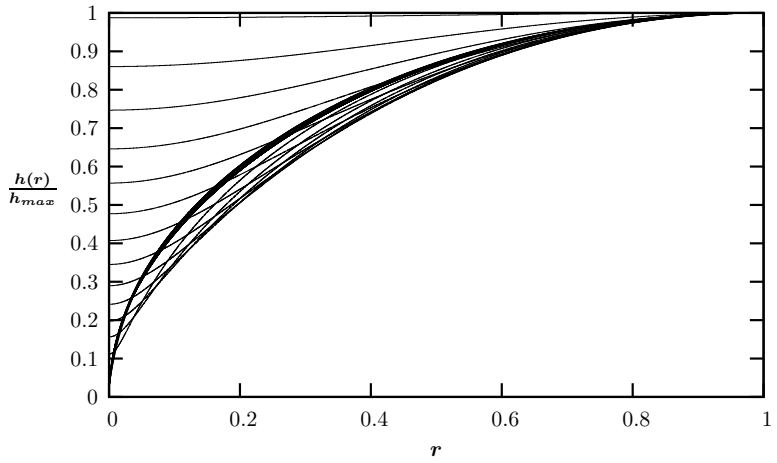

FIGURE 3.3.2: The family of scaled axisymmetric steady state solutions with minima at the origin.

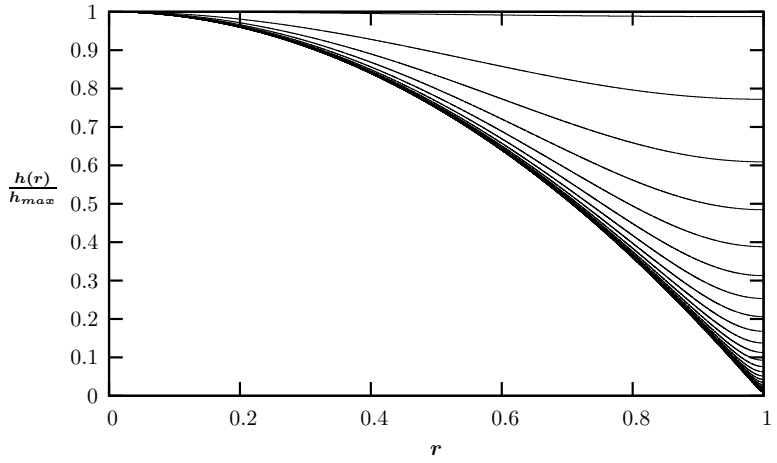

FIGURE 3.3.3: The family of scaled axisymmetric steady state solutions with minima at the outer edge, $r = 1$.

branches of solutions to the axisymmetric steady state rupture problem with p being a function of a parameter $\bar{h}$, Figure 3.3.7 shows the same on a log-log plot. Using log-log plot displays more clear the behavior of the first bifurcation curve as $h(0)$ goes closer to rupture.

The focus of our numerical calculations was evaluating the solutions corresponding to the first bifurcation branch and our goal is to find more solutions on the bifurcation curve as $h(0)$ gets smaller. From Figure 3.3.5 we can see that as the

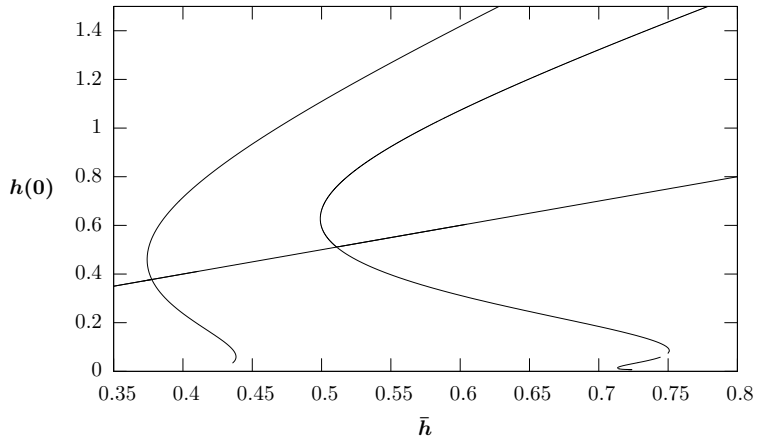

FIGURE 3.3.4: Bifurcation diagram of solutions to the axisymmetric steady state rupture problem.

height of fluid at the origin becomes thinner the bifurcation curve begins to oscillate and becomes multivalued for a given value of $\bar{h}$. The part of the bifurcation graph where the oscillations start to form corresponds to the part of the graph in Figure 3.3.7 where curve begins to spiral. To find the solution via shooting we have to have a good initial guess, the task which becomes harder as $h(0)$ goes to 0 and there are many solutions corresponding to the same pressure value.

The problem is even more clear from Figure 3.3.2 and Figure 3.3.3 which show a family of solutions on the first bifurcation branch. Solutions in Figure 3.3.3 correspond to solutions above the intersection of the first bifurcation curve and straight line in Figure 3.3.4. On the other hand, solutions in Figure 3.3.2 correspond to points in Figure 3.3.4 where the first bifurcation curve is below the straight line which represents all the uniform solutions. We can now see from Figure 3.3.2 that solutions close to rupture are approaching a singular form near 0 and thus are less likely to be chosen as a result of the shooting code. We need to see if there is some other standard method which can get us more solutions.

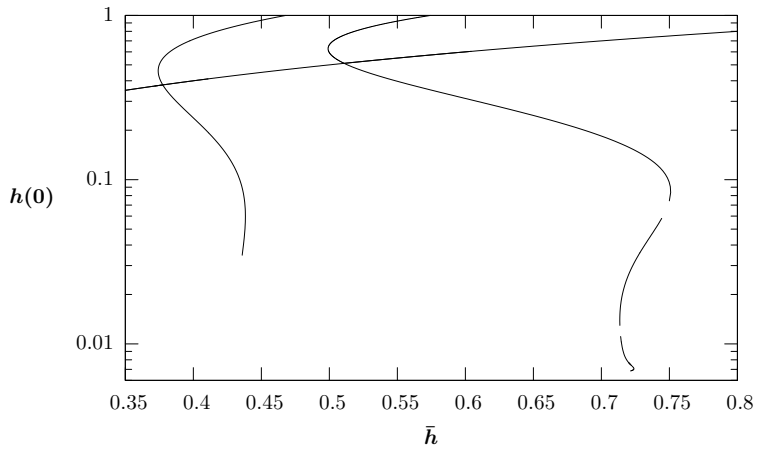

FIGURE 3.3.5: Semi-log plot of the first two bifurcation branches of solutions to the axisymmetric steady state rupture problem.

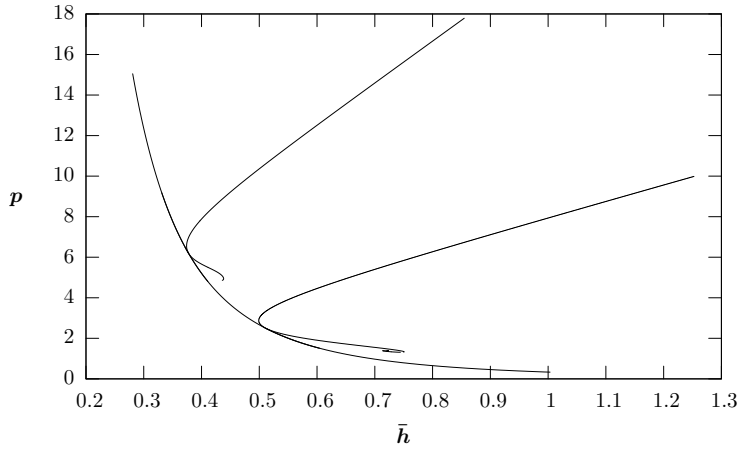

FIGURE 3.3.6: Pressure vs. height of thin film: bottom curve corresponds to solutions on the first bifurcation branch while the top corresponds to solutions on the second bifurcation branch.

3.3.2 Finite Difference Discretization and Newton's Method on Uniform Grid

Another standard way of solving a boundary value problem is by discretizing it using finite differences over, in the simplest case, an uniform grid.

We discretize (3.3.1a) rewritten in form

$$\frac{d^2h}{dr^2} + \frac{1}{r}\frac{dh}{dr} - \frac{1}{3}h^{-3} + \bar{p} = 0 \tag{3.3.18}$$

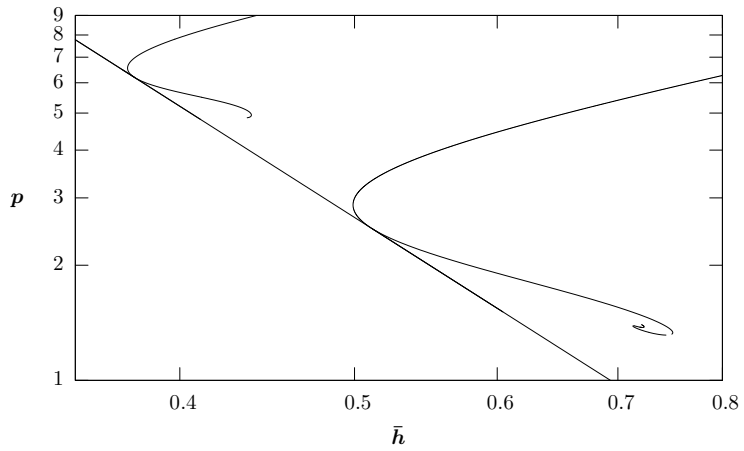

FIGURE 3.3.7: Log-log plot of pressure vs. height of thin film: bottom curve corresponds to solutions on the first bifurcation branch while the top corresponds to solutions on the second bifurcation branch.

over an equally spaced grid $r_i = i\Delta r$ for $i = 0, \ldots, N$ where $\Delta r = \frac{1}{N}$ so that $r_0 = 0$ and $r_N = 1$. Values h_0 and h_N correspond to values of $h(r)$ at $r = 0$ and $r = 1$ respectively. Using the centered difference scheme we obtain

$$\frac{h_{i-1} - 2h_i + h_{i+1}}{\Delta r^2} + \frac{1}{r_i}\frac{h_{i+1} - h_{i-1}}{r_{i+1} - r_{i-1}} - \frac{1}{3}h_i^{-3} + \bar{p} = 0. \tag{3.3.19}$$

or

$$\frac{h_{i-1} - 2h_i + h_{i+1}}{\Delta r^2} + \frac{h_{i+1} - h_{i-1}}{2i\Delta r^2} - \frac{1}{3}h_i^{-3} + \bar{p} = 0. \tag{3.3.20}$$

for $i = 1, \ldots, N$ with $h_{N+1} = h_{N-1}$, consequence of centered difference approximation to boundary condition at $r = 1$

$$0 = \left.\frac{dh}{dr}\right|_{r=1} \approx \frac{h_{N+1} - h_{N-1}}{2\Delta r}. \tag{3.3.21}$$

This scheme is second order accurate away from the origin.

When $i = 0$ we cannot use the above scheme because of division with zero in second term since $r_0 = 0$. To resolve that problem we find different way to express the corresponding derivative $\frac{1}{r}\frac{dh}{dr}$ at $r = 0$. Writing $h(r)$ as Taylor series around

$r = 0$

$$h(r) = h(0) + rh'(0) + \frac{r^2}{2}h''(0) + O(r^3) \tag{3.3.22}$$

we have

$$\frac{dh}{dr} = h'(0) + rh''(0) + O(r^2) \text{ for } r \to 0. \tag{3.3.23}$$

Boundary condition at $r = 0$ says $h'(0) = 0$ so

$$\lim_{r\to 0} \frac{1}{r}\frac{dh}{dr} = h''(0). \tag{3.3.24}$$

Now we can use that to approximate (3.3.18) at $r = 0$

$$\left.\frac{d^2h}{dr^2}\right|_{r=0} + \frac{1}{r}\left.\frac{dh}{dr}\right|_{r=0} - \frac{1}{3}h(0)^{-3} + \bar{p} = 2\left.\frac{d^2h}{dr^2}\right|_{r=0} - \frac{1}{3}h(0)^{-3} + \bar{p} \tag{3.3.25}$$

and using centered difference

$$\left.\frac{d^2h}{dr^2}\right|_{r=0} \approx \frac{h_1 - 2h_0 + h_{-1}}{\Delta r^2} + O(\Delta r^2) = 2\frac{h_1 - h_0}{\Delta r^2} \tag{3.3.26}$$

to obtain a corrected finite difference equation for $i = 0$

$$4\frac{h_1 - h_0}{\Delta r^2} - \frac{1}{3}h_0^{-3} + \bar{p} + O(\Delta r^2) = 0. \tag{3.3.27}$$

As the corrected finite difference equation at $r = 0$ is second order accurate as well as the centered finite difference scheme we use for the rest of the grid points, the best accuracy we can hope for is $O(\Delta r^2)$. We test our numerical code by solving it again for $\bar{p} = 1.8$ and check the error at $h(1)$ for different size of Δr. The test confirms that the scheme is second order accurate as expected.

Figure 3.3.9 and Figure 3.3.10 show the first two branches of bifurcation graph of steady state solutions to axisymmetric rupture problem numerically obtained via the finite difference scheme described above implemented with Newton's method.

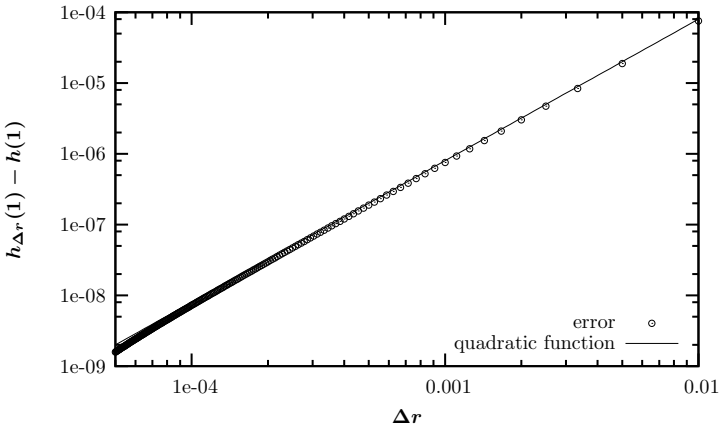

FIGURE 3.3.8: Numerical error of $h(1)$ when $p = 1.8$ for different numbers of grid points.

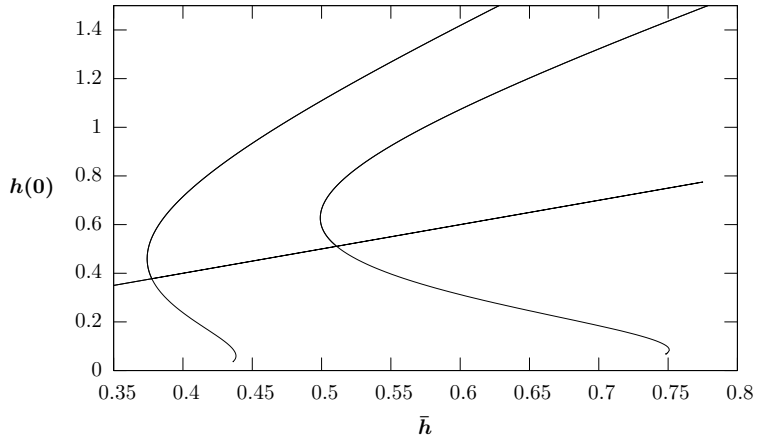

FIGURE 3.3.9: The bifurcation diagram of the solutions to the axisymmetric steady state problem using finite-difference scheme on uniform grid.

Not only we were not able to get more solutions, but with the finite difference scheme we were not able to get as many solutions as with the shooting method. As pressure parameter was made smaller the finite difference scheme was able to find the solutions easily using solutions at the previous pressure step as an initial condition. However, once the profile of the solution became closer to being singular at the origin the code was not able to evaluate those solutions using the previous solution as an initial condition. Profiles of the solutions close to rupture suggest that instead of the uniform grid we should use a grid which is more dense close to the origin.

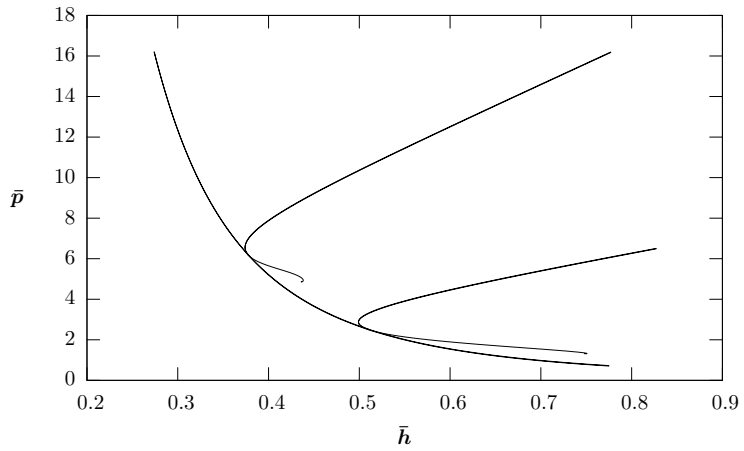

FIGURE 3.3.10: Graph of pressure vs. the average height of the thin film using finite-difference scheme on uniform grid.

3.3.3 Buckmire's Discretization Scheme and Newton's Method

In [10, 11] Buckmire introduced a novel method for computing numerical solutions to partial differential equations and ordinary differential equations written in cylindrical and spherical coordinates. This new scheme involves a particular discretization of the operator $\mathcal{R} \equiv r^p \frac{d}{dr}$, where $p = 1$ in the cylindrical case and $p = 2$ in the spherical case. Examples given by Buckmire deal with singular problems, more specifically, problems in which the solution is more sensitive and needs better resolution at the origin. As the axisymmetric rupture problem has a geometric singularity at $r = 0$ it is interesting to see if Buckmire's scheme would make a significant difference.

We consider the quantity $B(r)$ which is defined as

$$B(r) = \mathcal{R}h \equiv r^p \frac{dh}{dr}, \tag{3.3.28}$$

where $h = h(r)$ is a smooth, bounded function which operator $\mathcal{R}$ acts on. Following Buckmire's notation we choose grid $\{r_i\}_{i=0}^{N}$ on the interval $0 < r \leq 1$ so that

$$r_{-1} = 0 < r_0 < r_1 < r_2 < \ldots < r_i < \ldots < r_N = 1 \tag{3.3.29}$$

where

$$r_i = \left(\frac{1-\delta_i}{1+\delta_i}\right) r_{i+1} \tag{3.3.30}$$

with characteristics of grid discretization $\delta_i = \frac{r_{i+1}-r_i}{r_{i+1}+r_i}$. An uniform grid is a poor choice of domain discretization when there is a singular point in a domain ($r = 0$ in the axisymmetric rupture problem). In such case around $r = 0$ we would want more resolution via a denser set of grid points. Making δ_i small for all i would ensure that. Easy choice would be making all δ_i be the same value and we do so by letting $\delta = \epsilon^{-\frac{1}{N}}$ for all i where $\epsilon = r_0$ and describes how far away is the first grid point from the origin. Then

$$r_i = \delta^{N-i} \tag{3.3.31}$$

or

$$r_i = (r_0)^{\frac{N-i}{N}} = r_0 e^{-\frac{i}{N}\ln r_0}. \tag{3.3.32}$$

This discretization is exponential with many grid points close to $r = 0$. We also define our discretized quantities as $h_{i+1} \approx h(r_i)$ and $B_{i+\frac{1}{2}} = r^p \frac{dh}{dr}\big|_{r=r_{i+\frac{1}{2}}}$ where $r_{i+\frac{1}{2}} = \frac{r_i+r_{i+1}}{2}$. Buckmire proposes a scheme which he obtains by assuming that $B(r)$ is piecewise constant on each sub-interval (r_i, r_{i+1}) of the grid. On each interval $r_i \leq r \leq r_{i+1}$ we then have a boundary value problem

$$r^p \frac{dh}{dr} = B_{i+\frac{1}{2}} = constant. \tag{3.3.33}$$

$$h(r_i) = h_i \tag{3.3.34}$$

$$h(r_{i+1}) = h_{i+1}. \tag{3.3.35}$$

Solution of the ordinary differential equation (3.3.33) with $p = 1$ is $h(r) = B_{i+\frac{1}{2}} \ln(r) + C$ for $r_i \leq r \leq r_{i+1}$, and when boundary conditions (3.3.34) and (3.3.35) are applied

we obtain formula

$$B_{i+\frac{1}{2}} = \frac{h_{i+1} - h_i}{\log(\frac{r_{i+1}}{r_i})}. \tag{3.3.36}$$

Using this idea we can now discretize our problem

$$\frac{1}{r}\frac{\partial}{\partial r}\left(r\frac{dh}{dr}\right) - \frac{1}{3}h^{-3} + \bar{p} = 0 \text{ on } 0 \leq r \leq 1 \tag{3.3.37a}$$

$$h_r(0) = h_r(1) = 0, \tag{3.3.37b}$$

so that for $i = 1, \cdots, N-1$

$$\frac{1}{r_i}\frac{B_{i+\frac{1}{2}} - B_{i-\frac{1}{2}}}{r_{i+\frac{1}{2}} - r_{i-\frac{1}{2}}} - \frac{1}{3}h_i^{-3} + \bar{p} = 0 \tag{3.3.38}$$

with $B_{i+\frac{1}{2}}$ and $B_{i-\frac{1}{2}}$ as described by (3.3.36) so

$$\frac{2}{r_i\left(r_{i+1} - r_{i-1}\right)}\left(\frac{h_{i+1} - h_i}{\log\left(\frac{r_{i+1}}{r_i}\right)} - \frac{h_i - h_{i-1}}{\log\left(\frac{r_i}{r_{i-1}}\right)}\right) - \frac{1}{3}h_i^{-3} + \bar{p} = 0 \tag{3.3.39}$$

When $i = 0$ we assume $B_{-\frac{1}{2}} = 0$ since

$$B_{-\frac{1}{2}} \approx r\frac{dh}{dr}\bigg|_{r=0} = 0 \tag{3.3.40}$$

so

$$\frac{1}{r_1}\frac{B_{\frac{1}{2}}}{r_{\frac{1}{2}} - r_{-\frac{1}{2}}} - \frac{1}{3}h_0^{-3} + \bar{p} = 0. \tag{3.3.41}$$

To obtain a condition at $i = N$ we discretize boundary condition and obtain

$$\frac{r_{N-2} - r_{N-1} - 1}{r_{N-1} - 1}h_N + \frac{2 - r_{N-2}}{r_{N-1} - 1}h_{N-1} + h_{N-2} = 0. \tag{3.3.42}$$

To see how this new scheme compares to finite-difference scheme we will solve axisymmetric problem using both schemes on the uniform grid for different number of grid points. We test the numerical code by solving it for $\bar{p} = 1.8$ and then check the error at $h(1)$ for different size of Δr.

3.4 Conclusions and Further Work

The problem of rupture as seen in this chapter is not a problem that can be solved easily using traditional methods such as shooting via Newton or finite difference schemes. The difficulty lays in the near-singularity of the problem at the origin which lowers the accuracy of our schemes and as the solutions come closer to being singular at the origin methods stop being accurate.

There is still much work that can be done to find more solutions which occur closer to rupture. One thing would be improving on the shooting method by using a higher order Runge-Kutta method than the fourth order one used in this chapter. Another thing would be considering a non uniform grid with finite difference or scheme introduced by Buckmire. It would be interesting to solve both schemes on the exponential grid when ϵ is fixed and the number of grid points vary, and also when number of grid points is the same but distance from the origin to the first grid point varies. Yet another possibility is a connection which could be made to a similar problem from electrohydrodynamics, the so-called Emden equation

$$\frac{d^2y}{dx^2} + \frac{1}{x}\frac{dy}{dx} = \alpha + \frac{\beta}{y^2}. \tag{3.4.1}$$

Here variables y and x in (3.4.1) correspond to h and r in rupture problem, while parameters α and β correspond to $-\bar{p}$ and $\frac{1}{3}$ respectively. Note that the $\frac{1}{y^2}$ term corresponds to $\frac{1}{h^3}$ term. Equation (3.4.1)was studied by Ackerberg in [2] where he considered a special case of equation when parameter $\alpha = 0$, and with use of substitution transformed it into first-order problem. He then solved the equation with boundary conditions

$$\left.\frac{dy}{dx}\right|_{x=0} = 0, \tag{3.4.2a}$$

$$y(1) = 1. \tag{3.4.2b}$$

Finally, there is AUTO, continuation and bifurcation software for ordinary differential equations. This software is promising to solve the type of systems such as the rupture problem.

4

Spin coating: derivation of governing equations in rotating polar coordinates

4.1 Introduction

Spin coating is a method that has been widely used to coat uniform thin films on substrates in a variety of industrial applications such as manufacturing magnetic and optical discs, the production of phosphorous coatings on television screens and films on silicon wafers [14, 23]. The process of spinning can be separated into two phases [40]. In the first phase, a liquid droplet is placed in the center of a disk and the disk has begun to spin, the fluid layer is relatively thick so that the Reynolds number is significant, and inertial forces are important. As the disk is spun with constant angular velocity the liquid spreads outwards and the fluid layer thins out so that at some point inertial forces are no longer important. At that time phase two begins and the film continues to thin, a consequence of centrifugal force acting on the fluid (see Figure 4.1.1). Ideally, a drop of liquid is perfectly axisymmetric and its center coincides with the axis of the rotation. In the absence of temperature gradients the fluid is then expected to spread axisymmetrically due to centrifugal

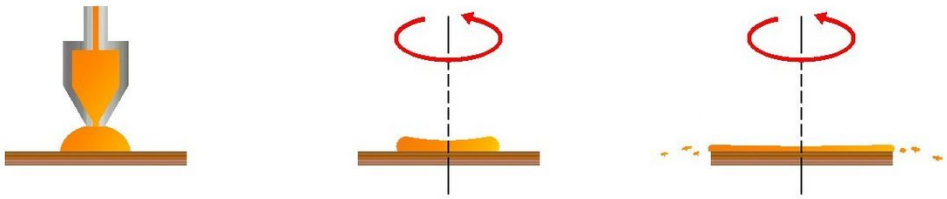

FIGURE 4.1.1: Liquid drop is deposited onto the center of the solid. As it is spun it spreads under the centrifugal force. Process ends once the excess fluid has spun off the solid and thin layer is left on the surface. (Source: http://www.indium.com/blogs/Jim-Hisert-Blog/)

force. In practice, however, it has been found that the spreading region of fluid becomes unstable at its edges, and forms "fingers" of liquid [46, 20, 35, 44]. Fluid then "prefers" to flow through the "fingers" leaving dry spots on the solid surface, a highly undesirable outcome in a coating process. This problem has made the study of rotating flows of thin films of high interest.

Pioneering work on spin coating was done by Emslie et al. [18] and involved simple analysis of axisymmetric flow on an infinite smooth disk with centrifugal force being balanced by viscous resistance. Since then much work has been done to expand the theory to include factors such as air shear [36], surface tension [49], non-Newtonian fluids [3], uneven solid substrates [17] and evaporation [42]. In all the studies mentioned above but [42] the effect of the Coriolis force has been neglected. The analytical investigation of the effect of the Coriolis force on the film heights and velocities has not been addressed until Momoniat and Mason in [37]. In it they assume an non-axisymmetric flow, and balance the viscous resistance in the azimuthal direction with the pressure gradient. This choice results in a nondimensionalization in which the scale of the azimuthal velocity is the same as that of the radial velocity. This nondimensionalization is a problem in the case of axisymmetric flow when the pressure gradient in the azimuthal direction is zero. As considered in [42], Myers and Charpin realized that the scales of azimuthal and radial velocities can be

quite different and instead they considered force balance in azimuthal direction to be between the viscous force and Coriolis force. In [38] they consider a thin layer of fluid subject to viscous resistance, centrifugal, Coriolis, gravity and surface tension forces and find that the azimuthal velocity term (Coriolis term) in radial velocity equation appears at the same order as inertia and is therefore negligible. Wu in [55] derives an evolutions equation for spin model in which he, like Myers and Charpin, includes effects of viscosity, centrifugal force, surface tension, and disjoining pressure but also considers forces of external air shearing and thermocapillarity (temperature dependent surface tension). The dimensionless equation he gives however excludes gravity, effect which Meyers and Charpin include. In [55] Wu then imposes different temperature profiles on the spinning disk, and shows that both the thermoviscosity and thermocapillarity effects significantly enhance film depletion rate when disk center is at a higher temperature than the outer edge. In this chapter we expand on the work of Myers and Charpin and Wu, and derive evolution equation which includes effects of viscosity, gravity, centrifugal force, surface tension, disjoining pressure as well as localized Marangoni forcing opposing the flow of the fluid. Following previous work done in the study of gravity flows and use of thermal effects to drive thin film dynamics [22, 55], we then in Chapter 5 study the influence of competing centrifugal and Marangoni forces on a variety of axisymmetric spin coating problems.

4.2 Converting inertial to rotational frames of reference

We derive the equations describing the flow in a thin film of viscous incompressible fluid on a rotating disk with respect to a reference frame attached to the disk (see Figure 4.2.1).

If $\vec{u}_I$ denotes the fluid velocity with respect to this fixed (inertial) frame and $\vec{u}_R$ denotes the fluid velocity with respect to a reference frame with the same origin and rotating with angular velocity $\vec{\omega}$ relative to the inertial frame, then to get from the

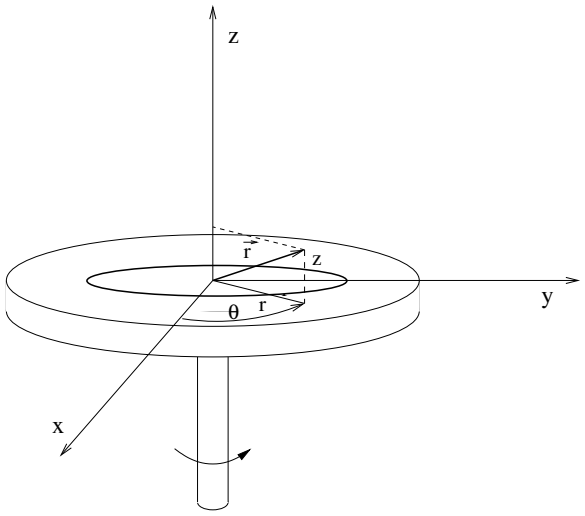

FIGURE 4.2.1: Thin layer of fluid is spun on a disk. Position vector $\vec{r}(x, y, z)$ in Cartesian coordinates corresponds to polar coordinates (r, θ, z).

inertial frame (I) of reference to rotational frame of reference (R) we have operator

$$\left(\frac{d}{dt}\right)_I = \left(\frac{d}{dt}\right)_R + \vec{\omega} \times . \tag{4.2.1}$$

If we denote $\vec{r} = (x, y, z)$ as the position vector of the fluid element, it follows that the relationship between the velocity in the inertial frame and rotation frame is described by

$$\left(\frac{d\vec{r}}{dt}\right)_I = \left(\frac{d\vec{r}}{dt}\right)_R + \vec{\omega} \times \vec{r} \tag{4.2.2}$$

and further more two accelerations are related as

$$\left(\frac{d^2\vec{r}}{dt^2}\right)_I = \left(\frac{d}{dt}\right)_R \left[\left(\frac{d\vec{r}}{dt}\right)_R + \vec{\omega} \times \vec{r}\right] + \vec{\omega} \times \left[\left(\frac{d\vec{r}}{dt}\right)_R + \vec{\omega} \times \vec{r}\right]. \tag{4.2.3}$$

Hence

$$\left(\frac{d^2\vec{r}}{dt^2}\right)_I = \left(\frac{d^2\vec{r}}{dt^2}\right)_R + \left(\frac{d\vec{\omega}}{dt}\right)_R \times \vec{r} + \vec{\omega} \times \left(\frac{d\vec{r}}{dt}\right)_R + \vec{\omega} \times \left(\frac{d\vec{r}}{dt}\right)_R + \vec{\omega} \times (\vec{\omega} \times \vec{r}), \tag{4.2.4}$$

which can be rewritten as

$$\vec{a}_I = \vec{a}_R + \left(\frac{d\vec{\omega}}{dt}\right)_R \times \vec{r} + 2\vec{\omega} \times \left(\frac{d\vec{r}}{dt}\right)_R + \vec{\omega} \times (\vec{\omega} \times \vec{r}) \tag{4.2.5}$$

and

$$\vec{a}_I = \vec{a}_R + \left(\frac{d\vec{\omega}}{dt}\right)_R \times \vec{r} + 2\vec{\omega} \times \vec{u}_R + \vec{\omega} \times (\vec{\omega} \times \vec{r}) \tag{4.2.6}$$

to finally obtain

$$\vec{a}_R = \vec{a}_I - \left(\frac{d\vec{\omega}}{dt}\right)_R \times \vec{r} - 2\vec{\omega} \times \vec{u}_R - \vec{\omega} \times (\vec{\omega} \times \vec{r}) \tag{4.2.7}$$

where $\left(\frac{d\vec{\omega}}{dt}\right)_R \times \vec{r}$ is the so called Euler force term, $2\vec{\omega} \times \vec{u}_R$ is Coriolis force term and $\vec{\omega} \times (\vec{r} \times \vec{\omega})$ is centrifugal force term [31, 34]. If angular velocity does not change with time, the Euler force is zero. Coriolis force is given by

$$2\vec{\omega} \times \vec{u}_R = \frac{2}{r} \begin{vmatrix} \hat{e}_r & r\hat{e}_\theta & \hat{e}_z \\ 0 & 0 & \Omega \\ u_r & ru_\theta & u_z \end{vmatrix} = 2\Omega(-u_\theta, u_r, 0) \tag{4.2.8}$$

where $\vec{\omega} = (0, 0, \Omega)$ and $\vec{u}_R = (u_r, u_\theta, u_z)$ [1].

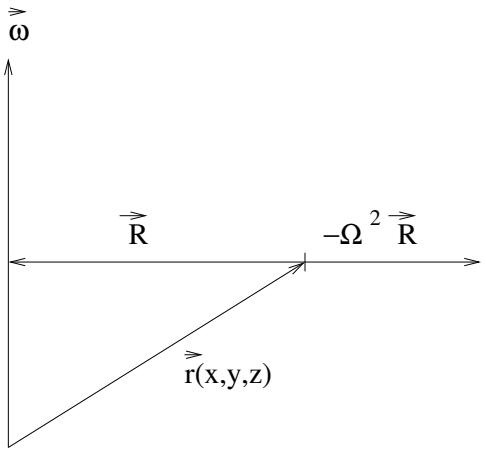

FIGURE 4.2.2: Centripetal acceleration on a particle at a position $\vec{r}(x, y, z)$ in a rotating reference frame of angular velocity $\vec{\omega}$. Vector $\vec{R}$ is a perpendicular projection of vector $\vec{r}$.

The centrifugal force can then be written in terms of the vector $\vec{R} = (x, y, 0)$ drawn perpendicularly to the axis of rotation, perpendicular projection of $\vec{r} = (x, y, z)$, (see Figure 4.2.2) since

$$\vec{\omega} \times \vec{r} = \vec{\omega} \times \vec{R}, \tag{4.2.9}$$

so

$$\begin{aligned}\vec{\omega}\times(\vec{\omega}\times\vec{r}) &= \vec{\omega}\times(\vec{\omega}\times\vec{R}) \\ &= (\vec{\omega}\cdot\vec{R})\vec{\omega}+(\vec{\omega}\cdot\vec{\omega})\vec{R} \\ &= -\Omega^2\vec{R} \\ &= -\vec{\nabla}\left(\tfrac{1}{2}\Omega^2 r^2\right)\end{aligned} \tag{4.2.10}$$

where in the third line we used the vector identity $\vec{A}\times\left(\vec{B}\times\vec{C}\right)=\left(\vec{A}\cdot\vec{C}\right)\vec{B}-\left(\vec{A}\cdot\vec{B}\right)\vec{C}$. Scalar $r=\sqrt{x^2+y^2}$ on the last line is the magnitude of vector $\vec{R}$.

In the case that the Euler term is zero (i.e. the angular velocity does not change with time) equation (4.2.6) can be rewritten as

$$\vec{a}_R=\vec{a}_I+2\Omega(-u_\theta,u_r,0)-\vec{\nabla}\left(\frac{1}{2}\Omega^2r^2\right). \tag{4.2.11}$$

In our problem $\vec{a}_I=\vec{g}$, the acceleration due to gravity.

4.3 Governing equations and boundary conditions

We begin with the Navier-Stokes and continuity equations relative to a frame of reference which rotates at with angular velocity along a fixed axis $\vec{\omega}=(0,0,\Omega)$ where Ω is constant

$$\vec{\nabla}\cdot\vec{u}=0 \tag{4.3.1a}$$

$$\begin{aligned}\rho\left(\frac{\partial\vec{u}}{\partial t}+\vec{u}\cdot\nabla\vec{u}\right) &= -\vec{\nabla}p+\mu\nabla^2\vec{u}-\nabla\Pi(h) \\ &\quad -\rho\left[\vec{g}+\left(\frac{d\vec{\omega}}{dt}\right)_r\times\vec{r}+2\Omega(-u_\theta,u_r,0)-\nabla\left(\frac{1}{2}\Omega^2r^2\right)\right].\end{aligned} \tag{4.3.1b}$$

where $\vec{u}=(u_r(r,\theta,z),u_\theta(r,\theta,z),u_z(r,\theta,z))$ is the fluid velocity relative to the rotating frame, and we assume that the shear stress due to the induced air flow is negligible. $\frac{\partial\vec{u}}{\partial t}$ is a rate of change of $\vec{u}$ at a fixed position $\vec{r}$ in that frame. Euler force term $\left(\frac{d\vec{\omega}}{dt}\right)_r$ is zero for constant angular velocity as it is the case in this problem. The

centrifugal force term can be incorporated into the "reduced pressure" p_R together with the force due to gravity

$$p_R = p + \rho g z - \frac{1}{2}\rho\Omega^2 r^2 + \frac{A'}{6\pi}\Pi(h). \tag{4.3.2}$$

Component-wise continuity and Navier-Stokes equations can then be rewritten as

$$\frac{1}{r}\frac{\partial}{\partial r}(ru_r) + \frac{1}{r}\frac{\partial u_\theta}{\partial \theta} + \frac{\partial u_z}{\partial z} = 0 \tag{4.3.3a}$$

$$\frac{\partial u_r}{\partial t} + u_r\frac{\partial u_r}{\partial r} + \frac{u_\theta}{r}\frac{\partial u_r}{\partial \theta} + u_z\frac{\partial u_r}{\partial z} - \frac{u_\theta^2}{r} = -\frac{1}{\rho}\frac{\partial p_R}{\partial r} + \frac{\mu}{\rho}\left(\nabla^2 u_r - \frac{u_r}{r^2} - \frac{2}{r^2}\frac{\partial u_\theta}{\partial \theta}\right) + 2\Omega u_\theta \tag{4.3.3b}$$

$$\frac{\partial u_\theta}{\partial t} + u_r\frac{\partial u_\theta}{\partial r} + \frac{u_\theta}{r}\frac{\partial u_\theta}{\partial \theta} + u_z\frac{\partial u_\theta}{\partial z} + \frac{u_r u_\theta}{r} = -\frac{1}{\rho r}\frac{\partial p_R}{\partial \theta} + \frac{\mu}{\rho}\left(\nabla^2 u_\theta - \frac{u_\theta}{r^2} + \frac{2}{r^2}\frac{\partial u_r}{\partial \theta}\right) - 2\Omega u_r \tag{4.3.3c}$$

$$\frac{\partial u_z}{\partial t} + u_r\frac{\partial u_z}{\partial r} + \frac{u_\theta}{r}\frac{\partial u_z}{\partial \theta} + u_z\frac{\partial u_z}{\partial z} = -\frac{1}{\rho}\frac{\partial p_R}{\partial z} + \frac{\mu}{\rho}\nabla^2 u_z. \tag{4.3.3d}$$

Assuming there is no slip between the fluid and the solid boundary, conditions at $z = 0$ are:

$$u_r|_{z=0} = 0, \tag{4.3.4a}$$

$$u_\theta|_{z=0} = 0, \tag{4.3.4b}$$

and no flux through the impermeable solid boundary

$$u_z|_{z=0} = 0. \tag{4.3.4c}$$

The kinematic boundary conditions at the fluid-air interface $z = h(r, \theta, t)$ are given by equations

$$u_z = \frac{\partial h}{\partial t} + u_r\frac{\partial h}{\partial r} + \frac{u_\theta}{r}\frac{\partial h}{\partial \theta}, \tag{4.3.5}$$

and

$$\tau\vec{n} = -\kappa\sigma\vec{n} + \nabla_s\sigma \tag{4.3.6}$$

where σ is the surface tension, s is the arc length along the interface, and τ is the stress tensor of the incompressible fluid

$$\tau = -p_R I + 2\mu E \tag{4.3.7}$$

with

$$\begin{aligned} E &= \frac{1}{2}\left[\nabla\vec{u} + (\nabla\vec{u})^T\right] \\ &= \frac{1}{2}\begin{vmatrix} \frac{\partial u_r}{\partial r} & \frac{1}{r}\frac{\partial u_r}{\partial \theta} & \frac{\partial u_r}{\partial z} \\ \frac{\partial u_\theta}{\partial r} & \frac{1}{r}\frac{\partial u_\theta}{\partial \theta} & \frac{\partial u_\theta}{\partial z} \\ \frac{\partial u_z}{\partial r} & \frac{1}{r}\frac{\partial u_z}{\partial \theta} & \frac{\partial u_z}{\partial z} \end{vmatrix} + \frac{1}{2}\begin{vmatrix} \frac{\partial u_r}{\partial r} & \frac{\partial u_\theta}{\partial r} & \frac{\partial u_z}{\partial r} \\ \frac{1}{r}\frac{\partial u_r}{\partial \theta} & \frac{1}{r}\frac{\partial u_\theta}{\partial \theta} & \frac{1}{r}\frac{\partial u_z}{\partial \theta} \\ \frac{\partial u_r}{\partial z} & \frac{\partial u_\theta}{\partial z} & \frac{\partial u_z}{\partial z} \end{vmatrix} \\ &= \frac{1}{2}\begin{vmatrix} 2\frac{\partial u_r}{\partial r} & \frac{\partial u_\theta}{\partial r} + \frac{1}{r}\frac{\partial u_r}{\partial \theta} & \frac{\partial u_r}{\partial z} + \frac{\partial u_z}{\partial r} \\ \frac{\partial u_\theta}{\partial r} + \frac{1}{r}\frac{\partial u_r}{\partial \theta} & \frac{2}{r}\frac{\partial u_\theta}{\partial \theta} & \frac{\partial u_\theta}{\partial z} + \frac{1}{r}\frac{\partial u_z}{\partial \theta} \\ \frac{\partial u_z}{\partial r} + \frac{\partial u_r}{\partial z} & \frac{1}{r}\frac{\partial u_z}{\partial \theta} + \frac{\partial u_\theta}{\partial z} & 2\frac{\partial u_z}{\partial z} \end{vmatrix}. \end{aligned} \tag{4.3.8}$$

Hence, for the incompressible Newtonian fluid

$$\tau = \begin{vmatrix} -p_R + 2\mu\frac{\partial u_r}{\partial r} & \mu(\frac{\partial u_\theta}{\partial r} + \frac{1}{r}\frac{\partial u_r}{\partial \theta}) & \mu(\frac{\partial u_r}{\partial z} + \frac{\partial u_z}{\partial r}) \\ \mu(\frac{\partial u_\theta}{\partial r} + \frac{1}{r}\frac{\partial u_r}{\partial \theta}) & -p_R + \frac{2\mu}{r}\frac{\partial u_\theta}{\partial \theta} & \mu(\frac{\partial u_\theta}{\partial z} + \frac{1}{r}\frac{\partial u_z}{\partial \theta}) \\ \mu(\frac{\partial u_z}{\partial r} + \frac{\partial u_r}{\partial z}) & \mu(\frac{1}{r}\frac{\partial u_z}{\partial \theta} + \frac{\partial u_\theta}{\partial z}) & -p_R + 2\mu\frac{\partial u_z}{\partial z} \end{vmatrix}. \tag{4.3.9}$$

Equation (4.3.5) is the kinematic boundary condition which says that normal component of the velocity of the fluid at the interface is balanced by the speed of the interface. Vector equation (4.3.6) has three components which are obtained by taking the dot product of the equation (4.3.6) with $\vec{n}$, $\vec{t}_r$ and $\vec{t}_\theta$ (equations (4.3.10), (4.3.11) and (4.3.12) respectively). In the normal direction normal stress is balanced by the product of the surface tension and mean curvature

$$\vec{n} \cdot \tau\vec{n} = -\kappa\sigma. \tag{4.3.10}$$

In the two tangential directions we balance the shear stress on the interface and the surface gradient of the surface tension σ,

$$\vec{t}_r \cdot \tau\vec{n} = \vec{t}_r \cdot \nabla_s\sigma \tag{4.3.11}$$

and

$$\vec{t}_\theta \cdot \tau\vec{n} = \vec{t}_\theta \cdot \nabla_s\sigma. \tag{4.3.12}$$

Here the unit normal and tangential vectors in polar coordinates are

$$\vec{n} = \frac{(-\frac{\partial h}{\partial r}, -\frac{1}{r}\frac{\partial h}{\partial \theta}, 1)}{\sqrt{1 + (\frac{\partial h}{\partial r})^2 + \frac{1}{r^2}(\frac{\partial h}{\partial \theta})^2}}, \tag{4.3.13a}$$

$$\vec{t}_r = \frac{(1, 0, \frac{\partial h}{\partial r})}{\sqrt{1 + (\frac{\partial h}{\partial r})^2}}, \tag{4.3.13b}$$

and

$$\vec{t}_\theta = \frac{(0, 1, \frac{1}{r}\frac{\partial h}{\partial \theta})}{\sqrt{1 + \frac{1}{r^2}(\frac{\partial h}{\partial \theta})^2}}, \tag{4.3.13c}$$

so that mean curvature of the interface

$$\begin{aligned}
\kappa &= -\nabla \cdot \vec{n} \\
&= -\frac{1}{r}\frac{\partial}{\partial r}\left[\frac{-r\frac{\partial h}{\partial r}}{\sqrt{1+\left(\frac{\partial h}{\partial r}\right)^2+\left(\frac{1}{r^2}\frac{\partial h}{\partial \theta}\right)^2}}\right] - \frac{1}{r}\frac{\partial}{\partial \theta}\left[\frac{-\frac{1}{r}\frac{\partial h}{\partial \theta}}{\sqrt{1+\left(\frac{\partial h}{\partial r}\right)^2+\left(\frac{1}{r^2}\frac{\partial h}{\partial \theta}\right)^2}}\right] - \frac{\partial}{\partial z}\left[\frac{1}{\sqrt{1+\left(\frac{\partial h}{\partial r}\right)^2+\left(\frac{1}{r^2}\frac{\partial h}{\partial \theta}\right)^2}}\right] \\
&= \frac{\frac{1}{r}\frac{\partial h}{\partial r}+\frac{\partial^2 h}{\partial r^2}+\frac{1}{r}\left(\frac{\partial h}{\partial r}\right)^3+\frac{1}{r^2}\frac{\partial^2 h}{\partial \theta^2}+\frac{2}{r^3}\frac{\partial h}{\partial r}\left(\frac{\partial h}{\partial \theta}\right)^2-\frac{2}{r^2}\frac{\partial h}{\partial r}\frac{\partial h}{\partial \theta}\frac{\partial}{\partial r}\left(\frac{\partial h}{\partial \theta}\right)+\frac{1}{r^2}\frac{\partial^2 h}{\partial r^2}\left(\frac{\partial h}{\partial \theta}\right)^2+\frac{1}{r^2}\frac{\partial^2 h}{\partial \theta^2}\left(\frac{\partial h}{\partial r}\right)^2}{\left[1+\left(\frac{\partial h}{\partial r}\right)^2+\left(\frac{1}{r^2}\frac{\partial h}{\partial \theta}\right)^2\right]^{\frac{3}{2}}} \\
&\approx \frac{\nabla^2 h}{|\nabla h|}.
\end{aligned} \tag{4.3.14}$$

We can now expand the terms in the vector equation (4.3.6)

$$\begin{aligned}
\tau\vec{n} = \; & \frac{1}{\sqrt{1+\left(\frac{\partial h}{\partial r}\right)^2+\left(\frac{1}{r}\frac{\partial h}{\partial \theta}\right)^2}} \\
& \cdot \begin{vmatrix} -\frac{\partial h}{\partial r}\left(-p_R + 2\mu\frac{\partial u_r}{\partial r}\right) - \frac{1}{r}\frac{\partial h}{\partial \theta}\mu\left(\frac{\partial u_\theta}{\partial r} + \frac{1}{r}\frac{\partial u_r}{\partial \theta}\right) + \mu\left(\frac{\partial u_r}{\partial z} + \frac{\partial u_z}{\partial r}\right) \\ -\frac{\partial h}{\partial r}\mu\left(\frac{\partial u_\theta}{\partial r} + \frac{1}{r}\frac{\partial u_r}{\partial \theta}\right) - \frac{1}{r}\frac{\partial h}{\partial \theta}\left(-p_R + \frac{2\mu}{r}\frac{\partial u_\theta}{\partial \theta}\right) + \mu\left(\frac{\partial u_\theta}{\partial z} + \frac{1}{r}\frac{\partial u_z}{\partial \theta}\right) \\ -\frac{\partial h}{\partial r}\mu\left(\frac{\partial u_z}{\partial r} + \frac{\partial u_r}{\partial z}\right) - \frac{1}{r}\frac{\partial h}{\partial \theta}\mu\left(\frac{1}{r}\frac{\partial u_z}{\partial \theta} + \frac{\partial u_\theta}{\partial z}\right) - p_R + 2\mu\frac{\partial u_z}{\partial z} \end{vmatrix}
\end{aligned} \tag{4.3.15}$$

and

$$\begin{aligned}
\kappa\sigma\vec{n} = \; & \frac{\sigma\left(\frac{1}{r}\frac{\partial h}{\partial r}+\frac{\partial^2 h}{\partial r^2}+\frac{1}{r}\left(\frac{\partial h}{\partial r}\right)^3+\frac{1}{r^2}\frac{\partial^2 h}{\partial \theta^2}+\frac{2}{r^3}\frac{\partial h}{\partial r}\left(\frac{\partial h}{\partial \theta}\right)^2-\frac{2}{r^2}\frac{\partial h}{\partial r}\frac{\partial h}{\partial \theta}\frac{\partial}{\partial r}\left(\frac{\partial h}{\partial \theta}\right)+\frac{1}{r^2}\frac{\partial^2 h}{\partial r^2}\left(\frac{\partial h}{\partial \theta}\right)^2+\frac{1}{r^2}\frac{\partial^2 h}{\partial \theta^2}\left(\frac{\partial h}{\partial r}\right)^2\right)}{\left(1+\left(\frac{\partial h}{\partial r}\right)^2+\left(\frac{1}{r}\frac{\partial h}{\partial \theta}\right)^2\right)^2} \\
& \times \left(-\frac{\partial h}{\partial r}, -\frac{1}{r}\frac{\partial h}{\partial \theta}, 1\right),
\end{aligned} \tag{4.3.16}$$

so that the stress balance condition in normal direction (4.3.10) becomes

$$\begin{aligned} -p \quad & \left[1+\left(\tfrac{\partial h}{\partial r}\right)^2+\tfrac{1}{r^2}\left(\tfrac{\partial h}{\partial \theta}\right)^2\right] \\ & +2\mu\tfrac{\partial u_r}{\partial r}\left(\tfrac{\partial h}{\partial r}\right)^2+\tfrac{2\mu}{r}\tfrac{\partial h}{\partial r}\tfrac{\partial h}{\partial \theta}\left(\tfrac{\partial u_\theta}{\partial r}+\tfrac{1}{r}\tfrac{\partial u_r}{\partial \theta}\right)-\tfrac{2\mu}{r}\tfrac{\partial h}{\partial \theta}\left(\tfrac{\partial u_\theta}{\partial z}+\tfrac{1}{r}\tfrac{\partial u_z}{\partial \theta}\right) \\ & -2\mu\tfrac{\partial h}{\partial r}\left(\tfrac{\partial u_z}{\partial r}+\tfrac{\partial u_r}{\partial z}\right)+\tfrac{2\mu}{r^3}\left(\tfrac{\partial h}{\partial \theta}\right)^2\tfrac{\partial u_\theta}{\partial \theta}+2\mu\tfrac{\partial u_z}{\partial z} \\ & +\sigma\frac{\frac{1}{r}\frac{\partial h}{\partial r}+\frac{\partial^2 h}{\partial r^2}+\frac{1}{r}\left(\frac{\partial h}{\partial r}\right)^3+\frac{1}{r^2}\frac{\partial^2 h}{\partial \theta^2}+\frac{2}{r^3}\frac{\partial h}{\partial r}\left(\frac{\partial h}{\partial \theta}\right)^2-\frac{2}{r^2}\frac{\partial h}{\partial r}\frac{\partial h}{\partial \theta}\frac{\partial}{\partial r}\left(\frac{\partial h}{\partial \theta}\right)+\frac{1}{r^2}\frac{\partial^2 h}{\partial r^2}\left(\frac{\partial h}{\partial \theta}\right)^2+\frac{1}{r^2}\frac{\partial^2 h}{\partial \theta^2}\left(\frac{\partial h}{\partial r}\right)^2}{\sqrt{1+\left(\frac{\partial h}{\partial r}\right)^2+\frac{1}{r^2}\left(\frac{\partial h}{\partial \theta}\right)^2}} \\ & =0. \end{aligned} \tag{4.3.17}$$

The tangential stress balance in the radial direction (4.3.11) expands to yield

$$\begin{aligned} -2\mu\tfrac{\partial h}{\partial r}\tfrac{\partial u_r}{\partial r} \quad & +2\mu\tfrac{\partial h}{\partial r}\tfrac{\partial u_z}{\partial z}+\mu\left(\tfrac{\partial u_z}{\partial r}+\tfrac{\partial u_r}{\partial z}\right)-\tfrac{\mu}{r}\tfrac{\partial h}{\partial \theta}\left(\tfrac{\partial u_\theta}{\partial r}+\tfrac{1}{r}\tfrac{\partial u_r}{\partial \theta}\right)-\mu\left(\tfrac{\partial h}{\partial r}\right)^2\left(\tfrac{\partial u_z}{\partial r}+\tfrac{\partial u_r}{\partial z}\right) \\ & -\tfrac{\mu}{r}\tfrac{\partial h}{\partial r}\tfrac{\partial h}{\partial \theta}\left(\tfrac{\partial u_\theta}{\partial z}+\tfrac{1}{r}\tfrac{\partial u_z}{\partial \theta}\right)=\tfrac{\partial \sigma}{\partial r}\sqrt{1+\left(\tfrac{\partial h}{\partial r}\right)^2+\tfrac{1}{r^2}\left(\tfrac{\partial h}{\partial \theta}\right)^2}\sqrt{1+\left(\tfrac{\partial h}{\partial r}\right)^2}, \end{aligned} \tag{4.3.18}$$

and finally the tangential stress balance in the azimuthal direction is

$$\begin{aligned} -\tfrac{2\mu}{r^2}\tfrac{\partial h}{\partial \theta}\tfrac{\partial u_\theta}{\partial \theta}+\tfrac{2\mu}{r}\tfrac{\partial h}{\partial \theta}\tfrac{\partial u_z}{\partial z} \quad & -\mu\tfrac{\partial h}{\partial r}\left(\tfrac{\partial u_\theta}{\partial r}+\tfrac{1}{r}\tfrac{\partial u_r}{\partial \theta}\right)-\tfrac{\mu}{r}\tfrac{\partial h}{\partial \theta}\tfrac{\partial h}{\partial r}\left(\tfrac{\partial u_z}{\partial r}+\tfrac{\partial u_r}{\partial z}\right) \\ & -\tfrac{\mu}{r^2}\left(\tfrac{\partial h}{\partial \theta}\right)^2\left(\tfrac{\partial u_\theta}{\partial z}+\tfrac{1}{r}\tfrac{\partial u_z}{\partial \theta}\right)+\mu\left(\tfrac{\partial u_\theta}{\partial z}+\tfrac{1}{r}\tfrac{\partial u_z}{\partial \theta}\right) \\ & =\tfrac{1}{r}\tfrac{\partial \sigma}{\partial \theta}\sqrt{1+\tfrac{1}{r^2}\left(\tfrac{\partial h}{\partial \theta}\right)^2+\tfrac{1}{r^2}\left(\tfrac{\partial h}{\partial \theta}\right)^2}\sqrt{1+\tfrac{1}{r^2}\left(\tfrac{\partial h}{\partial \theta}\right)^2}. \end{aligned} \tag{4.3.19}$$

4.4 Nondimensionalized system

We consider the length scales in the r direction defined by the radius R of the film of mean thickness H so that $H \ll R$, and introduce small parameter

$$\epsilon = \frac{H}{R}. \tag{4.4.1}$$

The dimensionless $\tilde{r}$ and $\tilde{z}$ coordinates are given by

$$r = R\tilde{r}, \tag{4.4.2}$$

and

$$z = H\tilde{z}. \tag{4.4.3}$$

The dimensionless fluid velocity in the r direction is scaled as

$$u_r = U_r \tilde{u_r} \tag{4.4.4}$$

where U_r is the characteristic velocity of the problem in r direction. We scale velocities in θ and z directions as

$$u_\theta = U_\theta \tilde{u_\theta}, \tag{4.4.5}$$

and

$$u_z = U_z \tilde{u_z}. \tag{4.4.6}$$

Time is scaled as

$$t = T\tilde{t} = \frac{R}{U_r}\tilde{t}, \tag{4.4.7}$$

angular velocity is scaled

$$\omega = \Omega\tilde{\omega}, \tag{4.4.8}$$

where Ω is some fixed reference rotation rate. Reduced pressure is scaled

$$p_R = P\tilde{p}_R. \tag{4.4.9}$$

We drop the tildes and write the scaled system. The conservation of mass equation

$$\frac{1}{r}\frac{\partial}{\partial r}(ru_r) + \frac{U_\theta}{U_r}\frac{1}{r}\frac{\partial u_\theta}{\partial \theta} + \frac{U_z}{\epsilon U_r}\frac{\partial u_z}{\partial z} = 0. \tag{4.4.10}$$

It follows $U_z = \epsilon U_r$, and $U_\theta = U_r$ for a non-axisymmetric problem.

In the radial direction the nondimensional Navier-Stokes equations become

$$\begin{aligned}\epsilon^2 \mathrm{Re} \quad & \left[\frac{\partial u_r}{\partial t} + u_r\frac{\partial u_r}{\partial r} + \frac{U_\theta}{U_r}\frac{u_\theta}{r}\frac{\partial u_r}{\partial \theta} + u_z\frac{\partial u_r}{\partial z} - \left(\frac{U_\theta}{U_r}\right)^2\frac{u_\theta^2}{r}\right] \\ & = -\frac{\partial p_R}{\partial r} + \epsilon^2\left[\frac{1}{r}\frac{\partial}{\partial r}\left(r\frac{\partial u_r}{\partial r}\right) + \frac{1}{r^2}\frac{\partial^2 u_r}{\partial \theta^2} - \frac{u_r}{r^2} - \frac{U_\theta}{U_r}\frac{2}{r^2}\frac{\partial u_\theta}{\partial \theta}\right] + \frac{\partial^2 u_r}{\partial z^2} + 2\frac{U_\theta}{U_r}\mathrm{Ek}^{-1}\omega u_\theta,\end{aligned} \tag{4.4.11}$$

in the azimuthal direction

$$\begin{aligned}\epsilon^2\mathrm{Re}\ & \left(\tfrac{\partial u_\theta}{\partial t}+u_r\tfrac{\partial u_\theta}{\partial r}+\tfrac{U_\theta}{U_r}\tfrac{u_\theta}{r}\tfrac{\partial u_\theta}{\partial \theta}+u_z\tfrac{\partial u_\theta}{\partial z}+\tfrac{u_r u_\theta}{r}\right)\\ &=-\left(\tfrac{U_\theta}{U_r}\right)^{-1}\tfrac{1}{r}\tfrac{\partial p_R}{\partial\theta}+\epsilon^2\left[\tfrac{1}{r}\tfrac{\partial}{\partial r}\left(r\tfrac{\partial u_\theta}{\partial r}\right)+\tfrac{1}{r^2}\tfrac{\partial^2 u_\theta}{\partial\theta^2}-\tfrac{u_\theta}{r^2}+\left(\tfrac{U_\theta}{U_r}\right)^{-1}\tfrac{2}{r^2}\tfrac{\partial u_r}{\partial\theta}\right]+\tfrac{\partial^2 u_\theta}{\partial z^2}\\ &\quad-2\left(\tfrac{U_\theta}{U_r}\right)^{-1}\mathrm{Ek}^{-1}\omega u_r,\end{aligned} \tag{4.4.12}$$

and in the z-direction

$$\epsilon^4\mathrm{Re}\left[\tfrac{\partial u_z}{\partial t}+u_r\tfrac{\partial u_z}{\partial r}+\tfrac{U_\theta}{U_r}\tfrac{u_\theta}{r}\tfrac{\partial u_z}{\partial\theta}+u_z\tfrac{\partial u_z}{\partial z}\right]=-\tfrac{\partial p_R}{\partial z}+\epsilon^2\left[\epsilon^2\tfrac{1}{r}\tfrac{\partial}{\partial r}\left(r\tfrac{\partial u_z}{\partial r}\right)+\epsilon^2\tfrac{1}{r^2}\tfrac{\partial u_z}{\partial\theta}+\tfrac{\partial^2 u_z}{\partial z^2}\right]. \tag{4.4.13}$$

Here the Reynolds number describing the ratio of inertial to viscous forces is

$$\mathrm{Re}=\frac{\rho U_r R}{\mu}=\frac{U_r R}{\nu}, \tag{4.4.14}$$

The Ekman number describing the ratio of viscous to centrifugal forces is

$$\mathrm{Ek}=\frac{\nu}{\Omega H^2}, \tag{4.4.15}$$

and the pressure scaling is

$$P=\frac{\mu R U_r}{H^2}. \tag{4.4.16}$$

We want to keep the effect of the centrifugal force, so from the scaling of reduced pressure

$$p_R=P\tilde{p_R}=P\left(\tilde{p}+\mathrm{St}^{-1}\tilde{z}-\frac{\tilde{\omega}^2\tilde{r}^2}{2}+\mathrm{Ha}\tilde{\Pi}(\tilde{h})\right) \tag{4.4.17}$$

we can obtain U_r

$$U_r=\frac{\rho\Omega^2 R H^2}{\mu}=\frac{\Omega^2 R H^2}{\nu}. \tag{4.4.18}$$

Here the inverse Stokes number represents the ratio of gravitational to viscous forces

$$\mathrm{St}^{-1}=\epsilon\frac{\rho g H^2}{\mu U_r} \tag{4.4.19}$$

and the Hamaker constant describing the strength of the disjoining pressure due to van der Waals forces

$$\mathrm{Ha} = \frac{A'\epsilon}{6\pi\mu U H^2}. \tag{4.4.20}$$

No slip boundary condition between the fluid and the solid boundary conditions at $z = 0$ stays the same

$$u_r|_{z=0} = 0, \tag{4.4.21}$$

$$u_\theta|_{z=0} = 0, \tag{4.4.22}$$

and similarly for no flux condition

$$u_z|_{z=0} = 0. \tag{4.4.23}$$

The kinematic boundary condition at the fluid-air interface $z = h(r, \theta, t)$ is given by equation

$$u_z = \frac{\partial h}{\partial t} + u_r \frac{\partial h}{\partial r} + \frac{U_\theta}{U_r}\frac{u_\theta}{r}\frac{\partial h}{\partial \theta}. \tag{4.4.24}$$

The stress boundary condition equations are little bit more involved. In the normal direction

$$\begin{aligned}
&-p\left[1+\epsilon^2\left\{\left(\tfrac{\partial h}{\partial r}\right)^2+\tfrac{1}{r^2}\left(\tfrac{\partial h}{\partial \theta}\right)^2\right]\right\}+2\epsilon^4\left[\tfrac{\partial u_r}{\partial r}\left(\tfrac{\partial h}{\partial r}\right)^2+\tfrac{1}{r}\tfrac{\partial h}{\partial r}\tfrac{\partial h}{\partial \theta}\left(\tfrac{U_\theta}{U_r}\tfrac{\partial u_\theta}{\partial r}+\tfrac{1}{r}\tfrac{\partial u_r}{\partial \theta}\right)\right]\\
&-2\epsilon^2\left(\tfrac{U_\theta}{U_r}\tfrac{\partial u_\theta}{\partial z}+\epsilon^2\tfrac{1}{r}\tfrac{\partial u_z}{\partial \theta}\right)-2\epsilon^4\left[\tfrac{\partial h}{\partial r}\left(\tfrac{\partial u_z}{\partial r}+\tfrac{\partial u_r}{\partial z}\right)-\tfrac{U_\theta}{U_r}\tfrac{1}{r^3}\left(\tfrac{\partial h}{\partial \theta}\right)^2\tfrac{\partial u_\theta}{\partial \theta}-\tfrac{\partial u_z}{\partial z}\right]\\
&+\frac{\mathrm{Ca}^{-1}}{\sqrt{1+\epsilon^2\left[\left(\frac{\partial h}{\partial r}\right)^2+\frac{1}{r^2}\left(\frac{\partial h}{\partial \theta}\right)^2\right]}}\left(\begin{array}{l}
\frac{1}{r}\frac{\partial h}{\partial r}+\frac{\partial^2 h}{\partial r^2}+\epsilon^2\frac{1}{r}\left(\frac{\partial h}{\partial r}\right)^3+\\
\frac{1}{r^2}\frac{\partial^2 h}{\partial \theta^2}+\frac{2\epsilon^2}{r^3}\frac{\partial h}{\partial r}\left(\frac{\partial h}{\partial \theta}\right)^2-\\
\frac{2\epsilon^2}{r^2}\frac{\partial h}{\partial r}\frac{\partial h}{\partial \theta}\frac{\partial}{\partial r}\left(\frac{\partial h}{\partial \theta}\right)+\epsilon^2\frac{1}{r^2}\frac{\partial^2 h}{\partial r^2}\left(\frac{\partial h}{\partial \theta}\right)^2+\\
\epsilon^2\frac{1}{r^2}\frac{\partial^2 h}{\partial \theta^2}\left(\frac{\partial h}{\partial r}\right)^2
\end{array}\right)\\
&=0.
\end{aligned} \tag{4.4.25}$$

In the radial direction the tangential stress boundary condition is

$$\begin{aligned}
-2\epsilon^2\tfrac{\partial h}{\partial r}\tfrac{\partial u_r}{\partial r}+2\epsilon^2\tfrac{\partial h}{\partial r}\tfrac{\partial u_z}{\partial z} \quad &+\epsilon^2\tfrac{\partial u_z}{\partial r}+\tfrac{\partial u_r}{\partial z}-\epsilon^2\tfrac{1}{r}\tfrac{\partial h}{\partial \theta}\left(\tfrac{U_\theta}{U_r}\tfrac{\partial u_\theta}{\partial r}+\tfrac{1}{r}\tfrac{\partial u_r}{\partial \theta}\right)\\
&-\epsilon^2\left(\tfrac{\partial h}{\partial r}\right)^2\left(\epsilon^2\tfrac{\partial u_z}{\partial r}+\tfrac{\partial u_r}{\partial z}\right)-\epsilon^2\tfrac{1}{r}\tfrac{\partial h}{\partial r}\tfrac{\partial h}{\partial \theta}\left(\tfrac{U_\theta}{U_r}\tfrac{\partial u_\theta}{\partial z}+\epsilon^2\tfrac{1}{r}\tfrac{\partial u_z}{\partial \theta}\right)\\
&=\tfrac{\partial \sigma}{\partial r}\sqrt{1+\epsilon^2\left[\left(\tfrac{\partial h}{\partial r}\right)^2+\tfrac{1}{r^2}\left(\tfrac{\partial h}{\partial \theta}\right)^2\right]}\sqrt{1+\epsilon^2\left(\tfrac{\partial h}{\partial r}\right)^2}
\end{aligned} \tag{4.4.26}$$

where we have used $\nabla_s\theta \approx (\frac{\partial\sigma}{\partial r}, \frac{1}{r}\frac{\partial\sigma}{\partial\theta}, 0) + O(\epsilon)$. The tangential stress boundary condition in the azimuthal direction is

$$\begin{aligned} -2\tfrac{U_\theta}{U_r}\epsilon^2\tfrac{1}{r^2}\tfrac{\partial h}{\partial\theta}\tfrac{\partial u_\theta}{\partial\theta} + 2\epsilon^2\tfrac{1}{r}\tfrac{\partial h}{\partial\theta}\tfrac{\partial u_z}{\partial z} \quad & -\epsilon^2\tfrac{\partial h}{\partial r}\left(\tfrac{U_\theta}{U_r}\tfrac{\partial u_\theta}{\partial r} + \tfrac{1}{r}\tfrac{\partial u_r}{\partial\theta}\right) - \epsilon^2\tfrac{1}{r}\tfrac{\partial h}{\partial\theta}\tfrac{\partial h}{\partial r}\left(\epsilon^2\tfrac{\partial u_z}{\partial r} + \tfrac{\partial u_r}{\partial z}\right) \\ & -\epsilon^2\tfrac{1}{r^2}\left(\tfrac{\partial h}{\partial\theta}\right)^2\left(\tfrac{U_\theta}{U_r}\tfrac{\partial u_\theta}{\partial z} + \epsilon^2\tfrac{1}{r}\tfrac{\partial u_z}{\partial\theta}\right) + \tfrac{U_\theta}{U_r}\tfrac{\partial u_\theta}{\partial z} + \epsilon^2\tfrac{1}{r}\tfrac{\partial u_z}{\partial\theta} \\ & = \tfrac{1}{r}\tfrac{\partial\sigma}{\partial\theta}\sqrt{1+\epsilon^2\left[\left(\tfrac{\partial h}{\partial r}\right)^2 + \tfrac{1}{r^2}\left(\tfrac{\partial h}{\partial\theta}\right)^2\right]}\sqrt{1+\epsilon^2\tfrac{1}{r^2}\left(\tfrac{\partial h}{\partial\theta}\right)^2}, \end{aligned} \tag{4.4.27}$$

where reduced capillary number is

$$\mathrm{Ca} = \epsilon^{-3}\frac{\mu U_r}{\sigma_0} \tag{4.4.28}$$

and scaled surface tension $\tilde{\sigma}$ is

$$\sigma = \frac{\mu U_r R}{H}\tilde{\sigma}. \tag{4.4.29}$$

4.5 Scaled axisymmetric problem

We first consider the axisymmetric problem with $\frac{\partial}{\partial\theta} \equiv 0$ so that scaled system simplifies to

$$\frac{1}{r}\frac{\partial}{\partial r}(ru_r) + \frac{\partial u_z}{\partial z} = 0 \tag{4.5.1}$$

$$\begin{aligned} \epsilon^2\mathrm{Re}\left(\tfrac{\partial u_r}{\partial t} + u_r\tfrac{\partial u_r}{\partial r} + u_z\tfrac{\partial u_r}{\partial z} - \left(\tfrac{U_\theta}{U_r}\right)^2\tfrac{u_\theta^2}{r}\right) = \; & -\tfrac{\partial p_R}{\partial r} + \epsilon^2\left[\tfrac{1}{r}\tfrac{\partial}{\partial r}\left(r\tfrac{\partial u_r}{\partial r}\right) - \tfrac{u_r}{r^2}\right] \\ & + \tfrac{\partial^2 u_r}{\partial z^2} + 2\tfrac{U_\theta}{U_r}\mathrm{Ek}^{-1}\omega u_\theta, \end{aligned} \tag{4.5.2a}$$

$$\begin{aligned} \epsilon^2\mathrm{Re}\left(\tfrac{\partial u_\theta}{\partial t} + u_r\tfrac{\partial u_\theta}{\partial r} + u_z\tfrac{\partial u_\theta}{\partial z} + \tfrac{u_r u_\theta}{r}\right) = \; & \epsilon^2\left[\tfrac{1}{r}\tfrac{\partial}{\partial r}\left(r\tfrac{\partial u_\theta}{\partial r}\right) - \tfrac{u_\theta}{r^2}\right] \\ & + \tfrac{\partial^2 u_\theta}{\partial z^2} - 2\left(\tfrac{U_\theta}{U_r}\right)^{-1}\mathrm{Ek}^{-1}\omega u_r, \end{aligned} \tag{4.5.2b}$$

$$\epsilon^4\mathrm{Re}\left(\frac{\partial u_z}{\partial t} + u_r\frac{\partial u_z}{\partial r} + u_z\frac{\partial u_z}{\partial z}\right) = -\frac{\partial p_R}{\partial z} + \epsilon^2\left[\epsilon^2\frac{1}{r}\frac{\partial}{\partial r}\left(r\frac{\partial u_z}{\partial r}\right) + \frac{\partial^2 u_z}{\partial z^2}\right]. \tag{4.5.2c}$$

with reduced pressure

$$p_R = p + \mathrm{St}^{-1} z - \frac{\omega^2 r^2}{2} + \mathrm{Ha}\Pi(h). \tag{4.5.3}$$

Assuming that in the azimuthal direction Coriolis force drives the flow, we keep the Coriolis force term at the leading order so

$$U_\theta = \mathrm{Ek}^{-1} U_r \tag{4.5.4}$$

or

$$\frac{U_\theta}{U_r} = \mathrm{Ek}^{-1}. \tag{4.5.5}$$

Note that using the scaling for the velocity in radial direction (4.4.18) we can rewrite $\epsilon^2\mathrm{Re}$ as follows

$$\epsilon^2\mathrm{Re} = \frac{H^2}{R^2}\frac{U_r R}{\nu} = \frac{H^2}{R\nu}\frac{\Omega^2 R H^2}{\nu} = \frac{\Omega^2 H^4}{\nu^2} = \mathrm{Ek}^{-2}. \tag{4.5.6}$$

Hence $\epsilon^2\mathrm{Re} = \left(\frac{U_\theta}{U_r}\right)^2$ and we can rewrite equations (4.5.2a),(4.5.2b) and (4.5.2c)

$$\begin{aligned}\epsilon^2\mathrm{Re}\left(\tfrac{\partial u_r}{\partial t} + u_r\tfrac{\partial u_r}{\partial r} + u_z\tfrac{\partial u_r}{\partial z} - \epsilon^2\mathrm{Re}\tfrac{u_\theta^2}{r}\right) = \; & -\tfrac{\partial p_R}{\partial r} + \epsilon^2\left[\tfrac{1}{r}\tfrac{\partial}{\partial r}\left(r\tfrac{\partial u_r}{\partial r}\right) - \tfrac{u_r}{r^2}\right] \\ & + \tfrac{\partial^2 u_r}{\partial z^2} + 2\epsilon^2\mathrm{Re}\omega u_\theta,\end{aligned} \tag{4.5.7a}$$

$$\epsilon^2\mathrm{Re}\left(\frac{\partial u_\theta}{\partial t} + u_r\frac{\partial u_\theta}{\partial r} + u_z\frac{\partial u_\theta}{\partial z} + \frac{u_r u_\theta}{r}\right) = \epsilon^2\left[\frac{1}{r}\frac{\partial}{\partial r}\left(r\frac{\partial u_\theta}{\partial r}\right) - \frac{u_\theta}{r^2}\right] + \frac{\partial^2 u_\theta}{\partial z^2} - 2\omega u_r, \tag{4.5.7b}$$

$$\epsilon^4\mathrm{Re}\left(\frac{\partial u_z}{\partial t} + u_r\frac{\partial u_z}{\partial r} + u_z\frac{\partial u_z}{\partial z}\right) = -\frac{\partial p_R}{\partial z} + \epsilon^2\left[\epsilon^2\frac{1}{r}\frac{\partial}{\partial r}\left(r\frac{\partial u_z}{\partial r}\right) + \frac{\partial^2 u_z}{\partial z^2}\right]. \tag{4.5.7c}$$

No slip boundary condition between the fluid and the solid boundary conditions at $z = 0$ stays the same:

$$u_r|_{z=0} = 0, \tag{4.5.8}$$

$$u_\theta|_{z=0} = 0, \tag{4.5.9}$$

and

$$u_z|_{z=0} = 0. \tag{4.5.10}$$

The kinematic boundary condition at the fluid-air interface $z = h(r, \theta, t)$ is given by equation

$$u_z = \frac{\partial h}{\partial t} + u_r \frac{\partial h}{\partial r}. \tag{4.5.11}$$

Stress condition equations are simplified to

$$\begin{aligned} -p\left[1+\epsilon^2\left(\tfrac{\partial h}{\partial r}\right)^2\right] + 2\epsilon^4 \tfrac{\partial u_r}{\partial r}\left(\tfrac{\partial h}{\partial r}\right)^2 - 2\mathrm{Ek}^{-1}\epsilon^2 \tfrac{\partial u_\theta}{\partial z} \quad & -2\epsilon^4\left[\tfrac{\partial h}{\partial r}\left(\tfrac{\partial u_z}{\partial r} + \tfrac{\partial u_r}{\partial z}\right) - \tfrac{\partial u_z}{\partial z}\right] \\ & +\mathrm{Ca}^{-1}\tfrac{\left[\frac{1}{r}\frac{\partial h}{\partial r}+\epsilon^2\frac{1}{r}\left(\frac{\partial h}{\partial r}\right)^3+\frac{\partial^2 h}{\partial r^2}\right]}{\sqrt{1+\epsilon^2\left(\frac{\partial h}{\partial r}\right)^2}} = 0 \end{aligned} \tag{4.5.12}$$

$$\begin{aligned} -2\epsilon^2\frac{\partial h}{\partial r}\frac{\partial u_r}{\partial r} + 2\epsilon^2\frac{\partial h}{\partial r}\frac{\partial u_z}{\partial z} + \epsilon^2\frac{\partial u_z}{\partial r} + \frac{\partial u_r}{\partial z} \quad & -\epsilon^2\left(\tfrac{\partial h}{\partial r}\right)^2\left(\epsilon^2\tfrac{\partial u_z}{\partial r} + \tfrac{\partial u_r}{\partial z}\right) \\ & = \tfrac{\partial \sigma}{\partial r}\left[1+\epsilon^2\left(\tfrac{\partial h}{\partial r}\right)^2\right] \end{aligned} \tag{4.5.13}$$

$$-\epsilon^2\frac{\partial h}{\partial r}\frac{\partial u_\theta}{\partial r} + \frac{\partial u_\theta}{\partial z} = 0. \tag{4.5.14}$$

4.6 Leading order axisymmetric problem

We seek the solution of the governing equations as a perturbation series in powers of the small parameter ϵ. We consider the lubrication approximation of the governing system by letting $\mathrm{Re}, \mathrm{Ca} = O(1)$, as $\epsilon = \frac{H}{R} \to 0$. We then have

$$\frac{1}{r}\frac{\partial}{\partial r}(r u_r) + \frac{\partial u_z}{\partial z} = 0, \tag{4.6.1}$$

$$\frac{\partial^2 u_r}{\partial z^2} = \frac{\partial p}{\partial r} - \omega^2 r + \mathrm{Ha}\frac{\partial \Pi(h)}{\partial r}, \tag{4.6.2}$$

$$\frac{\partial^2 u_\theta}{\partial z^2} = 2\omega u_r, \tag{4.6.3}$$

and

$$\frac{\partial p}{\partial z} = -\mathrm{St}^{-1}. \tag{4.6.4}$$

No slip boundary condition between the fluid and the solid boundary conditions at $z = 0$ stays the same:

$$u_r|_{z=0} = 0, \tag{4.6.5}$$

$$u_\theta|_{z=0} = 0, \tag{4.6.6}$$

and

$$u_z|_{z=0} = 0. \tag{4.6.7}$$

The kinematic boundary condition at the fluid-air interface $z = h(r,t)$ is given by equation

$$u_z = \frac{\partial h}{\partial t} + u_r \frac{\partial h}{\partial r}. \tag{4.6.8}$$

Stress condition equations at $z = h(r,t)$ are simplified to

$$p = -\mathrm{Ca}^{-1} \frac{1}{r} \frac{\partial}{\partial r} \left(r \frac{\partial h}{\partial r} \right), \tag{4.6.9}$$

$$\frac{\partial u_r}{\partial z} = \mathrm{Ma}, \tag{4.6.10}$$

and

$$\frac{\partial u_\theta}{\partial z} = 0 \tag{4.6.11}$$

where Marangoni number

$$\mathrm{Ma} = \epsilon \frac{\gamma \tau R}{\mu U_r} \tag{4.6.12}$$

represent ration of thermal surface tension to viscous forces as described in Chapter 2.

4.7 Solving the leading order axisymmetric problem

Integrating equation (4.6.4) gives

$$p(r,z) = C_1(r) - \mathrm{St}^{-1} z. \tag{4.7.1}$$

From the stress condition (4.6.9) we then have

$$C_1(r) = -\mathrm{Ca}^{-1} \frac{\partial}{\partial r}\left(r \frac{\partial h}{\partial r}\right) + \mathrm{St}^{-1} h \tag{4.7.2}$$

so

$$p(r,z) = -\mathrm{St}^{-1}(z-h) - \mathrm{Ca}^{-1} \frac{1}{r}\frac{\partial}{\partial r}\left(r \frac{\partial h}{\partial r}\right). \tag{4.7.3}$$

Now

$$\frac{\partial p}{\partial r} = \mathrm{St}^{-1}\frac{\partial h}{\partial r} - \mathrm{Ca}^{-1}\frac{\partial}{\partial r}\left(\frac{1}{r}\frac{\partial}{\partial r}\left(r\frac{\partial h}{\partial r}\right)\right) \tag{4.7.4}$$

so equation (4.6.2) yields

$$\frac{\partial^2 u_r}{\partial z^2} = \mathrm{St}^{-1}\frac{\partial h}{\partial r} - \mathrm{Ca}^{-1}\frac{\partial}{\partial r}\left(\frac{1}{r}\frac{\partial}{\partial r}\left(r\frac{\partial h}{\partial r}\right)\right) - \omega^2 r + \mathrm{Ha}\frac{\partial \Pi}{\partial r}. \tag{4.7.5}$$

Integrating once with respect to variable z gives first derivative of radial velocity

$$\frac{\partial u_r}{\partial z} = \left[\mathrm{St}^{-1}\frac{\partial h}{\partial r} - \mathrm{Ca}^{-1}\frac{\partial}{\partial r}\left(\frac{1}{r}\frac{\partial}{\partial r}\left(r\frac{\partial h}{\partial r}\right)\right) + \mathrm{Ha}\frac{\partial \Pi}{\partial r} - \omega^2 r\right] z + C_2(r). \tag{4.7.6}$$

Integrating once again with respect to variable z yields general equation for radial velocity $u_r(r,z)$

$$u_r(r,z) = \left[\mathrm{St}^{-1}\frac{\partial h}{\partial r} - \mathrm{Ca}^{-1}\frac{\partial}{\partial r}\left(\frac{1}{r}\frac{\partial}{\partial r}\left(r\frac{\partial h}{\partial r}\right)\right) + \mathrm{Ha}\frac{\partial \Pi}{\partial r} - \omega^2 r\right]\frac{z^2}{2} + C_2(r)z + C_3(r). \tag{4.7.7}$$

Boundary condition (4.6.5) yields $C_3(r) = 0$ and stress condition (4.6.10) gives

$$C_2(r) = \mathrm{Ma} - \left[\mathrm{St}^{-1}\frac{\partial h}{\partial r} - \mathrm{Ca}^{-1}\frac{\partial}{\partial r}\left(\frac{1}{r}\frac{\partial}{\partial r}\left(r\frac{\partial h}{\partial r}\right)\right) + \mathrm{Ha}\frac{\partial \Pi}{\partial r} - \omega^2 r\right] h \tag{4.7.8}$$

so

$$u_r(r,z) = \left[\mathrm{St}^{-1}\frac{\partial h}{\partial r} - \mathrm{Ca}^{-1}\frac{\partial}{\partial r}\left(\frac{1}{r}\frac{\partial}{\partial r}\left(r\frac{\partial h}{\partial r}\right)\right) + \mathrm{Ha}\frac{\partial \Pi}{\partial r} - \omega^2 r\right]\left(\frac{z^2}{2} - hz\right) + \mathrm{Ma}z \tag{4.7.9}$$

which has to satisfy the equation (4.6.3) so

$$\frac{\partial^2 u_\theta}{\partial z^2} = 2\omega\left[\mathrm{St}^{-1}\frac{\partial h}{\partial r} - \mathrm{Ca}^{-1}\frac{\partial}{\partial r}\left(\frac{1}{r}\frac{\partial}{\partial r}\left(r\frac{\partial h}{\partial r}\right)\right) + \mathrm{Ha}\frac{\partial \Pi}{\partial r} - \omega^2 r\right]\left(\frac{z^2}{2} - hz\right) + 2\mathrm{Ma}\omega z. \tag{4.7.10}$$

Integrating equation (4.7.10) once with respect to variable z yields

$$\begin{aligned}\tfrac{\partial u_\theta}{\partial z} = \;& \omega\left[\mathrm{St}^{-1}\tfrac{\partial h}{\partial r} - \mathrm{Ca}^{-1}\tfrac{\partial}{\partial r}\left(\tfrac{1}{r}\tfrac{\partial}{\partial r}\left(r\tfrac{\partial h}{\partial r}\right)\right) + \mathrm{Ha}\tfrac{\partial \Pi}{\partial r} - \omega^2 r\right]\left(\tfrac{z^3}{3} - hz^2\right) \\ & + \mathrm{Ma}\omega z^2 + C_4(r),\end{aligned} \tag{4.7.11}$$

and integrating second time with respect to the same variable gives

$$\begin{aligned}u_\theta = \;& \omega\left[\mathrm{St}^{-1}\tfrac{\partial h}{\partial r} - \mathrm{Ca}^{-1}\tfrac{\partial}{\partial r}\left(\tfrac{1}{r}\tfrac{\partial}{\partial r}\left(r\tfrac{\partial h}{\partial r}\right)\right) + \mathrm{Ha}\tfrac{\partial \Pi}{\partial r} - \omega^2 r\right]\left(\tfrac{z^4}{12} - \tfrac{hz^3}{3}\right) \\ & + \mathrm{Ma}\omega\tfrac{z^3}{3} + C_4(r)z + C_5(r).\end{aligned} \tag{4.7.12}$$

The azimuthal no slip boundary condition (4.6.6) determines $C_5(r) = 0$, and stress condition (4.6.11) yields an expression for $C_4(r)$

$$C_4(r) = 2\omega\left[\mathrm{St}^{-1}\frac{\partial h}{\partial r} - \mathrm{Ca}^{-1}\frac{\partial}{\partial r}\left(\frac{1}{r}\frac{\partial}{\partial r}\left(r\frac{\partial h}{\partial r}\right)\right) + \mathrm{Ha}\frac{\partial \Pi}{\partial r} - \omega^2 r\right]\frac{h^3}{3} - \mathrm{Ma}\omega h^2 \tag{4.7.13}$$

so

$$\begin{aligned}u_\theta = \;& \omega\left[\mathrm{St}^{-1}\tfrac{\partial h}{\partial r} - \mathrm{Ca}^{-1}\tfrac{\partial}{\partial r}\left(\tfrac{1}{r}\tfrac{\partial}{\partial r}\left(r\tfrac{\partial h}{\partial r}\right)\right) + \mathrm{Ha}\tfrac{\partial \Pi}{\partial r} - \omega^2 r\right]\left(\tfrac{z^4}{12} - \tfrac{hz^3}{3} + \tfrac{2h^3 z}{3}\right) \\ & + \mathrm{Ma}\omega\left(\tfrac{z^3}{3} - h^2 z\right).\end{aligned} \tag{4.7.14}$$

Integrating equation (4.6.1) together with boundary conditions (4.6.7) and (4.6.8) gives

$$\frac{\partial h}{\partial t} + \frac{1}{r}\frac{\partial}{\partial r}\int_0^h r u_r dz = 0 \tag{4.7.15}$$

so that the non-dimensional evolution equation is given by

$$\frac{\partial h}{\partial t}+\frac{1}{r}\frac{\partial}{\partial r}\left\{\frac{rh^3}{3}\left[\mathrm{Ca}^{-1}\frac{\partial}{\partial r}\left(\frac{1}{r}\frac{\partial}{\partial r}\left(r\frac{\partial h}{\partial r}\right)\right)-\mathrm{St}^{-1}\frac{\partial h}{\partial r}-\mathrm{Ha}\frac{\partial \Pi}{\partial r}+\omega^2 r\right]+\mathrm{Ma}\frac{rh^2}{2}\right\}=0 \tag{4.7.16}$$

where capillary number Ca characterizes the ratio of viscous to surface tension acting across the interface between a liquid and gas

$$\mathrm{Ca}=\epsilon^{-3}\frac{\mu U_r}{\sigma_0}=\frac{\rho\Omega^2R^4}{\sigma_0 H}, \tag{4.7.17}$$

Inverse Stokes number St^{-1} is a ratio of gravity and viscous forces

$$\mathrm{St}^{-1}=\epsilon\frac{\rho g H^2}{\mu U_r}=\frac{gH}{\Omega^2R^2}, \tag{4.7.18}$$

Hamaker number Ha

$$\mathrm{Ha}=\epsilon\frac{A'}{6\pi\mu U_r H^2}=\frac{A'}{6\pi\rho\Omega^2R^2H^3}, \tag{4.7.19}$$

Marangoni number Ma is a ratio of thermal surface tension and viscous forces

$$\mathrm{Ma}=\epsilon\frac{\gamma\tau R}{\mu U_r}=\frac{\gamma\tau}{\rho\Omega^2R}. \tag{4.7.20}$$

For hydrophilic materials when the fluid is spreading and completely wetting the surface we choose the disjoining pressure of the form

$$\Pi(h)=-\frac{1}{h^3}. \tag{4.7.21}$$

Note that the van der Waals term in the pressure expression is of the opposite sign of that in the rupture problem. This is caused by the difference in fluids and substrates in two problems. In the case of hydrophobic surface (water on a Teflon) van der

Waals forces promote rupture (positive sign) while in the case of hydrophilic materials (silicon oil over the silicon chip surface) they smooth the surface and promote spreading.

Written in the original dimensional variables evolution equation is then given by

$$\frac{\partial h}{\partial t} + \frac{1}{r}\frac{\partial}{\partial r}\left\{\frac{rh^3}{3}\left[\frac{\sigma}{\mu}\frac{\partial}{\partial r}\left(\frac{1}{r}\frac{\partial}{\partial r}\left(r\frac{\partial h}{\partial r}\right)\right) - \frac{\rho g}{\mu}\frac{\partial h}{\partial r} + \frac{A'}{6\pi\mu}\frac{\partial}{\partial r}\left(\frac{1}{h^3}\right) + \frac{\rho}{\mu}\omega^2 r\right] + \frac{\gamma\tau}{\mu}\frac{rh^2}{2}\right\} = 0 \tag{4.7.22}$$

which corresponds to two dimensional form of evolution of thin films equation (2.3.11) in polar coordinates. Here, in general,

$$h_t + \vec{\nabla}\cdot\left[\frac{h^3}{3}\left(\mathrm{Ca}^{-1}\vec{\nabla}\left(\nabla^2 h\right) - \mathrm{St}^{-1}\nabla h - \mathrm{Ha}\nabla\Pi + \vec{r}\omega^2\right) + \frac{h^2}{2}\mathrm{Ma}\nabla\sigma\right] = 0. \tag{4.7.23}$$

5

Solutions of spin coating problems

5.1 Introduction

We consider two different models of the spin coating problem; one to which we refer to as a spinning bucket problem, and one which we call a spinning droplet problem. In this chapter we present a detailed study of solutions to both problems. Analysis of both of the models is closely guided by the experiments performed by Professor Robert Behringer and Shomeek Mukhopadhyay at Duke University Physics Department. Figures 5.1 and 5.1.2 show their first and then final experimental set ups in which Plexiglas cylinder is mounted to a motor with controllable angular velocity. With this kind of set up we can perform experiments which correspond to both of the models we want to study.

In the spinning bucket experiment we perform a comprehensive discussion of the special case of Newton's rotating bucket experiment [30] (see Figure 5.1.3). Unlike in the original Newton's bucket experiment, we consider a relatively thin layer of fluid confined within an impermeable cylindrical container of finite size. Depending on the angular velocity of the rotation two resulting shapes form. If the angular velocity

FIGURE 5.1.1: The preliminary assembly of the rotating thin film experiment by Shomeek Mukhopadhyay

is less than some critical angular velocity, the surface of the fluid is a paraboloid of revolution (see profile in Figure 5.1). On the other hand if the angular velocity is very high the fluid ruptures and dry circular region forms around the center of the cylinder (see profile in Figure 5.1.5). Studying how the effects of centrifugal, gravity, surface tension as well as Marangoni forces influence the critical angular velocity separating the two shapes is something we study in this chapter.

The second model, the spinning drop, is a problem which is more closely related to the industrial process of spin coating. In the spinning drop model we replicate the process by considering a thin drop placed in the center of an impermeable cylindrical container of infinite size (see Figure 5.1). As the cylinder rotates, drop spreads coating the bottom of the cylinder with a thin film. This problem has a great similarity with problems of gravity driven forces. Following the previous work done in study of thermal effects to drive thin film dynamics in gravity flows we examine the behaviors which result from the competing Marangoni and centrifugal forces.

In both problems the thickness is assumed to be nonzero everywhere which means

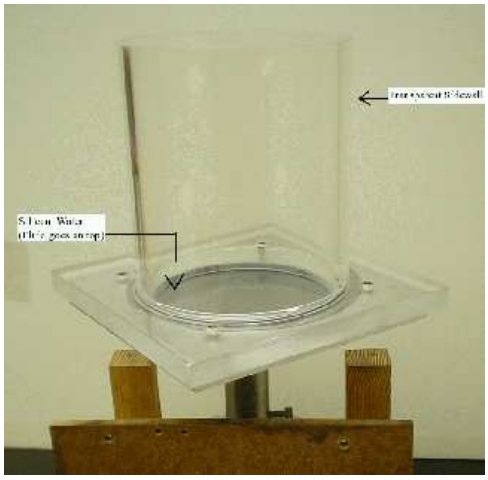

FIGURE 5.1.2: Another view of the experimental set up for the rotating thin film experiment by Shomeek Mukhopadhyay

that the initial condition in the spinning droplet problem will have to include a nonzero film of fluid on the whole surface of the cylinder. We also assume there is no flux of fluid through the boundary of the circular region with $0 \leq r \leq 1$, an area of the container in $r\theta$- plane,

$$\vec{n} \cdot \nabla p = \left. \frac{\partial p}{\partial r} \right|_{r=1} = 0, \tag{5.1.1}$$

and additionally, we take fluid surface to be normal to the container walls

$$\vec{n} \cdot \nabla h = \left. \frac{\partial h}{\partial r} \right|_{r=1} = 0. \tag{5.1.2}$$

Here $\vec{n}$ is the unit outer normal. The normal condition (5.1.2) means that we are neglecting any positive or negative meniscus on the wetting or non wetting walls of the container. In that case the uniform fluid layer solution $h(r, \theta) = \bar{h}$ is then an exact solution of the full problem.

Since evolution equation is a conservation equation, a consequence of the no flux boundary condition (3.2.1) is that the fluid volume

$$V(t) = \int_0^{2\pi} \int_0^1 h \, r dr d\theta = \pi \bar{h} \tag{5.1.3}$$

FIGURE 5.1.3: The interface of two immiscible liquids rotating around a vertical axis is an upward-opening circular paraboloid. (Source: `http://en.wikipedia.org/wiki/Bucket_argument`)

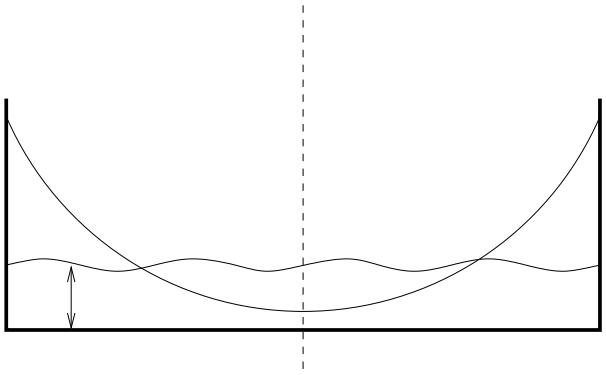

FIGURE 5.1.4: Initial profile and a parabolic profile for $\omega < \omega_c$ formed after some time.

is conserved

$$\frac{dV}{dt} = \frac{d}{dt}\left(\int_0^{2\pi}\int_0^1 h\, r dr d\theta\right) = 0. \tag{5.1.4}$$

In this chapter we both analytically (if possible) and numerically examine problems for various combinations of capillary, gravity, van der Waals, Marangoni and centrifugal forcing. We begin the chapter by testing the numerical scheme on a linear fourth order PDE with a known analytical solution. Further, we test the code on a nonlinear forth order problem of similar structure which does not include spin but

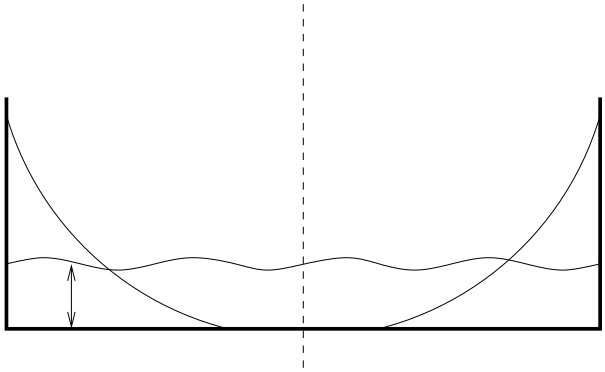

FIGURE 5.1.5: Initial profile and a truncated parabolic profile for $\omega > \omega_c$ formed after some time.

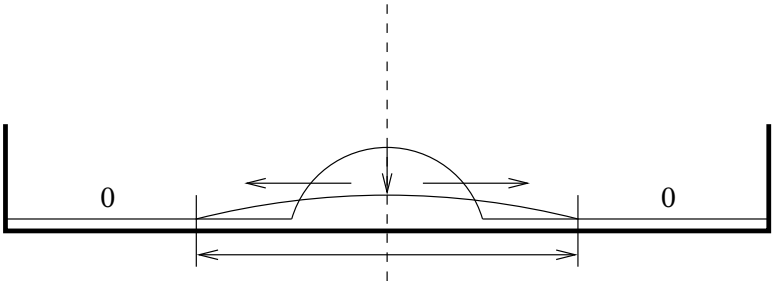

FIGURE 5.1.6: Initial profile and spreading profile at some later time of spinning droplet

has a known similarity solution. We then proceed implementing the code to find the critical angular velocities for steady state solutions for thee different cases:

1. centrifugal and gravity forces only,

2. centrifugal and surface tension forces only,

3. centrifugal, gravity and surface tension forces only.

Finally, we solve numerically full problem with full or linearized expression for curvature in the capillarity term.

5.2 Fourth order test problem for the linear thin film equation

Many of the difficulties associated with the full spin-coating problem are addressed by solving the linear fourth order heat equation

$$h_t + \nabla^4 h = 0 \tag{5.2.1}$$

in axisymmetric form

$$\frac{\partial h}{\partial t} + \frac{1}{r}\frac{\partial}{\partial r}\left\{ r\frac{\partial}{\partial r}\left[\frac{1}{r}\frac{\partial}{\partial r}\left(r\frac{\partial h}{\partial r}\right)\right]\right\} = 0. \tag{5.2.2}$$

We consider the axisymmetric fourth order heat equation (5.2.2) on a domain $0 \leq r \leq 1$, with boundary conditions

$$\left.\frac{\partial h}{\partial r}\right|_{r=0} = 0 \qquad \text{and} \qquad \left.\frac{\partial h}{\partial r}\right|_{r=1} = 0, \tag{5.2.3}$$

$$\left.\frac{\partial}{\partial r}\left[\frac{1}{r}\frac{\partial}{\partial r}\left(r\frac{\partial h}{\partial r}\right)\right]\right|_{r=1} = 0, \tag{5.2.4}$$

and initial condition $h(r,0) = h_0(r)$. Boundary conditions (5.2.3) a "no-meniscus" or zero inclination angle condition at the wall of the container (the fluid interface will be normal to the solid). Note that there is only one no flux condition (5.2.4). A no flux condition at $r = 0$ is not needed due to the regular singular point of the equation at the origin so some solutions are unbounded and rejected as unphysical. Also note that equation (5.2.4) can be rewritten as

$$\left.\frac{\partial}{\partial r}\left[\frac{1}{r}\frac{\partial}{\partial r}\left(r\frac{\partial h}{\partial r}\right)\right]\right|_{r=1} = \left.\left(\frac{\partial^3 h}{\partial r^3} + \frac{1}{r}\frac{\partial^2 h}{\partial r^2} - \frac{1}{r^2}\frac{\partial h}{\partial r}\right)\right|_{r=1} = \left.\left(\frac{\partial^3 h}{\partial r^3} + \frac{1}{r}\frac{\partial^2 h}{\partial r^2}\right)\right|_{r=1} = 0. \tag{5.2.5}$$

This system makes a good test problem because it has an analytical solution which can be found using method of separation of variables so we can verify the

stability and accuracy of our finite difference discretization for the thin film equation by testing our code on this simpler linear partial differential equation problem.

We assume solution of form

$$h(r,t) = \sum_{n=0}^{\infty} C_n T_n(t) R_n(r) \tag{5.2.6}$$

and substitute into the partial differential equation to obtain

$$\frac{1}{T_n}\frac{dT_n}{dt} = -\frac{1}{R_n}\frac{1}{r}\frac{d}{dr}\left\{ r\frac{d}{dr}\left[\frac{1}{r}\frac{d}{dr}\left(r\frac{dR_n}{dr}\right)\right]\right\} = -\lambda_n^4. \tag{5.2.7}$$

As left side of the equation is dependent on t, and right on r variable only, both sides have to be a constant. This immediately yields to two ordinary linear differential equations.

First we find a general solution $T_n(t)$ of the ordinary differential equation

$$\frac{dT_n}{dt} + \lambda_n^4 T_n = 0. \tag{5.2.8}$$

This solution is

$$T_n(t) = A_n e^{-\lambda_n^4 t}. \tag{5.2.9}$$

To solve the ordinary differential in radial direction we expand the equation to obtain

$$r^4\frac{d^4R_n}{dr^4} + 2r^3\frac{d^3R_n}{dr^3} - r^2\frac{d^2R_n}{dr^2} + r\frac{dR_n}{dr} - \lambda_n^4 r^4 R_n = 0. \tag{5.2.10}$$

General solution of this equation is

$$R_n(r) = B_n J_0(\lambda_n r) + C_n Y_0(\lambda_n r) + D_n I_0(\lambda_n r) + E_n K_0(\lambda_n r) \tag{5.2.11}$$

where J_0, Y_0, I_0 and K_0 are respectively Bessel functions of first, second, modified first and modified second kind of order zero. Solution (5.2.11) was found using Maple.

From (5.2.11)

$$\frac{dR_n}{dr} = -B_n\lambda_n J_1(\lambda_n r) - C_n\lambda_n Y_1(\lambda_n r) + D_n\lambda_n I_1(\lambda_n r) + E_n\lambda_n K_1(\lambda_n r) \tag{5.2.12}$$

where J_1, Y_1, I_1 and K_1 are respectively Bessel functions of first, second, modified first and modified second kind of order one. Since we are looking for a bounded solution, and $Y_1(r)$ and $K_1(r)$ blow up at $r = 0$, we get $C_n = E_n = 0$. The zero contact angle condition at $r = 1$ reduces the solution to form

$$R_n(r) = B_n J_0(\lambda_n r) + D_n I_0(\lambda_n r) \tag{5.2.13}$$

with

$$B_n J_1(\lambda_n) = D_n I_1(\lambda_n). \tag{5.2.14}$$

On the other hand the no flux boundary condition (5.2.4) determines that

$$B_n J_1(\lambda_n) = -D_n I_1(\lambda_n), \tag{5.2.15}$$

so we must take $D_n = 0$ and λ_n to satisfy $J_1(\lambda_n) = 0$ The solutions are:

$$R_n(r) = B_n J_0(\lambda_n) \tag{5.2.16}$$

where λ_n is a root of Bessel function of the first kind $J_1(\lambda_n)$ shown in Figure 5.2.1.

Finally, we have analytical solution of our test problem

$$h(r,t) = \sum_{n=0}^{\infty} h_n(r,t) = \sum_{n=0}^{\infty} F_n e^{-\lambda^4 t} J_0(\lambda_n r), \tag{5.2.17}$$

and we can numerically solve the problem and compare it to its analytical solution.

5.2.1 Numerical scheme

We consider the fourth-order heat equation (5.2.2)

$$\frac{\partial h}{\partial t} + \frac{1}{r}\frac{\partial}{\partial r}\left(r\frac{\partial p}{\partial r}\right) = 0 \tag{5.2.18a}$$

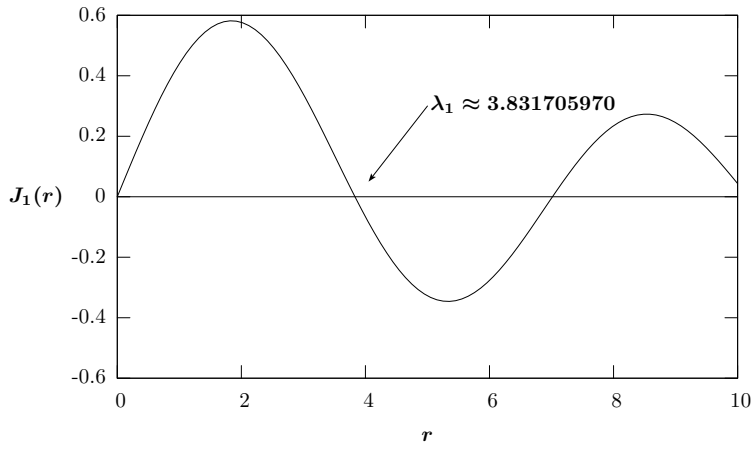

FIGURE 5.2.1: Bessel function of the first kind of the first order $J_1(r)$

on a domain $0 \leq r \leq 1$ where

$$p = \frac{1}{r}\frac{\partial}{\partial r}\left(r\frac{\partial h}{\partial r}\right). \tag{5.2.18b}$$

Boundary conditions are

$$\left.\frac{\partial h}{\partial r}\right|_{r=0} = 0 \qquad \text{and} \qquad \left.\frac{\partial h}{\partial r}\right|_{r=1} = 0, \tag{5.2.18c}$$

$$\left.\frac{\partial p}{\partial r}\right|_{r=1} = 0, \tag{5.2.18d}$$

and initial condition $h(r,0) = J_0(\lambda_1 r)$ where $\lambda_1 \approx 3.831705970$. Note, $\lambda_0 = 0$ gives the uniform constant, flat film solution $h_0(r) \equiv 1$.

We discretize the problem over an equally-spaced grid $r_i = i\Delta r$ for $i = 0, \ldots, N$ where $\Delta r = \frac{1}{N}$ so that $r_0 = 0$ and $r_N = 1$. Values h_0^j and h_N^j correspond to values of $h(r,t)$ at $r = 0$ and $r = 1$ at time $t_j = j\Delta t$. The initial condition at time $t_0 = 0$ is discretized as

$$h_i^0 = J(\lambda_1 r_i) \tag{5.2.19}$$

where $\lambda_1 \approx 3.831705970$. We use the backward Euler difference scheme to discretize in time. This scheme yields first order accuracy, $O(\Delta t)$. To discretize in space we

use second order accurate scheme, $O(\Delta r^2)$, the centered difference scheme. This results in an implicit method which does require more computational effort in each solution step but is unconditionally stable meaning that we can take as big of a time step as needed and the solution will still remain well behaved for linear problems. In contrast, using an explicit method (choosing a forward Euler difference scheme to discretize in time) we would be limited to a time step dependent on a size of a spatial step, $\Delta t \approx O(\Delta r^4)$. This would be very slow if we wanted good accuracy.

We obtain discretized equations (5.2.18a) and(5.2.18b)

$$\begin{aligned}
\frac{h_i^{j+1}-h_i^j}{\Delta t} &= -\frac{1}{r_i}\frac{r_{i+\frac{1}{2}}\frac{\partial p}{\partial r}\Big|_{i+\frac{1}{2}}^{j+1} - r_{i-\frac{1}{2}}\frac{\partial p}{\partial r}\Big|_{i-\frac{1}{2}}^{j+1}}{r_{i+\frac{1}{2}}-r_{i-\frac{1}{2}}} \\
&= -\frac{1}{r_i\Delta r}\left(r_{i+\frac{1}{2}}\frac{p_{i+1}^{j+1}-p_i^{j+1}}{r_{i+1}-r_i} - r_{i-\frac{1}{2}}\frac{p_i^{j+1}-p_{i-1}^{j+1}}{r_i-r_{i-1}}\right) \\
&= -\frac{1}{r_i\Delta r^2}\left[r_{i+\frac{1}{2}}\left(p_{i+1}^{j+1}-p_i^{j+1}\right) - r_{i-\frac{1}{2}}\left(p_i^{j+1}-p_{i-1}^{j+1}\right)\right] \\
&= -\frac{r_{i+\frac{1}{2}}}{r_i\Delta r^2}p_{i+1}^{j+1} + \frac{r_{i+\frac{1}{2}}}{r_i\Delta r^2}p_i^{j+1} + \frac{r_{i-\frac{1}{2}}}{r_i\Delta r^2}p_i^{j+1} - \frac{r_{i-\frac{1}{2}}}{r_i\Delta r^2}p_{i-1}^{j+1} \quad (5.2.20) \\
&= -\frac{r_{i+\frac{1}{2}}}{r_i\Delta r^2}p_{i+1}^{j+1} + \frac{2}{\Delta r^2}p_i^{j+1} - \frac{r_{i-\frac{1}{2}}}{r_i\Delta r^2}p_{i-1}^{j+1}, \quad (5.2.21)
\end{aligned}$$

and

$$\begin{aligned}
p_i^{j+1} &= \frac{1}{r_i}\frac{r_{i+\frac{1}{2}}\frac{\partial h}{\partial r}\Big|_{i+\frac{1}{2}}^{j+1} - r_{i-\frac{1}{2}}\frac{\partial h}{\partial r}\Big|_{i-\frac{1}{2}}^{j+1}}{r_{i+\frac{1}{2}}-r_{i-\frac{1}{2}}} \\
&= \frac{1}{r_i\Delta r}r_{i+\frac{1}{2}}\frac{h_{i+1}^{j+1}-h_i^{j+1}}{r_{i+1}-r_i} - r_{i-\frac{1}{2}}\frac{h_i^{j+1}-h_{i-1}^{j+1}}{r_i-r_{i-1}} \\
&= \frac{1}{r_i\Delta r^2}\left[r_{i+\frac{1}{2}}\left(h_{i+1}^{j+1}-h_i^{j+1}\right) - r_{i-\frac{1}{2}}\left(h_i^{j+1}-h_{i-1}^{j+1}\right)\right]. \quad (5.2.22)
\end{aligned}$$

Combining two discretizations we have

$$\begin{aligned}\frac{h_i^{j+1}-h_i^j}{\Delta t} &= -\frac{r_{i+\frac{1}{2}}}{r_i r_{i+1}\Delta r^4}\left[r_{i+\frac{3}{2}}\left(h_{i+2}^{j+1}-h_{i+1}^{j+1}\right)-r_{i+\frac{1}{2}}\left(h_{i+1}^{j+1}-h_i^{j+1}\right)\right]\\ &+\frac{2}{r_i\Delta r^4}\left[r_{i+\frac{1}{2}}\left(h_{i+1}^{j+1}-h_i^{j+1}\right)-r_{i-\frac{1}{2}}\left(h_i^{j+1}-h_{i-1}^{j+1}\right)\right]\\ &-\frac{r_{i-\frac{1}{2}}}{r_i r_{i-1}\Delta r^4}\left[r_{i-\frac{1}{2}}\left(h_i^{j+1}-h_{i-1}^{j+1}\right)-r_{i-\frac{3}{2}}\left(h_{i-1}^{j+1}-h_{i-2}^{j+1}\right)\right]\end{aligned}$$

for $i=2,\ldots,N$. Here

$$h_{N+1}^{j+1}=h_{N-1}^{j+1} \tag{5.2.23}$$

is a consequence of centered difference, second order accurate, discretization of the no inclination angle boundary condition at $r=1$

$$\left.\frac{\partial h}{\partial r}\right|_{r=1}=0=\frac{h_{N+1}^{j+1}-h_{N-1}^{j+1}}{2\Delta r}+O(\Delta r^2). \tag{5.2.24}$$

Similarly, by discretizing the no-flux condition at $r=1$ using centered differences

$$\begin{aligned}\left.\frac{\partial}{\partial r}\left[\frac{1}{r}\frac{\partial}{\partial r}\left(r\frac{\partial h}{\partial r}\right)\right]\right|_{r=1} &= \left.\left[\frac{\partial}{\partial r}\left(\frac{1}{r}\frac{\partial h}{\partial r}+\frac{\partial^2 h}{\partial r^2}\right)\right]\right|_{r=1}\\ &= \left.\left(\frac{\partial^3 h}{\partial r^3}+\frac{1}{r}\frac{\partial^2 h}{\partial r^2}-\frac{1}{r^2}\frac{\partial h}{\partial r}\right)\right|_{r=1}\\ &= \frac{h_{N+2}^{j+1}-2h_{N+1}^{j+1}+2h_{N-1}^{j+1}-h_{N-2}^{j+1}}{2\Delta r^3}\\ &\quad+\frac{h_{N+1}^{j+1}-2h_N^{j+1}+h_{N-1}^{j+1}}{\Delta r^2}\\ &\quad+\frac{h_{N+1}^{j+1}-h_{N-1}^{j+1}}{2\Delta r}+O(\Delta r^2)\\ &= \frac{h_{N+2}^{j+1}-h_{N-2}^{j+1}+4\Delta r(h_{N-1}^{j+1}-h_N^{j+1})}{2\Delta r^3}+O(\Delta r^2) \qquad (5.2.25)\\ &= 0\end{aligned}$$

we obtain

$$h_{N+2}^{j+1} = h_{N-2}^{j+1} - 4\Delta r \left(h_{N-1}^{j+1} - h_N^{j+1}\right) + O(\Delta r^2). \tag{5.2.26}$$

When $i = 0$ and $i = 1$ we cannot use the above scheme (5.2.23) because of division with zero in some of the terms. We have to find other ways to express conditions at those points.

For $i = 0$ discretize the no meniscus boundary condition at $r = 0$ using second order forward differences

$$\left.\frac{\partial h}{\partial r}\right|_{r=0} = \frac{-3h_0^{j+1} + 4h_1^{j+1} - h_2^{j+1}}{2\Delta r} + O(\Delta r^2) = 0 \tag{5.2.27}$$

so

$$h_0^{j+1} = \frac{4h_1^{j+1} - h_2^{j+1}}{3} + O(\Delta r^2) \tag{5.2.28}$$

For $i = 1$ we can see that in the general expression division by zero occurs in the fourth term of equation (5.2.20), expression for pressure p_{-1}^{j+1}. To resolve that problem we have to find a different way to express the pressure in terms of boundary conditions. Assuming solution of form

$$h(r,t) = \sum_{n=0}^{\infty} c_n(t) r^n = c_0(t) + c_1(t) r + c_2(t) r^2 + \ldots + O(r^3) \tag{5.2.29}$$

for $r \to 0$ we have

$$\frac{\partial h}{\partial r} = c_1(t) + 2c_2(t) r + O(r^2). \tag{5.2.30}$$

The no slip boundary condition (5.2.3) at $r = 0$ makes $c_1(t) = 0$ so for small r

$$\left.\frac{1}{r}\frac{\partial h}{\partial r}\right|_{r=0} = \lim_{r\to 0}\frac{1}{r}\frac{\partial h}{\partial r} = 2c_2(t) = \lim_{r\to 0}\frac{\partial^2 h}{\partial r^2} = \left.\frac{\partial^2 h}{\partial r^2}\right|_{r=0}. \tag{5.2.31}$$

Now we can use that to approximate

$$\begin{aligned}
\frac{1}{r}\frac{\partial}{\partial r}\left(r\frac{\partial h}{\partial r}\right)\Big|_{r=0} &= \left(\frac{\partial^2 h}{\partial r^2}+\frac{1}{r}\frac{\partial h}{\partial r}\right)\Big|_{r=0} \\
&= 2\frac{\partial^2 h}{\partial r^2}\Big|_{r=0} \\
&= 2\frac{h_1-2h_0+h_{-1}}{\Delta r^2}+O(\Delta r^2) \\
&= 4\frac{h_1-h_0}{\Delta r^2}+O(\Delta r^2). \qquad (5.2.32)
\end{aligned}$$

This gives a modified scheme for $i=1$

$$\begin{aligned}
\frac{h_1^{j+1}-h_1^j}{\Delta t} &= -\frac{r_{\frac{3}{2}}}{r_1 r_2 \Delta r^4}\left[r_{\frac{5}{2}}\left(h_3^{j+1}-h_2^{j+1}\right)-r_{\frac{3}{2}}\left(h_2^{j+1}-h_1^{j+1}\right)\right] \qquad (5.2.33) \\
&\quad +\frac{2}{r_1\Delta r^4}\left[r_{\frac{3}{2}}\left(h_2^{j+1}-h_1^{j+1}\right)-r_{\frac{1}{2}}\left(h_1^{j+1}-h_0^{j+1}\right)\right] \\
&\quad -\frac{4r_{\frac{1}{2}}}{r_1\Delta r^4}\left(h_1^{j+1}-h_0^{j+1}\right).
\end{aligned}$$

All together discretized differential equations (5.2.28), (5.2.33) and (5.2.23) make a system of $N+1$ linear equations, $A\vec{h}=\vec{0}$. Matrix A is a five banded matrix with two sub diagonals and two super diagonals. To solve band-diagonal sets of equation we use in combination Numerical Recipes routines bandec and banbnks [41]. We first call on bandec routine which constructs an LU decomposition of a row wise permutation of A.

The mass of the system is conserved so

$$\frac{d}{dt}\int_0^1 h(r,t)rdr=0. \qquad (5.2.34)$$

We use (5.2.2) to rewrite the mass conservation equation (5.2.34)

$$\begin{aligned}\frac{d}{dt}\int_0^1 h(r,t)rdr &= \int_0^1 \frac{\partial h}{\partial t} rdr \\ &= -\int_0^1 \frac{\partial}{\partial r}\left[\frac{1}{r}\left(r\frac{\partial p}{\partial r}\right)\right] dr \\ &= -\frac{1}{r}\frac{\partial}{\partial r}\left(r\frac{\partial p}{\partial r}\right)\Bigg|_0^1 = 0. \end{aligned} \tag{5.2.35}$$

Using the backward difference approximation for time derivative and trapezoid rule to represent the integral we can approximate

$$\int_0^1 h(r)rdr = \Delta r^2 \sum_{i=1}^{N-1} ih_i + \Delta r\frac{h_N}{2} + O(\Delta r^2) \tag{5.2.36}$$

Figure 5.2.2 shows error $|M_{\Delta r}(T) - M_0|$ with respect to Δr and shows that error goes by $O(\Delta r^2)$ which is expected by the centered difference approximation. This confirms that boundary conditions are satisfied and there is no fluid flux escaping or coming in through boundaries meaning that the mass is conserved.

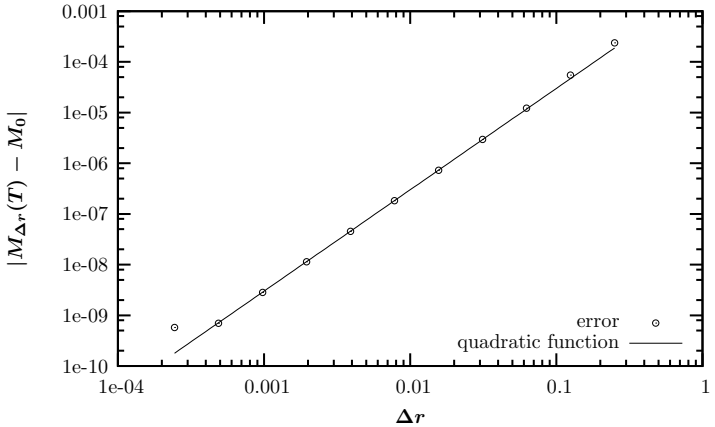

FIGURE 5.2.2: Plot of error $|M_{\Delta r}(T) - M_0|$ where $T = 10^{-2}$ and M_0 initial mass at time $t = 0$ vs Δr for linear fourth order test problem.

Figure 5.2.3 shows the numerical solution compared to the exact analytical solution. We confirm the second order accuracy in space by plotting the error at $h(0,T)$

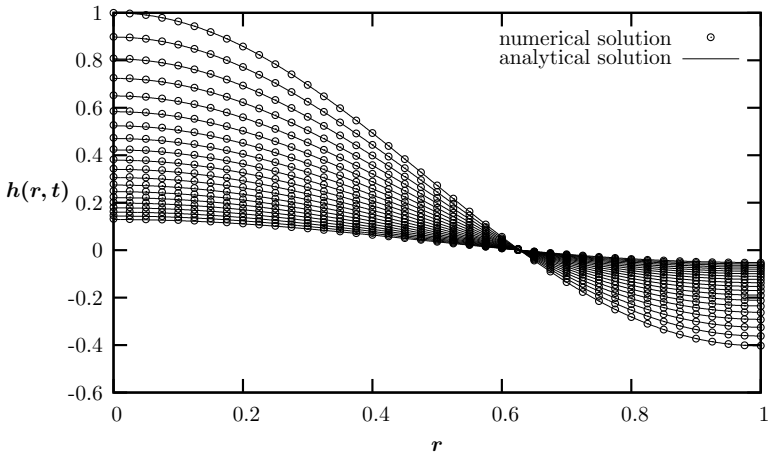

FIGURE 5.2.3: Numerical and analytical solution of linear test problem (5.2.2) in polar coordinates

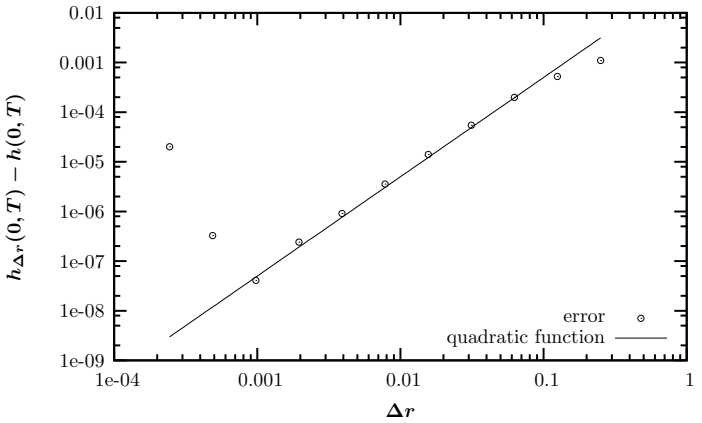

FIGURE 5.2.4: Plot of error at $h(0,T)$ where $T = 10^{-2}$ vs Δr for the linear fourth order test problem.

when $T = 10^{-2}$ for solutions calculated with different step size Δr, as well as plotting the L_2 norm of the error vector $h_{\Delta r}(r,T) - h(r,t)$. We keep constant time step $\Delta t = 10^{-8}$. Figure 5.2.4, the log-log plot of the numerical error at $h(0,T)$ vs Δr, and Figure 5.2.5, the plot of L2 norm of $h_{\Delta r}(r,T) - h(r,T)$ vs Δr, show the second order accuracy as expected. We similarly test the dependence on time by plotting the error at $h(0,T)$ when $T = 10^{-2}$ for solutions calculated with different step size Δt as well as plotting the L2 norm of the error vector $h_{\Delta t}(r,T) - h(r,t)$. We keep constant spacial step $\Delta r = 10^{-3}$. Figure 5.2.6, the log-log plot of the numerical error

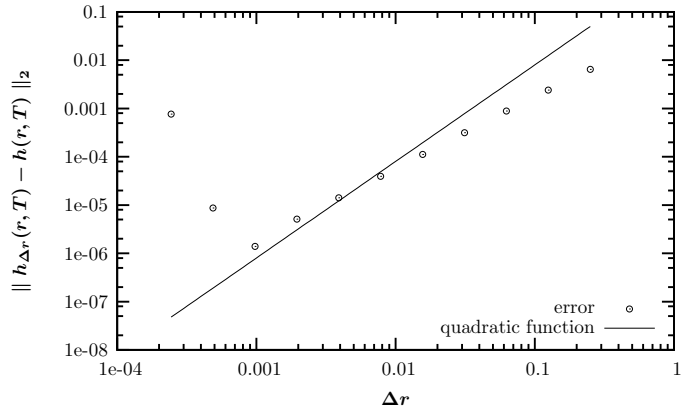

FIGURE 5.2.5: Plot of L2 norm of $h_{\Delta r}(r,T) - h(r,T)$ where $T = 10^{-2}$ vs Δr for the linear fourth order test problem.

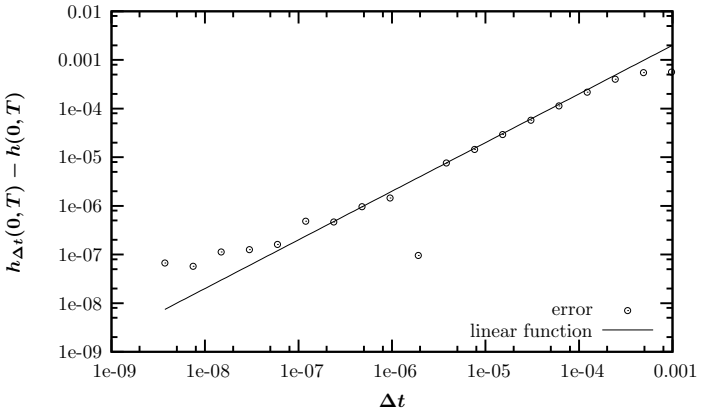

FIGURE 5.2.6: Plot of error at $h(0,T)$ where $T = 10^{-2}$ vs Δt for the linear fourth order test problem.

at $h(0,T)$ vs Δt, and Figure 5.2.7, the plot of L2 norm of $h_{\Delta t}(r,T) - h(r,T)$ vs Δt, show the expected first order accuracy.

5.3 Fourth order nonlinear test problem for the thin film equation

We now test our code on a nonlinear test problem which has a similarity solution so it will be easy to verify the accuracy of our numerical method. We consider the nonlinear fourth order partial differential equation

$$\frac{\partial h}{\partial t} + \frac{1}{r}\frac{\partial}{\partial r}\left\{ r h^n \frac{\partial}{\partial r}\left[\frac{1}{r}\frac{\partial}{\partial r}\left(r \frac{\partial h}{\partial r} \right) \right] \right\} = 0 \tag{5.3.1}$$

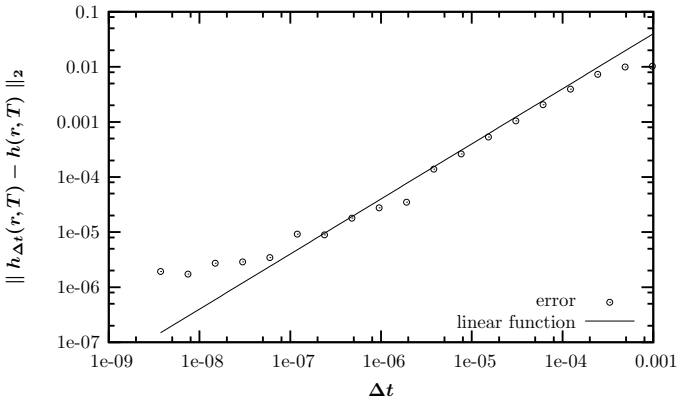

FIGURE 5.2.7: Plot of L2 norm of $h_{\Delta t}(r,T) - h(r,T)$ where $T = 10^{-2}$ vs Δt for the linear fourth order test problem.

with $n = 1$. In our full problem $n = 3$ but the features and the difficulties are the same. Boundary conditions are no slip

$$\left.\frac{\partial h}{\partial r}\right|_{r=0} = 0 \qquad \text{and} \qquad \left.\frac{\partial h}{\partial r}\right|_{r=1} = 0, \tag{5.3.2}$$

and no flux

$$\left.\frac{\partial}{\partial r}\left[\frac{1}{r}\frac{\partial}{\partial r}\left(r\frac{\partial h}{\partial r}\right)\right]\right|_{r=1} = 0. \tag{5.3.3}$$

This problem was chosen because it has an analytic closed-form solution. To solve analytically we assume self-similar solution of form

$$h(r,t) = \frac{1}{\tau^2}H(\eta,s), \qquad \eta = \frac{r}{\tau}, \qquad s = \ln\tau \tag{5.3.4}$$

with $\tau = \alpha(t-t_0)^\beta$, and substitute into the governing partial differential equation [52]. The resulting equation is

$$\frac{\beta}{\alpha^2}(t-t_0)^{-2\beta-1}\left(-2H - \eta\frac{\partial H}{\partial \eta} + \frac{\partial H}{\partial s}\right) = -\frac{(t-t_0)^{-8\beta}}{\alpha^8}\frac{1}{\eta}\frac{\partial}{\partial \eta}\left\{\eta H\frac{\partial}{\partial \eta}\left[\frac{1}{\eta}\frac{\partial}{\partial \eta}\left(\eta\frac{\partial H}{\partial \eta}\right)\right]\right\} \tag{5.3.5}$$

so $\beta = \frac{1}{6}$ and $\alpha = 6^{\frac{1}{6}}$. Hence $\tau = [6(t-t_0)]^{\frac{1}{6}}$ and

$$\frac{\partial H}{\partial s} = 2H + \eta\frac{\partial H}{\partial \eta} - \frac{1}{\eta}\frac{\partial}{\partial \eta}\left\{\eta H\frac{\partial}{\partial \eta}\left[\frac{1}{\eta}\frac{\partial}{\partial \eta}\left(\eta\frac{\partial H}{\partial \eta}\right)\right]\right\}. \tag{5.3.6}$$

Similarity solution $\bar{H}(\eta)$ is

$$\bar{H}(\eta) = \frac{1}{32}\left(L^2 - \eta^2\right)^2, \tag{5.3.7}$$

so that $h(\eta,\tau) = \frac{1}{32\tau^2}(L^2-\eta^2)^2$. In terms of r and t

$$h(r,t) = \frac{1}{32\left[6\left(t-t_0\right)\right]^{\frac{1}{3}}}\left[L^2 - \frac{r^2}{\left[6\left(t-t_0\right)\right]^{\frac{1}{3}}}\right]^2. \tag{5.3.8}$$

We use this to set up our initial condition $h(0,r)$.

5.3.1 Numerical scheme

We discretize the non-linear test problem (5.3.1) so that the numerical scheme becomes

$$\begin{aligned}\frac{h_i^{j+1}-h_i^j}{\Delta t} \quad & + \frac{r_{i+\frac{1}{2}}h_{i+\frac{1}{2}}}{r_i r_{i+1}\Delta r^4}\left[r_{i+\frac{3}{2}}(h_{i+2}^{j+1}-h_{i+1}^{j+1}) - r_{i+\frac{1}{2}}(h_{i+1}^{j+1}-h_i^{j+1})\right] \\ & - \frac{r_{i+\frac{1}{2}}h_{i+\frac{1}{2}}}{r_i^2\Delta r^4}\left[r_{i+\frac{1}{2}}(h_{i+1}^{j+1}-h_i^{j+1}) - r_{i-\frac{1}{2}}(h_i^{j+1}-h_{i-1}^{j+1})\right] \\ & - \frac{r_{i-\frac{1}{2}}h_{i-\frac{1}{2}}}{r_i^2\Delta r^4}\left[r_{i+\frac{1}{2}}(h_{i+1}^{j+1}-h_i^{j+1}) - r_{i-\frac{1}{2}}(h_i^{j+1}-h_{i-1}^{j+1})\right] \\ & + \frac{r_{i-\frac{1}{2}}h_{i-\frac{1}{2}}}{r_i r_{i-1}\Delta r^4}\left[r_{i-\frac{1}{2}}(h_i^{j+1}-h_{i-1}^{j+1}) - r_{i-\frac{3}{2}}(h_{i-1}^{j+1}-h_{i-2}^{j+1})\right] \quad = 0\end{aligned} \tag{5.3.9}$$

for $i = 2,\ldots,N$ with $h_{N+1}^{j+1} = h_{N-1}^{j+1}$ and $h_{N+2}^{j+1} = h_{N-2}^{j+1} - 4\Delta r(h_{N-1}^{j+1} - h_N^{j+1})$, consequence of centered difference approximation to boundary conditions (5.3.2) and (5.3.3) at $r = 1$, same as in the linear problem.

Following the linear problem, for $i = 0$ we use boundary condition (5.3.2) at $r = 0$ using the second order forward difference

$$\left.\frac{\partial h}{\partial r}\right|_{r=0} = \frac{-3h_0^{j+1} + 4h_1^{j+1} - h_2^{j+1}}{2\Delta r} + O(\Delta r^2) = 0 \tag{5.3.10}$$

and for $i = 1$ we use

$$\begin{aligned}\tfrac{h_1^{j+1}-h_1^j}{\Delta t} \quad & + \tfrac{r_{\frac{5}{2}} h_{\frac{5}{2}}}{r_1 r_2 \Delta r^4}\left[r_{\frac{5}{2}}(h_3^{j+1}-h_2^{j+1}) - r_{\frac{3}{2}}(h_2^{j+1}-h_1^{j+1})\right] \\ & - \tfrac{r_{\frac{3}{2}} h_{\frac{3}{2}}}{r_1^2 \Delta r^4}\left[r_{\frac{3}{2}}(h_2^{j+1}-h_1^{j+1}) - r_{\frac{1}{2}}(h_1^{j+1}-h_0^{j+1})\right] \\ & - \tfrac{r_{\frac{1}{2}} h_{\frac{1}{2}}}{r_1^2 \Delta r^4}\left[r_{\frac{3}{2}}(h_2^{j+1}-h_1^{j+1}) - r_{\frac{1}{2}}(h_1^{j+1}-h_0^{j+1})\right] \\ & + \tfrac{4 r_{\frac{1}{2}} h_{\frac{1}{2}}}{r_1 \Delta r^4}(h_1^{j+1}-h_0^{j+1}) = 0\end{aligned}$$

Like in the linear test problem we use bandec and banbks Numerical recepies routines [41] to solve, in this case, nonlinear system of $N+1$ equations at each step of the Newton iteration until desired error tolerance is achieved (10^{-14}). For the initial condition we use similarity solution to form a profile of a drop on a prewetted surface of thickness $\delta = 0.0001$

$$h(r,0) = \begin{cases} \frac{1}{32[6(-t_0)]^{\frac{1}{3}}}\left[L^2 - \frac{r^2}{[6(-t_0)]^{\frac{1}{3}}}\right]^2 + \delta, & r < r_0 \\ \delta, & r \geq r_0 \end{cases}$$

Here $L = r_0\left[6\left(0-t_0\right)\right]^{-\frac{1}{6}}$. We set initial drop radius $r_0 = 0.1$ and initial time $t_0 = -5 \cdot 10^{-7}$ so that the height of the droplet at the origin at time $t = 0$ is unit height. To that we add the prewetting height $\delta = 0.0001$ which adds to the initial height of the drop (at $t = 0$ the height of the drop is $h(0,0) = 1.0001$). Figure 5.3.1 shows this initial solution with $\delta = 0.02$ in order for the profile to be more clear. It is evident that the prewetting layer height is significantly smaller than the size of the drop.

Figure 5.3.1 shows profile of the solution evolving through time. Here the height of the drop at the origin, $h(0,t)$, gets smaller as the time t increases. In log-log plot of $h(0,t)$ vs. t shown in Figure 5.3.1 we can see that this height evaluated by the numerical code decays as expected by the similarity solution. Similarity solution at $r = 0$ is given by

$$h(0,t) = \frac{L^4}{32\left[6\left(t-t_0\right)\right]^{\frac{1}{3}}} \tag{5.3.11}$$

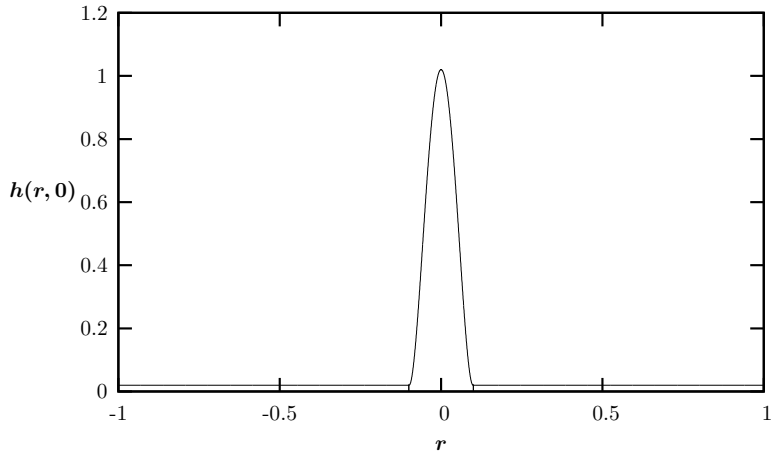

FIGURE 5.3.1: The similarity solution at time $t = 0$ when initial drop radius is $r_0 = 0.1$ and we set $h(0,0) = 1 + \delta$ so that $t_0 \approx -5 \times 10^{-7}$. In our code $\delta = 0.0001$ but in this plot $\delta = 0.02$ to better see the form of the initial profile.

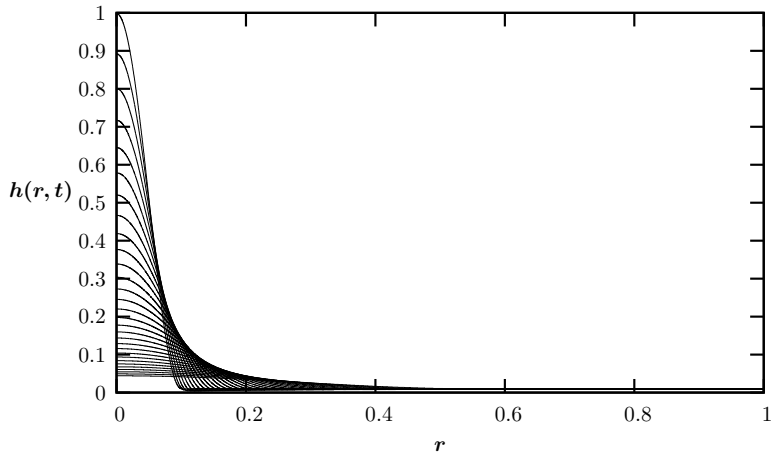

FIGURE 5.3.2: Solution profiles of nonlinear test problem evolving through time evaluated numerically

so log-log plot of $h(0,t)$ vs $t - t_0$ is a straight line with slope $-\frac{1}{3}$ and y-intercept $\log(\frac{L^2}{32 \cdot 6^{\frac{1}{3}}})$.

5.4 Spin coating problem steady state solutions

We now begin our study of three steady state problems related to our full spin coating evolution equations. In this section we only consider the bucket model.

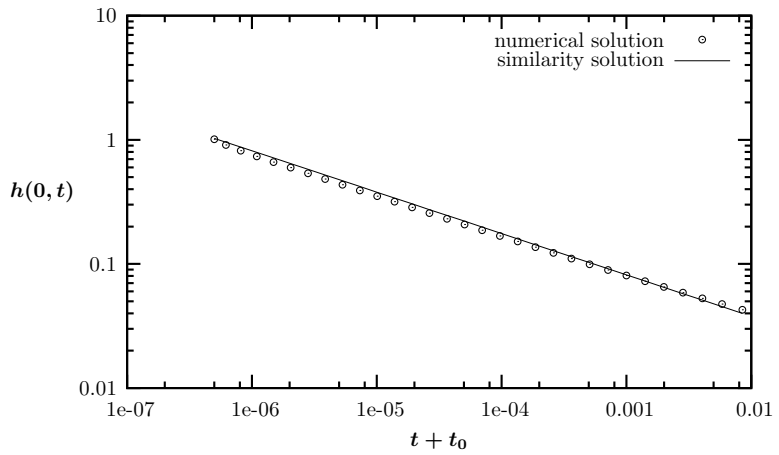

FIGURE 5.3.3: Plot of height of the drop at the origin, $h(0,t)$, vs. time for nonlinear test problem

Each evolution begins with the flat thin film in a cylinder which is being spun with some constant angular velocity ω.

5.4.1 Steady state solutions for $\mathrm{Ca}^{-1} = 0$, $\mathrm{Ma} = 0$ *and* $\mathrm{Ha} = 0$ - *centrifugal and gravity forces only*

In this problem we assume that the driving forces are centrifugal and gravity force and neglect capillary, surface tension and any forces due to van der Waals intermolecular interaction. This models an experiment in which layer of fluid being spun in a bucket is of a medium thickness.

We are looking for a steady state solution to second order PDE problem

$$\frac{\partial h}{\partial t} + \frac{1}{r}\frac{\partial}{\partial r}\left[\frac{rh^3}{3}\frac{\partial}{\partial r}\left(-\mathrm{St}^{-1}h + \frac{\omega^2 r^2}{2}\right)\right] = 0 \tag{5.4.1}$$

with boundary conditions

$$\left.\frac{\partial h}{\partial r}\right|_{r=0} = 0 \tag{5.4.2a}$$

$$\left.\frac{\partial}{\partial r}\left(-\mathrm{St}^{-1}h + \frac{\omega^2 r^2}{2}\right)\right|_{r=1} = 0. \tag{5.4.2b}$$

where ω is the constant angular velocity of the spin.

To solve the problem we first integrate steady state form of equation (5.4.1) and obtain

$$\frac{\partial}{\partial r}\left(-\mathrm{St}^{-1}h + \frac{\omega^2 r^2}{2}\right) = 0. \tag{5.4.3}$$

Note that boundary condition (5.4.2b) is now satisfied and gives us no more information. We integrate now (5.4.3) to get

$$h(r) = \frac{\mathrm{St}}{2}\omega^2 r^2 + C_0. \tag{5.4.4}$$

This general solution not only satisfies boundary condition (5.4.2b) at $r = 1$ but also boundary condition at $r = 0$, equation (5.4.2a). Constant C_0 is determined by the conservation of mass.

If in the beginning of the experiment, before the spin, we had a flat layer of fluid we can write the initial condition as $h(r) = \bar{h}$. Total mass is then

$$\int_0^{2\pi}\int_0^1 h(r) r dr d\theta = 2\pi\int_0^1 \bar{h} r dr = \pi\bar{h}. \tag{5.4.5}$$

Since mass is conserved

$$\begin{aligned}\int_0^{2\pi}\int_0^1 h(r) r dr d\theta &= 2\pi\int_0^1\left(\frac{\mathrm{St}}{2}\omega^2 r^3 + C_0 r\right)dr \\ &= 2\pi\left(\frac{\mathrm{St}}{8}\omega^2 r^4 + C_0\frac{r^2}{2}\right)\Bigg|_0^1 \\ &= \frac{\mathrm{St}}{4}\pi\omega^2 + \pi C_0. \end{aligned}\tag{5.4.6}$$

Setting equations (5.4.5) and (5.4.6) equal to each other gives us the value of constant C_0

$$C_0 = \bar{h} - \frac{\mathrm{St}}{4}\omega^2. \tag{5.4.7}$$

We now have that the steady state solution depends on the uniform initial condition and constant St in this manner

$$h(r) = \frac{\mathrm{St}}{2}\omega^2 r^2 + \bar{h} - \frac{\mathrm{St}}{4}\omega^2. \tag{5.4.8}$$

Note that function $h(r)$ becomes negative when initial height of the fluid $\bar{h} < \frac{\mathrm{St}}{4}\omega^2$, or when angular velocity

$$\omega > \sqrt{\frac{4\bar{h}}{\mathrm{St}}} = \omega_c. \tag{5.4.9}$$

When angular velocity ω is greater than this critical angular velocity ω_c a dry spot occurs so that

$$h(r) = 0 \text{ for } r \leq r_c. \tag{5.4.10}$$

where $r = r_c$ is a critical radius within which there is no fluid and which depends on the angular velocity. Steady state solution (5.4.8) in this case does not hold and we have to look for a different solution profile.

Equation (5.4.4) is the general form of the steady state solution with constant C_0 which is in the case when the angular velocity $\omega > \omega_c$ determined by the boundary condition at $r = r_c$

$$h(r_c) = \frac{\mathrm{St}}{2}\omega^2 r_c^2 + C_0 = 0. \tag{5.4.11}$$

It follows

$$C_0 = -\frac{\mathrm{St}}{2}\omega^2 r_c^2 \tag{5.4.12}$$

so the weak steady state solution when $\omega < \omega_c$ is then

$$h(r) = \frac{\mathrm{St}}{2}\omega^2 \left(r^2 - r_c^2\right). \tag{5.4.13}$$

As in the case with small angular velocities, mass has to be conserved so

$$\begin{aligned}\int_0^{2\pi}\int_{r_c}^1 h(r)r\,dr\,d\theta &= 2\pi\int_{r_c}^1\left(\frac{\mathrm{St}}{2}\omega^2 r^3-\frac{\mathrm{St}}{2}\omega^2 r_c^2 r\right)dr\\ &= 2\pi\left(\frac{\mathrm{St}}{8}\omega^2 r^4-\frac{\mathrm{St}}{4}\omega^2 r_c^2 r^2\right)\Big|_{r_c}^1\\ &= \pi\left(\frac{\mathrm{St}}{4}\omega^2-\frac{\mathrm{St}}{2}\omega^2 r_c^2-\frac{\mathrm{St}}{4}\omega^2 r_c^4+\frac{\mathrm{St}}{2}\omega^2 r_c^4\right)\\ &= \pi\frac{\mathrm{St}}{4}\omega^2\left(1-2r_c^2+r_c^4\right) \qquad (5.4.14)\end{aligned}$$

has to be the same as the mass before the spin (5.4.5). This condition yields the critical radius for $\omega > \omega_c$

$$r_c = \sqrt{1-\frac{\omega_c}{\omega}} \qquad (5.4.15)$$

where $\omega_c = \sqrt{\frac{4\bar{h}}{\mathrm{St}}}$ is angular velocity for which the profile of the spun film changes from parabolic to ruptured parabolic (see Figure 5.1 and Figure 5.1.5).

Finally, we can write a steady solution of the PDE problem (5.4.1) when $\omega > \omega_c$

$$h(r) = \begin{cases} 0 & \text{if } 0 < r \le r_c, \\ \frac{\mathrm{St}}{2}\omega^2\left(r^2-r_c^2\right) & \text{if } r_c < r < 1. \end{cases} \qquad (5.4.16)$$

We test the code solving the dynamical equation (5.4.1) and matching the long time solution with the steady state solutions (5.4.8) and (5.4.13). We set Stokes number $\mathrm{St} = 1$ and initial height of flat fluid $\bar{h} = 1$ constant for all the plots. Critical angular velocity is then $\omega_c = 2$.

Figure 5.4.1 shows the numerical solutions to the PDE evolving over the time (plotted every $\Delta t = 0.1$) when $\omega = 1 < \omega_c$. As the time increases the height of the PDE solution profiles at the origin is decreasing and the parabolic shapes are converging to the plot of the steady state solution. Figure 5.4.2 shows the same but for the problem when angular velocity $\omega = 2.1 > \omega_c$.

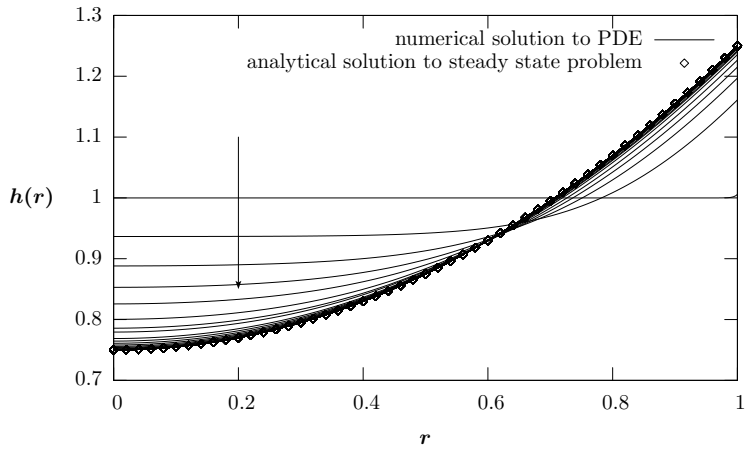

FIGURE 5.4.1: Evolution of the numerical solution to the PDE compared to the analytical solution of the steady state problem for $\omega = 1$ when St $= 1$, and $\bar{h} = 1$ ($\omega_c = 2$).

The plot in Figure 5.4.3 shows the relation between the r_c and $\frac{\omega}{\omega_c}$ obtained by numerically solving the full problem for a range of ω. The numerical solution is compared to the analytical relationship between the r_c and ω (5.4.15). To calculate r_c in numerical code we check for the smallest value of $h(r,t)$ at grid points. This would not a big issue if the graph of the function was smooth and consequently its

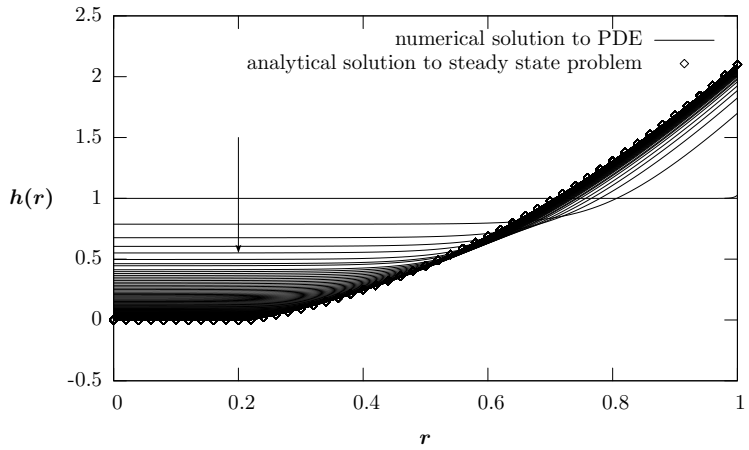

FIGURE 5.4.2: Evolution of the numerical solution to the PDE compared to the analytical solution of the steady state problem for $\omega = 2.1$ when St $= 1$, and $\bar{h} = 1$ ($\omega_c = 2$).

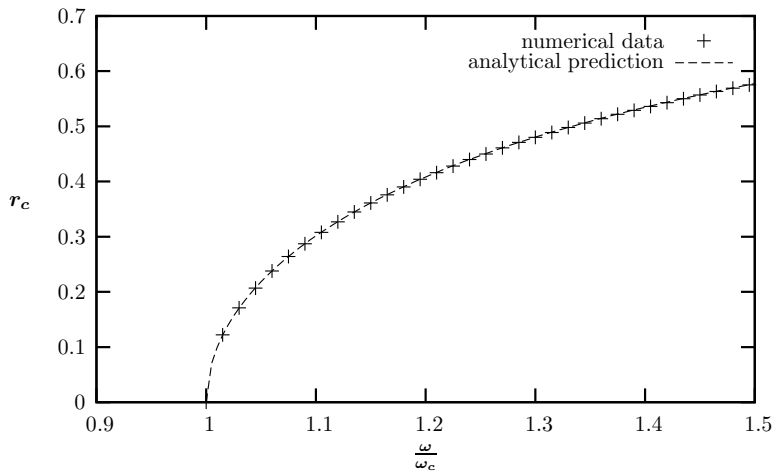

FIGURE 5.4.3: Comparison of numerical data plot r_c vs. $\frac{\omega}{\omega_c}$ with the predicted analytical solution from equation (5.4.15) with $\omega_c = 2$.

numerical approximation was smooth. But profiles of solution to the PDE when $\omega > \omega_c$ are not differentiable, and therefore not smooth at r_c. Graphs $h(r) = 0$ for $r \leq r_c$ and piecewise parabolic profile described by equation (5.4.13) for $r > r_c$ meet in a cusp at $r = r_c$. Figure 5.4.4 shows a blow up of the part of the plot around $r = r_c$. This plot was done with $\Delta r = 10^{-4}$ and initial $\Delta t = 10^{-5}$. Error tolerance on Newton's method is 10^{-10}. With the time flat part of the numerical solution lowers towards the analytical steady state solution, however, with time oscillations form in the flat line solution. Figure 5.4.5 shows log-log plot of the height of the fluid at the origin $h(0,t)$ through time t. The height decays with $O\left(t^{-\frac{1}{2}}\right)$ which is slower than the exponential convergence in linear test problem. This slower convergence to the steady state height is due to the non smooth weak solution (5.4.16).

5.4.2 Steady state solutions for $\mathrm{St}^{-1} = 0$, $\mathrm{Ma} = 0$ *and* $\mathrm{Ha} = 0$ - *centrifugal and surface tension forces only*

In this problem we consider a thin layer of fluid rotating so that dominant forces are centrifugal and surface tension forces while we neglect gravity, and forces due to disjoining pressure and thermocapillarity. We are looking for a steady state solution

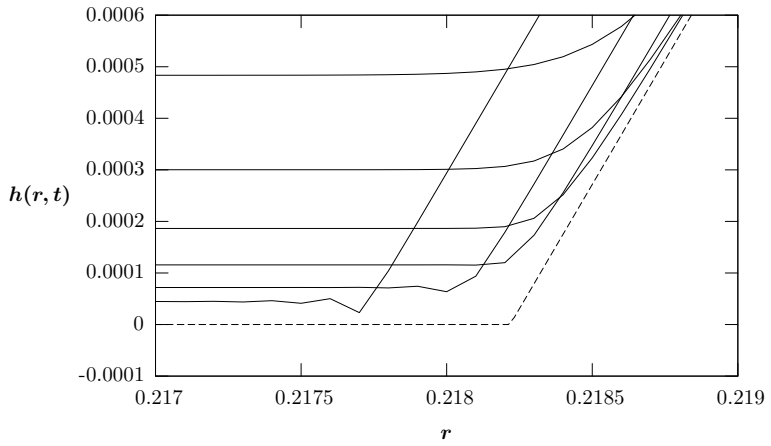

FIGURE 5.4.4: Enlargement of the long time solutions to the PDE around $r = r_c = \sqrt{1 - \frac{2}{2.1}} \approx 0.2182$. (Spacial step is $\Delta r = 10^{-4}$.)

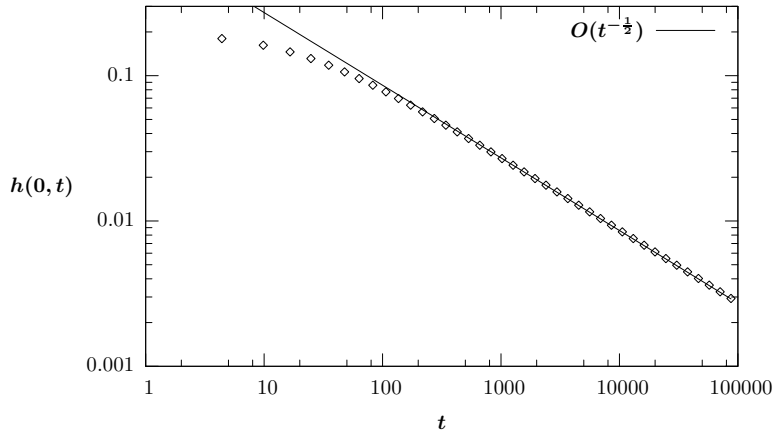

FIGURE 5.4.5: Log-log plot of $h(0,t)$ vs t shows that the height of the film at the origin decays as $\frac{1}{\sqrt{t}}$.

to the fourth order PDE problem

$$\frac{\partial h}{\partial t} + \frac{1}{r}\frac{\partial}{\partial r}\left[\frac{rh^3}{3}\frac{\partial}{\partial r}\left(\frac{1}{\mathrm{Ca}}\frac{1}{r}\frac{\partial}{\partial r}\left(r\frac{\partial h}{\partial r}\right) + \frac{\omega^2 r^2}{2}\right)\right] = 0 \tag{5.4.17}$$

with boundary conditions

$$\left.\frac{\partial h}{\partial r}\right|_{r=0} = 0 \tag{5.4.18a}$$

$$\left.\frac{\partial h}{\partial r}\right|_{r=1} = 0 \tag{5.4.18b}$$

$$\left.\frac{\partial}{\partial r}\left(\frac{1}{\mathrm{Ca}}\frac{1}{r}\frac{\partial}{\partial r}\left(r\frac{\partial h}{\partial r}\right)+\frac{\omega^2 r^2}{2}\right)\right|_{r=1} = 0. \tag{5.4.18c}$$

where ω is the constant angular velocity of the spin.

To solve the problem we first integrate steady state form of equation (5.4.17) and obtain

$$\frac{d}{dr}\left(\frac{1}{\mathrm{Ca}}\frac{1}{r}\frac{d}{dr}\left(r\frac{dh}{dr}\right)+\frac{\omega^2 r^2}{2}\right) = 0. \tag{5.4.19}$$

Integrating second time yields

$$\frac{1}{\mathrm{Ca}}\frac{1}{r}\frac{d}{dr}\left(r\frac{dh}{dr}\right)+\frac{\omega^2 r^2}{2} = C_0. \tag{5.4.20}$$

We now rewrite the resulting equation as

$$\frac{d}{dr}\left(r\frac{dh}{dr}\right) = -\frac{\mathrm{Ca}\omega^2 r^3}{2} + C_0 \mathrm{Ca} r \tag{5.4.21}$$

and integrate once again to obtain

$$\frac{dh}{dr} = -\frac{\mathrm{Ca}\omega^2 r^3}{8} + \frac{C_0 \mathrm{Ca}}{2} r + \frac{C_1}{r}. \tag{5.4.22}$$

Integrating once more gives the general steady solution of the PDE (5.4.17)

$$h(r) = -\frac{\mathrm{Ca}\omega^2 r^4}{32} + \frac{C_0 \mathrm{Ca} r^2}{4} + C_1 \ln r + C_2. \tag{5.4.23}$$

Since we are looking for a bounded solution, no meniscus boundary condition at $r = 0$ implies $C_1 = 0$. At $r = 1$ no meniscus boundary condition on the other hand says

$$\left.\frac{dh}{dr}\right|_{r=1} = -\frac{\mathrm{Ca}\omega^2}{8} + \frac{C_0 \mathrm{Ca}}{2} = 0 \tag{5.4.24}$$

so that $C_0 = \frac{\omega^2}{4}$. As the no-flux condition is already satisfied the steady state solution is of the form

$$h(r) = -\frac{\mathrm{Ca}\omega^2 r^4}{32} + \frac{\mathrm{Ca}\omega^2 r^2}{16} + C_2. \tag{5.4.25}$$

If we begun the experiment with a flat layer of fluid $h(r) = \bar{h}$ then total mass at the beginning is

$$\int_0^{2\pi}\int_0^1 h(r) r dr d\theta = 2\pi \int_0^1 \bar{h} r dr = \pi \bar{h}. \tag{5.4.26}$$

Since mass stays conserved

$$\int_0^{2\pi}\int_0^1 h(r) r dr d\theta = 2\pi \int_0^1 \left(-\frac{\mathrm{Ca}\omega^2 r^5}{32} + \frac{\mathrm{Ca}\omega^2 r^3}{16} + C_2 r \right) dr = \pi \bar{h} \tag{5.4.27}$$

so

$$C_2 = \bar{h} - \frac{\mathrm{Ca}\omega^2}{48}. \tag{5.4.28}$$

The steady state solution depends on the initial uniform height, angular velocity ω and capillary constant Ca

$$h(r) = -\frac{\mathrm{Ca}\omega^2 r^4}{32} + \frac{\mathrm{Ca}\omega^2 r^2}{16} + \bar{h} - \frac{\mathrm{Ca}\omega^2}{48}. \tag{5.4.29}$$

The problem occurs once function $h(r)$ becomes negative, when $\bar{h} < \frac{\mathrm{Ca}\omega^2}{48}$, or when angular velocity ω is greater than critical angular velocity ω_c

$$\omega_c = \sqrt{\frac{48\bar{h}}{\mathrm{Ca}}}. \tag{5.4.30}$$

For angular velocities greater than critical angular velocity a dry spot occurs and there is r_c, critical radius, such that for $r \leq r_c$ there is no fluid

$$h(r) = 0, \qquad \text{for} \qquad r \leq r_c \tag{5.4.31}$$

and

$$\left.\frac{\partial h}{\partial r}\right|_{r=r_c} = 0. \tag{5.4.32}$$

At $r = r_c$

$$h(r_c) = -\frac{\mathrm{Ca}\omega^2 r_c^4}{32} + \frac{C_0 \mathrm{Ca} r_c^2}{4} + C_1 \ln r_c + C_2 = 0 \tag{5.4.33}$$

so

$$C_2 = \frac{\mathrm{Ca}\omega^2 r_c^4}{32} - \frac{C_0 \mathrm{Ca} r_c^2}{4} - C_1 \ln r_c \tag{5.4.34}$$

and

$$h(r) = -\frac{\mathrm{Ca}\omega^2}{32}\left(r^4 - r_c^4\right) + \frac{C_0 \mathrm{Ca}}{4}\left(r^2 - r_c^2\right) + C_1 \ln \frac{r}{r_c} \tag{5.4.35}$$

for $r > r_c$. Now

$$\frac{\partial h}{\partial r} = -\frac{\mathrm{Ca}\omega^2}{8} r^3 + \frac{C_0 \mathrm{Ca}}{2} r + \frac{C_1}{r} \tag{5.4.36}$$

so the no meniscus boundary condition at $r = 1$ becomes

$$-\frac{\mathrm{Ca}\omega^2}{8} + \frac{C_0 \mathrm{Ca}}{2} + C_1 = 0 \tag{5.4.37}$$

and

$$C_1 = \frac{\mathrm{Ca}\omega^2}{8} - \frac{C_0 \mathrm{Ca}}{2}. \tag{5.4.38}$$

Similarly from the boundary condition at $r = r_c$ (5.4.32)

$$-\frac{\mathrm{Ca}\omega^2}{8} r_c^3 + \frac{C_0 \mathrm{Ca}}{2} r_c + \frac{C_1}{r_c} = 0, \tag{5.4.39}$$

so we substitute in for C_1

$$-\frac{\mathrm{Ca}\omega^2}{8} r_c^3 + \frac{C_0 \mathrm{Ca}}{2} r_c + \frac{1}{r_c}\left(\frac{\mathrm{Ca}\omega^2}{8} - \frac{C_0 \mathrm{Ca}}{2}\right) = 0, \tag{5.4.40}$$

to get

$$C_0 = \frac{\omega^2}{4}\left(r_c^2+1\right) \tag{5.4.41}$$

and

$$C_1 = \frac{\mathrm{Ca}\omega^2}{8} - \frac{C_0\mathrm{Ca}}{2} = \frac{\mathrm{Ca}\omega^2}{8} - \frac{\mathrm{Ca}\omega^2}{8}\left(r_c^2+1\right) = -\frac{\mathrm{Ca}\omega^2 r_c^2}{8}. \tag{5.4.42}$$

Now the weak solution for $\omega > \omega_c$ is given by

$$h(r) = \begin{cases} 0 & \text{if } 0 < r \le r_c, \\ \frac{\mathrm{Ca}\omega^2}{8}\left[-\frac{\left(r^4-r_c^4\right)}{4} + \frac{\left(r_c^2+1\right)\left(r^2-r_c^2\right)}{2} - r_c^2\ln\frac{r}{r_c}\right] & \text{if } r_c < r \le 1. \end{cases} \tag{5.4.43}$$

As mass has to be conserved, at the steady state

$$\begin{aligned} \int_0^{2\pi}\int_{r_c}^1 h(r) r\,dr\,d\theta &= \frac{\pi\mathrm{Ca}\omega^2}{4}\int_{r_c}^1\left[-\frac{r^5 - r r_c^4}{4} + \left(r_c^2+1\right)\frac{r^3 - r r_c^2}{2} - r r_c^2\ln\frac{r}{r_c}\right]dr \\ &= \frac{\pi\mathrm{Ca}\omega^2}{4}\left[-\frac{r^6}{24} + \left(r_c^2+1\right)\frac{r^4}{8} - r_c^4\frac{r^2}{8} - r_c^2\frac{r^2}{2}\ln\frac{r}{r_c}\right]\Bigg|_{r_c}^1 \\ &= \frac{\pi\mathrm{Ca}\omega^2}{96}\left(r_c^6 - 6r_c^4 + 3r_c^2 + 2 - 12r_c^2\ln\frac{1}{r_c}\right) \\ &= \pi\bar{h} \end{aligned} \tag{5.4.44}$$

with $\bar{h}$ initial height of the fluid before rotation. It follows

$$r_c^6 - 6r_c^4 + 3r_c^2 + 2 - 12r_c^2\ln\frac{1}{r_c} = \frac{96\bar{h}}{\mathrm{Ca}\omega^2} \tag{5.4.45}$$

or

$$r_c^6 - 6r_c^4 + 3r_c^2 + 2 - 12r_c^2\ln\frac{1}{r_c} = 2\left(\frac{\omega_c}{\omega}\right)^2 \tag{5.4.46}$$

where

$$\omega_c = \sqrt{\frac{48\bar{h}}{\mathrm{Ca}}}. \tag{5.4.47}$$

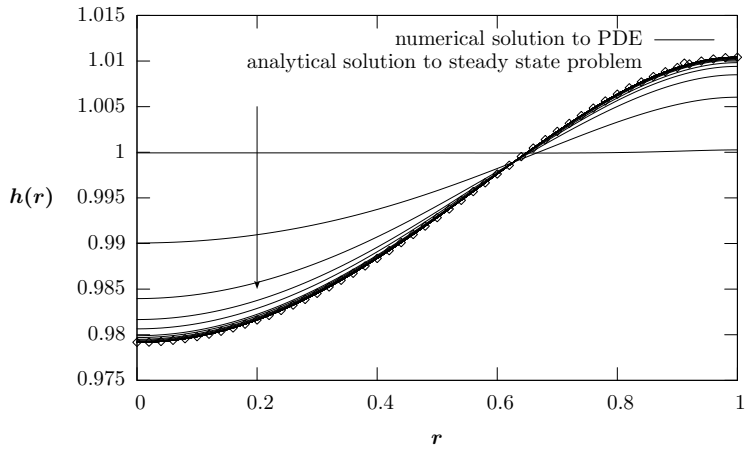

FIGURE 5.4.6: The evolution of numerical solution every $\Delta t = 0.01$, and analytical solution to the steady state problem for $\omega = 1$ when Ca $= 1$, and $\bar{h} = 1$ ($\omega_c = 4\sqrt{3}$).

We test the code solving the PDE numerically and matching the long time solution with the analytical steady state solution. Figure 5.4.6 shows the numerical and the steady state solution for angular velocity $\omega = 1$ of the fluid for Ca $= 1$ and $\bar{h} = 1$ when critical angular velocity $\omega_c = 4\sqrt{3}$. Figure 5.4.7 shows the numerical and the steady state solution when angular velocity $\omega = 4\sqrt{3} + 5 > \omega_c$ with the same values of Ca and $\bar{h}$. As time goes on initial flat fluid surface evolves into a shape which with time converges to the predicted steady state solution. Figure 5.4.8 is enlarged long time numerical solution to the PDE around r_c compared to the analytical solution of the steady state problem for $\omega = \omega_c + 5$. Like in the gravity and centrifugal forces only case, the numerical code chooses r_c by finding the lowest bound on $h(r)$.

Figure 5.4.9 shows the relation between the r_c and $\frac{\omega}{\omega_c}$ obtained by solving the full problem and is compared to the analytical relation (5.4.46) obtained for the steady state solution when $\omega > \omega_c$. There is an error introduced into the analytical solution as it also had to be found numerically. Two data sets are very close to each other. The better accuracy can be obtained by making spacial step smaller and running the code which solves the PDE for a longer time. Figure 5.4.10 shows log-log plot of the height of the fluid at the origin $h(0, t)$ through time t. The height decays with

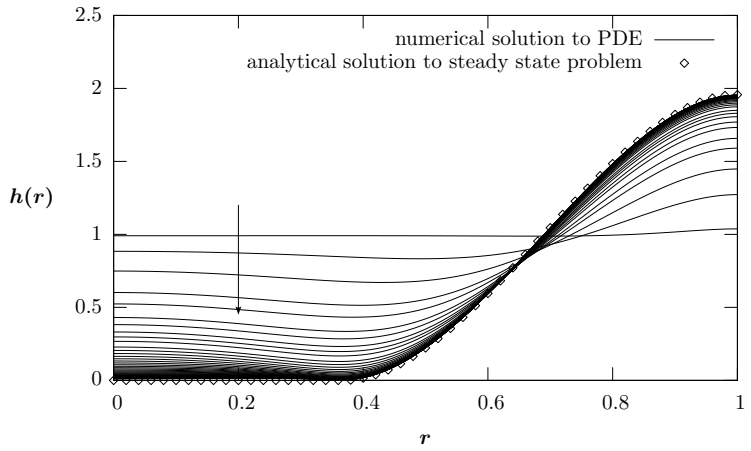

FIGURE 5.4.7: Long time numerical solution to PDE compared to the analytical solution to steady state problem for $\omega = 4\sqrt{3} + 5 < \omega_c = 4\sqrt{3}$ when Ca $= 1$, and $\bar{h} = 1$.

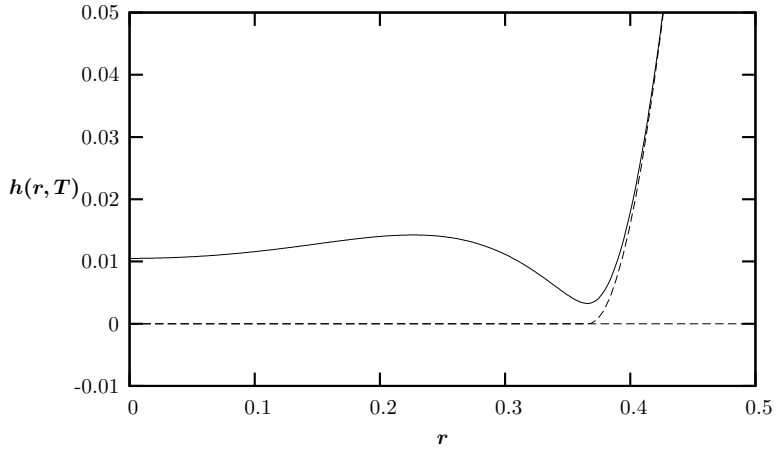

FIGURE 5.4.8: Enlargement of the long time numerical solution and steady state analytical solution of the PDE problem when $\omega = \omega_c + 5$, Ca $= 1$ and $\bar{h} = 1$ near r_c.

$O(t^{-4/5})$ which is slower than the exponential convergence in linear test problem but faster than the spin in which gravity and centrifugal forces are dominant and which has a cusp at $r = r_c$.

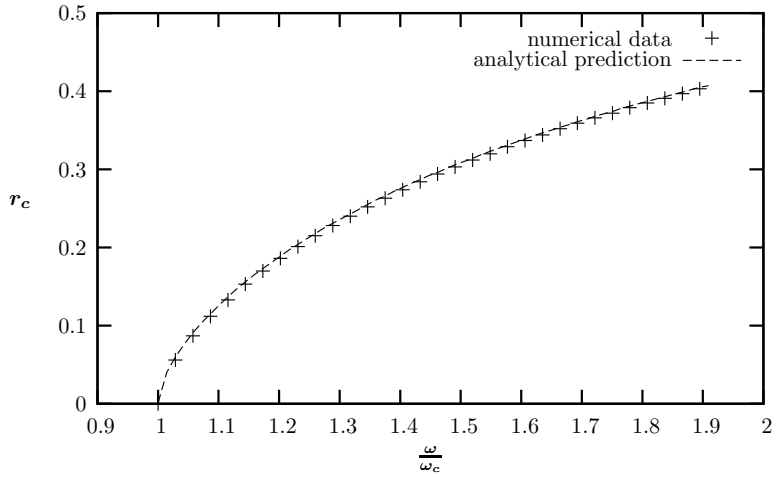

FIGURE 5.4.9: Comparison of numerical data plot r_c vs. $\frac{\omega}{\omega_c}$ with the analytical solution from equation (5.4.46).

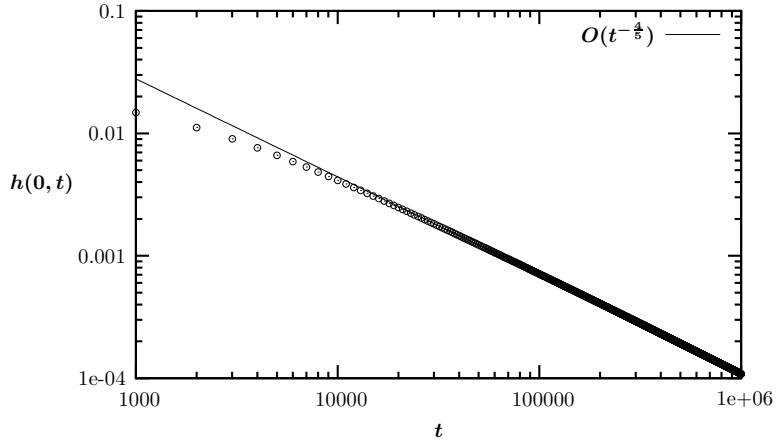

FIGURE 5.4.10: Log-log plot of $h(0,t)$ vs t shows that the height of the film at the origin decays as $t^{-\frac{4}{5}}$.

5.4.3 Steady state solutions for Ma = 0 *and* Ha = 0 - *gravity, centrifugal and surface tension forces only*

We consider a rotating thin film under the influence of gravity, centrifugal and surface tension forces and neglect the effects of van der Waals and Marangoni forcing. We are looking for a steady state solution to the fourth order nonlinear PDE problem

$$\frac{\partial h}{\partial t} + \frac{1}{r}\frac{\partial}{\partial r}\left[\frac{rh^3}{3}\frac{\partial}{\partial r}\left(\frac{1}{\mathrm{Ca}}\frac{1}{r}\frac{\partial}{\partial r}\left(r\frac{\partial h}{\partial r}\right) - \mathrm{St}^{-1}h + \frac{\omega^2 r^2}{2}\right)\right] = 0 \qquad (5.4.48)$$

with boundary conditions

$$\left.\frac{\partial h}{\partial r}\right|_{r=0} = 0 \tag{5.4.49a}$$

$$\left.\frac{\partial h}{\partial r}\right|_{r=1} = 0 \tag{5.4.49b}$$

$$\left.\frac{\partial}{\partial r}\left(\frac{1}{\mathrm{Ca}}\frac{1}{r}\frac{\partial}{\partial r}\left(r\frac{\partial h}{\partial r}\right) - \mathrm{St}^{-1}h + \frac{\omega^2 r^2}{2}\right)\right|_{r=1} = 0 \tag{5.4.49c}$$

where ω is the constant angular velocity of the spin.

To solve for the steady state solution we first integrate steady state form of (5.4.48) to obtain

$$\frac{d}{dr}\left(\frac{1}{\mathrm{Ca}}\frac{1}{r}\frac{d}{dr}\left(r\frac{dh}{dr}\right) - \mathrm{St}^{-1}h + \frac{\omega^2 r^2}{2}\right) = 0. \tag{5.4.50}$$

Integrating once again yields

$$\frac{1}{\mathrm{Ca}}\frac{1}{r}\frac{d}{dr}\left(r\frac{dh}{dr}\right) - \mathrm{St}^{-1}h + \frac{\omega^2 r^2}{2} = C_0. \tag{5.4.51}$$

Using Maple we can find the solution

$$h(r) = C_1 I_0\left(\sqrt{\mathrm{Bo}}r\right) + C_2 K_0\left(\sqrt{\mathrm{Bo}}r\right) + \frac{\mathrm{St}}{2}\omega^2 r^2 + 2\frac{\mathrm{St}^2}{\mathrm{Ca}}\omega^2 - C_0\mathrm{St} \tag{5.4.52}$$

where Bond number, the ratio of gravity and surface tension is given by

$$\mathrm{Bo} = \mathrm{St}^{-1}\cdot\mathrm{Ca} = \epsilon^{-2}\frac{\rho g H^2}{\sigma_0} = \frac{\rho g R^2}{\sigma_0}. \tag{5.4.53}$$

It follows

$$\frac{dh}{dr} = C_1\sqrt{\mathrm{Bo}}I_1\left(\sqrt{\mathrm{Bo}}r\right) - C_2\sqrt{\mathrm{Bo}}K_1\left(\sqrt{\mathrm{Bo}}r\right) + \mathrm{St}\omega^2 r. \tag{5.4.54}$$

Since we are looking for bounded solutions the no meniscus boundary condition at $r = 0$ gives $C_2 = 0$. Furthermore, from the no meniscus boundary condition at $r = 1$

$$C_1 = -\frac{\mathrm{St}\omega^2}{\sqrt{\mathrm{Bo}} I_1\left(\sqrt{\mathrm{Bo}}\right)}, \tag{5.4.55}$$

so

$$h(r) = -\frac{\mathrm{St}}{\sqrt{\mathrm{Bo}}}\omega^2 \frac{I_0\left(\sqrt{\mathrm{Bo}} r\right)}{I_1\left(\sqrt{\mathrm{Bo}}\right)} + \frac{\mathrm{St}}{2}\omega^2 r^2 + 2\frac{\mathrm{St}^2}{\mathrm{Ca}}\omega^2 - C_0\mathrm{St} \tag{5.4.56}$$

is the steady state solution with flux condition at $r = 1$ is already satisfied.

To find the constant C_0 we use conservation of mass

$$\begin{aligned} \int_0^{2\pi}\int_0^1 h(r) r dr d\theta &= 2\pi \int_0^1 \left(-\tfrac{\mathrm{St}}{\sqrt{\mathrm{Bo}}}\omega^2 r \tfrac{I_0\left(\sqrt{\mathrm{Bo}} r\right)}{I_1\left(\sqrt{\mathrm{Bo}}\right)} + \tfrac{\mathrm{St}}{2}\omega^2 r^3 + 2\tfrac{\mathrm{St}^2}{\mathrm{Ca}}\omega^2 r - C_0 \mathrm{St} r \right) dr \\ &= \pi\mathrm{St}\left(\tfrac{4\mathrm{St}}{\mathrm{Ca}}\omega^2 + \tfrac{\omega^2}{4} - C_0 \right) \\ &= \pi\bar{h} \end{aligned} \tag{5.4.57}$$

where $\bar{h}$ is the initial height of the flat thin layer of fluid before the spin. We now have

$$C_0 = \frac{4\mathrm{St}}{\mathrm{Ca}}\omega^2 + \frac{\omega^2}{4} - \mathrm{St}^{-1}\bar{h}. \tag{5.4.58}$$

The steady state solution depends on the initial uniform height $\bar{h}$ and constants St, Ca and Bo as

$$h(r) = -\frac{\mathrm{St}}{\sqrt{\mathrm{Bo}}}\omega^2 \frac{I_0\left(\sqrt{\mathrm{Bo}} r\right)}{I_1\left(\sqrt{\mathrm{Bo}}\right)} + \frac{\mathrm{St}}{2}\omega^2 r^2 - \frac{2\mathrm{St}^2}{\mathrm{Ca}}\omega^2 - \frac{\mathrm{St}}{4}\omega^2 + \bar{h}. \tag{5.4.59}$$

This steady state solution breaks down once function $h(r)$ becomes negative or when initial height of a flat thin film before spin

$$\bar{h} < \frac{\mathrm{St}}{\sqrt{\mathrm{Bo}}} \frac{\omega^2}{I_1\left(\sqrt{\mathrm{Bo}}\right)} + \frac{2\mathrm{St}^2}{\mathrm{Ca}}\omega^2 + \frac{\mathrm{St}}{4}\omega^2. \tag{5.4.60}$$

The critical angular velocity ω_c for which this happens is given by

$$\omega_c = \sqrt{\bar{h}\left[\frac{2\mathrm{St}^2}{\mathrm{Ca}} + \frac{\mathrm{St}}{4} + \frac{\mathrm{St}}{\sqrt{\mathrm{Bo}}}\frac{1}{I_1\left(\sqrt{\mathrm{Bo}}\right)}\right]^{-1}}. \tag{5.4.61}$$

When $\omega > \omega_c$ a dry spot occurs so that $h(r) = 0$ for all $r \leq r_c$, where r_c is some critical radius depending on ω. The general solution

$$h(r) = C_1 I_0\left(\sqrt{\mathrm{Bo}}r\right) + C_2 K_0\left(\sqrt{\mathrm{Bo}}r\right) + \frac{\mathrm{St}}{2}\omega^2 r^2 + 2\frac{\mathrm{St}^2}{\mathrm{Ca}}\omega^2 - C_0\mathrm{St} \tag{5.4.62}$$

is then subject to boundary conditions

$$h(r_c) = 0, \tag{5.4.63a}$$

$$\left.\frac{dh}{dr}\right|_{r=r_c} = 0, \tag{5.4.63b}$$

as well as

$$\left.\frac{dh}{dr}\right|_{r=1} = 0. \tag{5.4.63c}$$

Hence

$$h(r_c) = C_1 I_0\left(\sqrt{\mathrm{Bo}}r_c\right) + C_2 K_0\left(\sqrt{\mathrm{Bo}}r_c\right) + \frac{\mathrm{St}}{2}\omega^2 r_c^2 + 2\frac{\mathrm{St}^2}{\mathrm{Ca}}\omega^2 - C_0\mathrm{St} = 0, \tag{5.4.64}$$

$$\left.\frac{dh}{dr}\right|_{r=r_c} = C_1\sqrt{\mathrm{Bo}}I_1\left(\sqrt{\mathrm{Bo}}r_c\right) - C_2\sqrt{\mathrm{Bo}}K_1\left(\sqrt{\mathrm{Bo}}r_c\right) + \mathrm{St}\omega^2 r_c = 0, \tag{5.4.65}$$

and

$$\left.\frac{dh}{dr}\right|_{r=1} = C_1\sqrt{\mathrm{Bo}}I_1\left(\sqrt{\mathrm{Bo}}\right) - C_2\sqrt{\mathrm{Bo}}K_1\left(\sqrt{\mathrm{Bo}}\right) + \mathrm{St}\omega^2 = 0. \tag{5.4.66}$$

From (5.4.66)

$$C_1 = C_2\frac{K_1\left(\sqrt{\mathrm{Bo}}\right)}{I_1\left(\sqrt{\mathrm{Bo}}\right)} - \frac{\mathrm{St}}{\sqrt{\mathrm{Bo}}I_1\left(\sqrt{\mathrm{Bo}}\right)}\omega^2 \tag{5.4.67}$$

so substituting into (5.4.65) we have

$$C_2\sqrt{\mathrm{Bo}}\left[\frac{I_1\left(\sqrt{\mathrm{Bo}}r_c\right)}{I_1\left(\sqrt{\mathrm{Bo}}\right)}K_1\left(\sqrt{\mathrm{Bo}}\right)-K_1\left(\sqrt{\mathrm{Bo}}r_c\right)\right]+\mathrm{St}\omega^2\left[r_c-\frac{I_1\left(\sqrt{\mathrm{Bo}}r_c\right)}{I_1\left(\sqrt{\mathrm{Bo}}\right)}\right]=0. \tag{5.4.68}$$

We now have constant C_2

$$C_2=-\omega^2\frac{\mathrm{St}}{\sqrt{\mathrm{Bo}}}\left[r_c-\frac{I_1\left(\sqrt{\mathrm{Bo}}r_c\right)}{I_1\left(\sqrt{\mathrm{Bo}}\right)}\right]\cdot\left[\frac{I_1\left(\sqrt{\mathrm{Bo}}r_c\right)}{I_1\left(\sqrt{\mathrm{Bo}}\right)}K_1\left(\sqrt{\mathrm{Bo}}\right)-K_1\left(\sqrt{\mathrm{Bo}}r_c\right)\right]^{-1}. \tag{5.4.69}$$

Substituting into equation (5.4.64) yields constant C_0

$$C_0=C_1\mathrm{St}^{-1}I_0\left(\sqrt{\mathrm{Bo}}r_c\right)+C_2\mathrm{St}^{-1}Y_0\left(\sqrt{\mathrm{Bo}}r_c\right)+\frac{\omega^2r_c^2}{2}+\frac{2\mathrm{St}}{\mathrm{Ca}}\omega^2 \tag{5.4.70}$$

so finally we have the weak steady state solution when $\omega>\omega_c$

$$h(r)=\begin{cases}0 & \text{if } 0<r\le r_c,\\ C_1\left[I_0\left(\sqrt{\mathrm{Bo}}r\right)-I_0\left(\sqrt{\mathrm{Bo}}r_c\right)\right] & \\ +C_2\left[K_0\left(\sqrt{\mathrm{Bo}}r\right)-K_0\left(\sqrt{\mathrm{Bo}}r_c\right)\right]+\frac{\mathrm{St}}{2}\omega^2\left(r^2-r_c^2\right) & \text{if } r_c<r\le 1.\end{cases} \tag{5.4.71}$$

where C_1 and C_2 are given by (5.4.67) and (5.4.69) respectively.

Using the conservation of mass we can find the relationship between r_c and ω

$$\int_0^{2\pi}\int_{r_c}^1 h(r)r\,dr\,d\theta=\pi\bar{h} \tag{5.4.72}$$

which is much more complicated than for the previous cases and we find it numerically using the trapezoid rule. Figure 5.4.11 shows the relation between the r_c and ω obtained by solving the full problem and is compared to the analytically found relationship. The analytical r_c was obtained numerically by finding the node which the most closely satisfies equation (5.4.72).

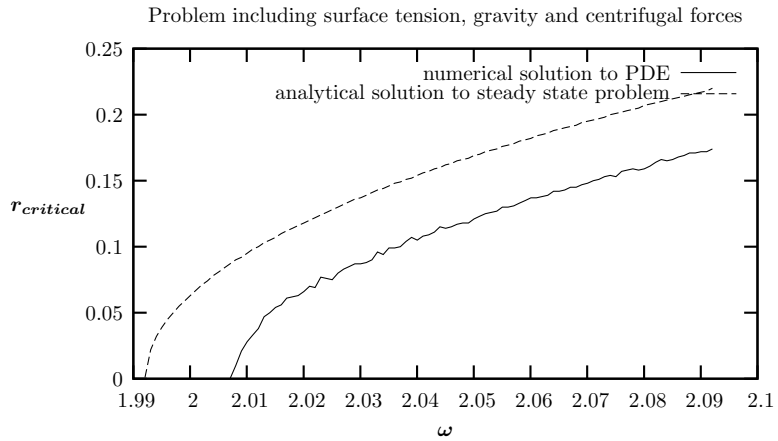

FIGURE 5.4.11: Comparison of numerical data plot r_c vs. ω with the predicted analytical solution.

5.5 Full dynamical problem - with Marangoni forcing

We now consider a full dynamical problem including surface tension, gravity, centrifugal, capillary and disjoint pressure forces

$$\frac{\partial h}{\partial t} + \frac{1}{r}\frac{\partial}{\partial r}\left\{\frac{rh^3}{3}\Big[\mathrm{Ca}^{-1}\frac{\partial}{\partial r}\left(\frac{1}{r}\frac{\partial}{\partial r}\left(r\frac{\partial h}{\partial r}\right)\right) - \mathrm{St}^{-1}\frac{\partial h}{\partial r} + \mathrm{Ha}\frac{\partial}{\partial r}\left(\frac{1}{h^3}\right) + \omega^2 r\Big] + \mathrm{Ma}\frac{rh^2}{2}\right\} = 0 \tag{5.5.1}$$

with boundary conditions

$$\left.\frac{\partial h}{\partial r}\right|_{r=0} = 0 \tag{5.5.2a}$$

$$\left.\frac{\partial h}{\partial r}\right|_{r=1} = 0 \tag{5.5.2b}$$

$$\left[\mathrm{Ca}^{-1}\frac{\partial}{\partial r}\left(\frac{1}{r}\frac{\partial}{\partial r}\left(r\frac{\partial h}{\partial r}\right)\right) - \mathrm{St}^{-1}\frac{\partial h}{\partial r} + \mathrm{Ha}\frac{\partial}{\partial r}\left(\frac{1}{h^3}\right) + \omega^2 r + \frac{3\mathrm{Ma}}{2h}\right]\Bigg|_{r=1} = 0 \tag{5.5.2c}$$

To solve the full problem we use numerical methods, more specific; finite difference via Newton's method.

We want to discretize the full PDE (5.5.1). We let $r_i = i\Delta r$ for $i = 0, \ldots, N$ where $\Delta r = \frac{1}{N}$ so that $r_0 = 0$ and $r_N = 1$. Values h_0^j and h_N^j correspond to values of $h(r,t)$ at $r = 0$ and $r = 1$ at time $t_j = j\Delta t$.

Finite difference

$$
\begin{aligned}
&\tfrac{h_i^{j+1}-h_i^j}{\Delta t} \\
&+\tfrac{1}{r_i\Delta r}\Bigg\{ \quad \tfrac{r_{i+\frac{1}{2}}\left(h_{i+\frac{1}{2}}^{j+1}\right)^3}{3}\Bigg[\quad \mathrm{Ca}^{-1}\tfrac{\partial}{\partial r}\left(\tfrac{1}{r}\tfrac{\partial}{\partial r}\left(r\tfrac{\partial h}{\partial r}\right)\right)\Big|_{i+\frac{1}{2}} \\
&\qquad\qquad -\mathrm{St}^{-1}\tfrac{h_{i+1}^{j+1}-h_i^{j+1}}{\Delta r} + \tfrac{\mathrm{Ha}}{\Delta r}\left(\tfrac{1}{\left(h_{i+1}^{j+1}\right)^3} - \tfrac{1}{\left(h_i^{j+1}\right)^3}\right) + \omega^2 r_{i+\frac{1}{2}}\Bigg] \\
&\qquad -\tfrac{r_{i-\frac{1}{2}}\left(h_{i-\frac{1}{2}}^{j+1}\right)^3}{3}\Bigg[\quad \mathrm{Ca}^{-1}\tfrac{\partial}{\partial r}\left(\tfrac{1}{r}\tfrac{\partial}{\partial r}\left(r\tfrac{\partial h}{\partial r}\right)\right)\Big|_{i-\frac{1}{2}} \\
&\qquad\qquad -\mathrm{St}^{-1}\tfrac{h_i^{j+1}-h_{i-1}^{j+1}}{\Delta r} + \tfrac{\mathrm{Ha}}{\Delta r}\left(\tfrac{1}{\left(h_i^{j+1}\right)^3} - \tfrac{1}{\left(h_{i-1}^{j+1}\right)^3}\right) + \omega^2 r_{i-\frac{1}{2}}\Bigg] \\
&\qquad\qquad +\mathrm{Ma}\tfrac{r_{i+\frac{1}{2}}\left(h_{i+\frac{1}{2}}^{j+1}\right)^2}{2} - \mathrm{Ma}\tfrac{r_{i-\frac{1}{2}}\left(h_{i-\frac{1}{2}}^{j+1}\right)^2}{2}\Bigg\} = 0
\end{aligned}
\tag{5.5.3}
$$

where

$$
\begin{aligned}
\tfrac{\partial}{\partial r}\left(\tfrac{1}{r}\tfrac{\partial}{\partial r}\left(r\tfrac{\partial h}{\partial r}\right)\right)\Big|_{i+\frac{1}{2}} &= \tfrac{1}{r_{i+1}\Delta r^3}\left[r_{i+\frac{3}{2}}\left(h_{i+2}^{j+1}-h_{i+1}^{j+1}\right) - r_{i+\frac{1}{2}}\left(h_{i+1}^{j+1}-h_i^{j+1}\right)\right] \\
&\quad -\tfrac{1}{r_i\Delta r^3}\left[r_{i+\frac{1}{2}}\left(h_{i+1}^{j+1}-h_i^{j+1}\right) - r_{i-\frac{1}{2}}\left(h_i^{j+1}-h_{i-1}^{j+1}\right)\right]
\end{aligned}
\tag{5.5.4}
$$

and

$$
\begin{aligned}
\tfrac{\partial}{\partial r}\left(\tfrac{1}{r}\tfrac{\partial}{\partial r}\left(r\tfrac{\partial h}{\partial r}\right)\right)\Big|_{i-\frac{1}{2}} &= \tfrac{1}{r_i\Delta r^3}\left[r_{i+\frac{1}{2}}\left(h_{i+1}^{j+1}-h_i^{j+1}\right) - r_{i-\frac{1}{2}}\left(h_i^{j+1}-h_{i-1}^{j+1}\right)\right] \\
&\quad -\tfrac{1}{r_{i-1}\Delta r^3}\left[r_{i-\frac{1}{2}}\left(h_i^{j+1}-h_{i-1}^{j+1}\right) - r_{i-\frac{3}{2}}\left(h_{i-1}^{j+1}-h_{i-2}^{j+1}\right)\right]
\end{aligned}
\tag{5.5.5}
$$

for $i = 2, \ldots, N$ with $h_{N+1}^{j+1} = h_{N-1}^{j+1}$ and $h_{N+2}^{j+1} \approx h_{N-2}^{j+1} - 4\Delta r\left(h_{N-1}^{j+1} - h_N^{j+1}\right) - 2\Delta r^3\mathrm{Ca}\left(\omega^2 + \frac{3\mathrm{Ma}}{2h_N^{j+1}}\right)$ (consequence of centered difference approximation to boundary conditions at $r = 1$).

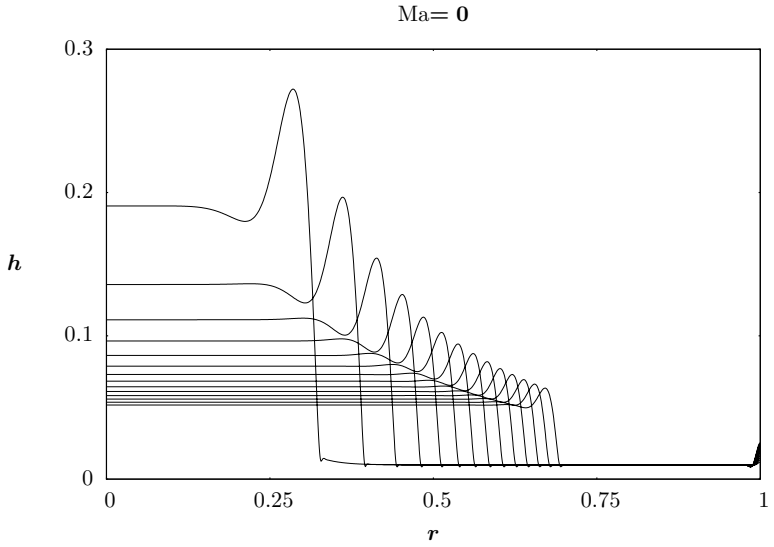

FIGURE 5.5.1: Flow of a drop driven by centrifugal and surface tension forces (Ca = 1, $\omega = 10$).

For $i = 0$ we use boundary condition at $r = 0$ using the second order forward difference:

$$\left.\frac{\partial h}{\partial r}\right|_{r=0} = \frac{-3h_0^{j+1} + 4h_1^{j+1} - h_2^{j+1}}{2\Delta r} + O(\Delta r^2) = 0 \tag{5.5.6}$$

and for $i = 1$ we use

$$\begin{aligned} \left.\frac{\partial}{\partial r}\left(\frac{1}{r}\frac{\partial}{\partial r}\left(r\frac{\partial h}{\partial r}\right)\right)\right|_{i-\frac{1}{2}} &= \frac{1}{r_i \Delta r^3}\left[r_{i+\frac{1}{2}}(h_{i+1}^{j+1} - h_i^{j+1}) - r_{i-\frac{1}{2}}(h_i^{j+1} - h_{i-1}^{j+1})\right] \\ &\quad -\frac{4}{\Delta r^3}\left(h_i^{j+1} - h_{i-1}^{j+1}\right) \end{aligned} \tag{5.5.7}$$

Figure 5.5.1 shows the spreading of a drop under the influence of centrifugal and surface tension forces where gravity, disjoining pressure and Marangoni forces have been neglected. The influence of adding the positive Marangoni forcing is shown in Figure 5.5.2. This forcing caused by the surface tension gradient, consequence of a cooler center of the disk compared to the outer edges, is acting against the centrifugal force making the spreading of the fluid slower.

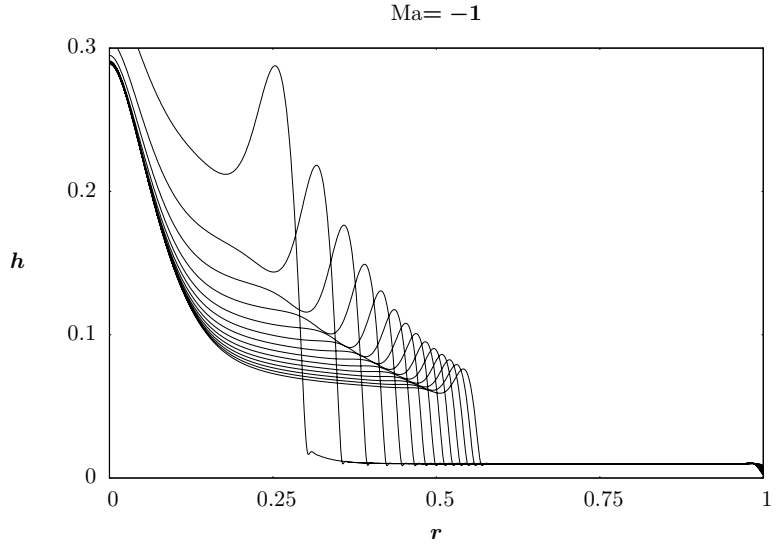

FIGURE 5.5.2: Flow of a drop driven by centrifugal, surface tension and Marangoni forces (Ca = 1, Ma = 1, $\omega = 10$).

6

Future Work

In this work we studied only axisymmetric flow problems of rotating thin films. To model fingering instabilities which have been observed in spin coating experiments we would need to consider a full problem in which the height $h(r, \theta, t)$ is also dependent on angle θ [44, 20, 35, 46, 50]. The simplest such problem would be

$$h_t + \nabla \cdot (h^3 \nabla \nabla^2 h) = 0 \tag{6.0.1}$$

with surface tension as a dominating force. This equation is written out in full cylindrical coordinates as

$$\begin{aligned} h_t &+ \frac{1}{r}\frac{\partial}{\partial r}\left[r h^3 \frac{\partial}{\partial r}\left(\frac{1}{r}\frac{\partial}{\partial r}\left(r \frac{\partial h}{\partial r} \right) + \frac{1}{r^2}\frac{\partial^2 h}{\partial \theta^2} \right) \right] \\ &+ \frac{1}{r}\frac{\partial}{\partial \theta}\left[\frac{h^3}{r}\frac{\partial}{\partial \theta}\left(\frac{1}{r}\frac{\partial}{\partial r}\left(r \frac{\partial h}{\partial r} \right) + \frac{1}{r^2}\frac{\partial^2 h}{\partial \theta^2} \right) \right] = 0. \end{aligned} \tag{6.0.2}$$

In order to solve two dimensional partial differential equation (6.0.2), a fast alternative to a standard method like the Crank-Nicolson would be Alternating Direction Implicit (ADI) method [54]. This method simplifies problem from solving for the height of the fluid over the full two-dimensional surface to solving along lines in one

direction and then alternating with solving along lines in the perpendicular direction. Equation (6.0.2) is not only harder to solve than its axisymmetric form because it has more singular terms but also because it has terms which have mixed derivatives. This problem in computation has been studied by Beam and Warming [4].

Studying equation (6.0.2) would be a first step towards understanding the full non-axisymmetric evolution equation which would also include influence of centrifugal, gravity, van der Waals and Marangoni forces. This is necessary in order to examine how thermal effects drive thin film dynamics in spin coating problems. By analogy with gravity driven flows, the radially driven flow can be expected to have a contact line that is unstable to transverse perturbation and the development of long fingers. In further work we want to examine the behaviors that can result from the competition of Marangoni effects with centrifugal acceleration. Marangoni forces in the spreading layers of fluid can be induced by imposing a constant gradient in radial outward direction of the center of the spinning disk.

Bibliography

[1] D.J. Acheson. *Elementary fluid dynamics*. Oxford University Press Inc., New York, NY, 1990.

[2] R.C. Ackerberg. On a nonlinear differential equation of electrohydrodynamics. *Proceedings of the Royal Society of London. Series A, Mathematical and Physical Sciences*, 312(1508):129–140, 1969.

[3] A. Acrivos, M.G. Shah, and E.E. Petersen. On the flow of a non-Newtonian liquid on a rotating disk. *Journal Of Applied Physics*, 31:963–968, 1960.

[4] R.M. Beam and R.F. Warming. Alternating direction implicit methods for parabolic equations with a mixed derivative. *SIAM Journal on Scientific and Statistical Computing*, 1(1):131–166, 1980.

[5] A.L. Bertozzi. The mathematics of moving contact lines in thin liquid films. *Notices of the American Mathematical Society*, 45(6):689–697, 1998.

[6] A.L. Bertozzi, G. Grun, and T.P. Witelski. Dewetting films: bifurcations and concentrations. *Nonlinearity*, 14(6):1569–1592, 2001.

[7] A.L. Bertozzi and M.C. Pugh. The lubrication approximation for thin viscous films: the moving contact line with porous media cut-off of van der Waals interactions. *Nonlinearity*, 7(6):1535–1564, 1994.

[8] A.L. Bertozzi and M.C. Pugh. The lubrication approximation for thin viscous films: regularity and long-term behavior of wear solutions. *Communications on Pure and Applied Mathematics*, 49(2):85–123, 1996.

[9] A.L. Bertozzi and M.C. Pugh. Long wave instabilities and saturation on thin film equations. *Communications on Pure and Applied Mathematics*, 51(6):625–661, 1998.

[10] R. Buckmire. Investigations of nonstandard, Mickens-type, finite-difference schemes for singular boundary value problems in cylindrical and spherical coordinates. *Numerical Methods for Partial Differential Equations*, 19(3):380–398, 2003.

[11] R. Buckmire. Application of a Mickens finite-difference scheme to the cylindrical Bratu-Gelfand problem. *Numerical Methods for Partial Differential Equations*, 20(3):327–337, 2004.

[12] J.P. Burelbach, S.G. Bankoff, and S.H. Davis. Nonlinear stability of evaporating/condensing liquid films. *Journal of Fluid Mechanics*, 195:463–494, 1988.

[13] A.J. Chorin and J.E. Marsden. *A mathematical introduction to fluid mechanics*. Springer-Verlag, New York, NY, 1992.

[14] F.C. Chou, M.W. Wang, S.C. Gong, and Z.G. Wang. Reduction of photoresist usage during spin coating. *Journal Of Electronic Materials*, 30(4):432–438, 2001.

[15] I. G. Currie. *Fundamental mechanics of fluids*. McGraw-Hill, New York, NY, 1993.

[16] I.E. Dzyaloshinskii, E.M. Lifshitz, and L.P. Pitaevskii. General theory of van der Waals' forces. *Soviet Phys.*, 4(2):153, 1961.

[17] Stillwagon L. E. and Larson R. G. Leveling of thin films over uneven substrates during spin coating. *Physics of Fluids A*, 2(11):1973–1944, 1990.

[18] A.G. Emslie, F.T. Bonner, and L.G. Peck. Flow of a viscous liquid on a rotating disk. *Journal Of Applied Physics*, 29:858, 1958.

[19] C.A.J. Fletcher. *Computational techniques for fluid dynamics*. Springer-Verlag, Berlin, Germany, 1991.

[20] N. Fraysse and G.M. Homsy. An experimental study of rivulet instabilities in centrifugal spin coating of viscous Newtonian and non-Newtonian fluids. *Physics of Fluids*, 6(4):1491–1504, 1994.

[21] R.W. Griffiths. The dynamics of lava flows. *Annual Review of Fluid Mechanics*, 32:477–518, 2000.

[22] R.P. Haskett, T.P. Witelski, and J. Sur. Localized Marangoni forcing in driven thin films. *Physica D*, 209:117–134, 2005.

[23] S. Hirasawa, Y. Saito, H. Nezu, N. Ohashi, and H. Maruyama. Analysis of drying shrinkage and flow due to surface tension on spin-coated films on topographic substrates. *IEEE Transactions on Semiconductor Manufacturing*, 10(4):438–444, 1997.

[24] L.M. Hocking. The influence of intermolecular forces on thin fluid layers. *Physics of Fluids A: Fluid Dynamics*, 5(4):793–799, 1993.

[25] L.M. Hocking. The spreading of drops with intermolecular forces. *Physics of Fluids A: Fluid Dynamics*, 6(10):3224–3228, 1994.

[26] C. Huh and L.E. Scriven. Hydrodynamic model of a steady movement of a solid/liquid/fluid contact line. *Journal Of Colloid Interface Science*, 35:85–101, 1971.

[27] H.E. Huppert. The propagation of two-dimensional and axisymmetric viscous gravity currents over a rigid horizontal surface. *Journal of Fluid Mechanics*, 121:43–58, 1982.

[28] H.E. Huppert and J.E. Simpson. The slumping of gravity currents. *Journal of Fluid Mechanics*, 99:785–799, 1980.

[29] C.-C. Hwang, C.-K. Lin, and W.-Y. Uen. A nonlinear three-dimensional rupture theory of thin liquid films. *Journal of Colloid and Interface Science*, 190:250–252, 1997.

[30] T.R.N. Jansson, M.P. Haspang, K.H. Jensen, P. Hersen, and T. Bohr. Polygons on a rotating fluid surface. *Physical Review Letters*, 96(17):153, 2006.

[31] P.K. Kundu and I.M. Cohen. *Fluid mechanics*. Elsevier Academic Press Inc., 2004.

[32] E. Lauga, M.P. Brenner, and H.A. Stone. Microfluidics: The no-slip boundary condition. In C. Tropea, A. Yarin, and J.F. Foss, editors, *Handbook of experimental fluid dynamics*. Springer, 2007.

[33] R.S. Laugesen and M.C. Pugh. Linear stability of steady states for thin film and Cahn-Hilliard type equations. *Archive for Rational Mechanics and Analysis*, 154:3–51, 2000.

[34] J.E. Marsden and T.S. Ratiu. *Introduction to mechanics and symmetry: a basic exposition of classical mechanical systems*. Springer-Verlag, 1994.

[35] F. Melo, J.F. Joanny, and S. Fauve. Fingering instability of spinning drops. *Physics Review Letters*, 63(18):1958–1961, 1989.

[36] S. Middleman. The effects of induced air flow on the spin coating of viscous liquids. *Journal Of Applied Physics*, 62(6):2530–2532, 1987.

[37] E. Momoniat and D.P. Mason. Investigation of the effect of the Coriolis force on a thin fluid film on a rotating disk. *International Journal of Non-Linear Mechanics*, 33(6):1069–1088, 1998.

[38] T.G. Myers and J.P.F. Charpin. The effect of the Coriolis force on axisymmetric rotating thin film flows. *International Journal of Non-Linear Mechanics*, 36:629–635, 2001.

[39] C.L.M.H. Navier. Memoire sur les lois du mouvement des fluides. *Mmoires de l'Acadmie Royale des Sciences de l'Institut de France*, 6:389–440, 1822.

[40] A. Oron, S.H. Davis, and S.G. Bankoff. Long-scale evolution of thin liquid films. *Reviews of Modern Physics*, 69(3):931–980, 1997.

[41] W.H. Press, S.A. Teukolsky, W.T. Vetterling, and B.P. Flannery. *Numerical Recipes: The art of scientific computing*. Cambridge University Press, New York, NY, 2007.

[42] B. Reisfeld, S.G. Bankoff, and S.H. Davis. The dynamics of thin liquid films during spin coating: Films with constant rates of evaporation. *Journal Of Applied Physics*, 70(10):5258–5266, 1991.

[43] O. Reynolds. On the theory of lubrication and its application to Mr. Beauchamp tower's experiments, including an experimental determination of the viscosity of olive oil. *Philosophical Transactions of the Royal Society of London*, 6:389–440, 1822.

[44] L.W. Schwartz and R.V. Roy. Theoretical and numerical results for spin coating of viscous liquids. *Physics of Fluids*, 16(3):569–584, 2004.

[45] A. Sharma and E. Ruckenstein. An analytical nonlinear theory of thin film rupture and its application to wetting films. *Journal of Colloid Interface Science*, 113:456–479, 1986.

[46] M. A. Spaid and G.M. Homsy. Stability of viscoelastic dynamic contact lines: An experimental study. *Phys. Fluids*, 9(4), 1997.

[47] J.C. Strikwerda. *Finite difference schemes and partial differential equations*. Society for Industrial and Applied Math, Philadelphia, PA, 2004.

[48] G.F. Teletzke, H.T. Davis, and L.E. Scriven. How liquids spread on solids. *Chemical Engineering Comm.*, 55:41–81, 1987.

[49] Y.-O. Tu. Depletion and retention of fluid on a rotating disk. *Trans. ASME, Journal of Lubrication Technology*, 105:625–629, 1983.

[50] M.W. Wang and F.C. Chou. Fingering instability and maximum radius at high rotational Bond number. *Journal Of Electochemical Society*, 148(5):283–290, 2001.

[51] M.B. Williams and S.H. Davis. Nonlinear theory of film rupture. *Journal of Colloid and Interface Science*, 90:220–220, 1982.

[52] T.P. Witelski and A.J. Bernoff. Stability of self-similar solutions for van der Waals driven thin film rupture. *Physics of Fluids*, 11(9):2443–2445, 1999.

[53] T.P. Witelski and A.J. Bernoff. Dynamics of three-dimensional thin film rupture. *Physica D*, 147:155–176, 2000.

[54] T.P. Witelski and M. Bowen. ADI schemes for fourth-order nonlinear diffusion equations. *Applied Numerical Mathematics*, 45(2-3):331–351, 2003.

[55] L. Wu. Spin coating of thin films on an axisymmetrically heated disk. *Physics of Fluids*, 18(3):063602–8, 2006.

[56] Q. Wu and H. Wong. A slope-dependent disjoining pressure for non-zero contact angles. *Journal of Fluid Mechanics*, 506):157–185, 2004.

[57] S.G. Yiantsios and R.H. Davis. Close approach and deformation of two viscous drops due to gravity and van der Waals forces. *Journal of Colloid and Interface Science*, 144:412–433, 1991.

[58] S.G. Yiantsios and B.G. Higgins. Rupture of thin films. *Journal of Colloid and Interface Science*, 147:341–350, 1991.

[59] W.W. Zhang and J.R. Lister. Similarity solutions for van der Waals rupture of a thin film on a solid substrate. *Physics of Fluids*, 11(9):2454–2462, 1999.

Biography

The author, Mihaela Froehlich (nèe Guberović) was born to Marija and Milan Guberović in Nova Gradiška, Croatia on May 8th, 1981. Following the completion of her pre-university schooling at the XV. Gymnasium in Zagreb, Croatia in 1999 she begun her undergraduates studies at Virginia Military Institute, Lexington, Virginia. She was graduated from there in 2003 with Bachelor of Science degrees in Mathematics and Physics. Following the graduation she continued her studies in mathematics at Duke University in Durham, North Carolina.